NAVAL POSTGRADUATE SCHOOL
Monterey, California

THESIS

MECHANICAL CHARACTERISTICS OF A SUPERPLASTIC ALUMINUM-10.2%Mg-0.1%Zr ALLOY

by

Thomas S. Hartmann

June 1985

Thesis Advisor: T. R. McNelley

Approved for public release; distribution is unlimited

SECURITY CLASSIFICATION OF THIS PAGE (When Data Entered)

REPORT DOCUMENTATION PAGE

READ INSTRUCTIONS BEFORE COMPLETING FORM

1. REPORT NUMBER	2. GOVT ACCESSION NO. / 3. RECIPIENT'S CATALOG NUMBER
4. TITLE (and Subtitle): Mechanical Characteristics of a Superplastic Aluminum-10.2%Mg-0.1%Zr Alloy	5. TYPE OF REPORT & PERIOD COVERED: Master's Thesis; June 1985
	6. PERFORMING ORG. REPORT NUMBER
7. AUTHOR(s): Thomas S. Hartmann	8. CONTRACT OR GRANT NUMBER(s)
9. PERFORMING ORGANIZATION NAME AND ADDRESS: Naval Postgraduate School, Monterey, California 93943-5100	10. PROGRAM ELEMENT, PROJECT, TASK AREA & WORK UNIT NUMBERS
11. CONTROLLING OFFICE NAME AND ADDRESS: Naval Postgraduate School, Monterey, California 93943-5100	12. REPORT DATE: June 1985
	13. NUMBER OF PAGES: 97
14. MONITORING AGENCY NAME & ADDRESS (if different from Controlling Office)	15. SECURITY CLASS. (of this report): Unclassified
	15a. DECLASSIFICATION/ DOWNGRADING SCHEDULE

16. DISTRIBUTION STATEMENT (of this Report)

Approved for public release; distribution is unlimited

17. DISTRIBUTION STATEMENT (of the abstract entered in Block 20, if different from Report)

18. SUPPLEMENTARY NOTES

19. KEY WORDS (Continue on reverse side if necessary and identify by block number)

Superplasticity, Aluminum, Aluminum-Magnesium Alloys, Thermomechanical Processing, Annealing, Recrystallization, Creep Models, Activation Energy, Strain Rate Sensitivity Coefficient

20. ABSTRACT (Continue on reverse side if necessary and identify by block number)

The elevated temperature mechanical characteristics of an aluminum-magnesium-zirconium alloy were studied. Thermomechanical processing consisted of solution treating and hot working at 440°C and then warm rolling at 300°C to 94% reduction. Subsequent treatments included annealing at 200°C for one hour, and recrystallizing for one minute at 440°C. Tensile testing of warm rolled, annealed, and

DD FORM 1 JAN 73 1473 EDITION OF 1 NOV 65 IS OBSOLETE

S N 0102-LF-014-6601

SECURITY CLASSIFICATION OF THIS PAGE (When Data Entered)

20. (Continued)

recrystallized material was conducted at various strain rates and temperatures. The data was analyzed to determine strain-rate sensitivity coefficients and activation energies, in turn to be correlated with microstructural data concurrently obtained on this superplastic alloy. This material exhibits particularly good ambient properties in addition to the superplasticity.

Approved for public release; distribution is unlimited

Mechanical Characteristics of a Superplastic Aluminum-10.2%Mg-0.1%Zr Alloy

by

Thomas S. Hartmann
Lieutenant Commander, United States Navy
B.S., Texas A&M University, 1976

Submitted in partial fulfillment of the
requirements for the degree of

MASTER OF SCIENCE IN MECHANICAL ENGINEERING

from the

NAVAL POSTGRADUATE SCHOOL
June 1985

ABSTRACT

The elevated temperature mechanical characteristics of an aluminum-magnesium-zirconium alloy were studied. Thermomechanical processing consisted of solution treating and hot working at 440°C and then warm rolling at 300°C to 94% reduction. Subsequent treatments included annealing at 200°C for one hour, and recrystallizing for one minute at 440°C. Tensile testing of warm rolled, annealed, and recrystallized material was conducted at various strain rates and temperatures. The data was analyzed to determine strain-rate sensitivity coefficients and activation energies, in turn to be correlated with microstructural data concurrently obtained on this superplastic alloy. This material exhibits particularly good ambient properties in addition to the superplasticity.

TABLE OF CONTENTS

LIST OF TABLES

LIST OF FIGURES

ACKNOWLEDGEMENT

I would like to thank my advisor, Professor T. R. McNelley, and Dr. E. W. Lee for their expert assistance and guidance in conducting this research, the Naval Air Systems Command and Mr. Richard Schmidt for their financial support and continued interest in superplastic aluminum alloys, and finally, my co-workers and friends, M. E. Alcamo and D. B. Berthold, whose concurrent work enabled this thesis to be more in-depth.

I. INTRODUCTION

Considerable attention has been devoted to superplastic materials over the last twenty years, and a wide range of experimental observations are recorded in the scientific literature. The utility of superplastic alloys is associated with special methods of deformation processing, and in the case of ultrafine-grained materials, excellent room temperature mechanical properties. Sheet forming by vacuum or pressure may be slow, but complex parts can be made often in a single operation with a relatively inexpensive female die [Ref. 1]. The net result is a cost savings for certain components which are manufactured in moderate numbers. Stewart [Ref. 2] notes the excellent response of superplastic alloys to closed die forging. Again complex parts may be formed, slowly but in a single operation. The finished part has exceptional dimensional accuracy, surface smoothness, and nondirectional properties. The forging loads are comparatively small.

A large number of fine-grained metals and alloys often exhibit large neck-free elongation when deformed superplastically at elevated temperatures and at low strain rates. Various attempts have been made to explain this superplastic phenomena in terms of creep models, but as yet no single model is universally accepted.

This research examined the mechanical properties of an Al-10%Mg-0.1%Zr alloy in the superplastic regime. The choice of high Magnesium content evolved from previous research at the Naval Postgraduate School [Refs. 3-14]. This work showed that when a high Magnesium content alloy was solution treated, hot worked and then subsequently warm worked, the resultant microstructure consisted of elongated, unrecrystallized grains containing a fine subgrain structure and with uniform beta phase precipitation. This structure results in an alloy that has a high strength to weight ratio, with good ductility, fatigue resistance, and is stress corrosion cracking resistant. The Zirconium was added in an attempt to get a fine dispersion of precipitates which would further refine the structure by grain boundary pinning. Such refinement is necessary for superplastic behavior.

The present research was intended to provide further insight into mechanisms of superplastic behavior in this alloy. To accomplish this, tensile testing was conducted over a wide range of temperatures, 20°C to 425°C, and strain rates, 6.67×10^{-5} to 1.67×10^{-1} s^{-1}. The test matrix was devised to provide data to allow computation of activation energies and strain rate sensitivity coefficients over this range of strain rates and temperatures. These parameters would thus facilitate correlation of the observed charactistics in this alloy to those predicted by current

creep models. Additionally, specimens were recrystallized or annealed, prior to testing in an attempt to relate the elevated temperature characteristics of this alloy with those of recent previous work [Refs. 11-14], on Al-10%Mg-0.5%Mn alloys. The Al-10%Mg-0.1%Zr alloy was studied concurrently with Alcamo [Ref. 15] and Berthold [Ref. 16] who examined microstructural and related mechanical characteristics of this alloy.

II. BACKGROUND

A. SUPERPLASTIC BEHAVIOR

1. Scope

Superplasticity is the ability of a material to deform to exceptionally high elongations. A 200% elongation is considered the threshold value of superplasticity [Ref. 17] and values of greater than 1000% have frequently been reported. The important mechanical and microstructural features necessary for superplasticity are generally agreed to be fine, equiaxed grains with high angle grain boundaries, temperature in the range 0.5-0.7 Tm, low strain rates, and a high strain rate sensitivity coefficient, m. These features and several creep models will be discussed in the following sections.

2. Strain Rate Sensitivity

Deformation at elevated temperatures is a thermally activated process, and superplasticity is observed only at elevated temperatures. For a thermally activated process, the flow stress is a function of strain, strain rate, and temperature. The flow process, σ, is related to strain rate, $\dot{\varepsilon}$, by:

$$\sigma = k\dot{\varepsilon}^m \qquad \text{(eqn. 2.1)}$$

where k is a temperature dependent material constant, and m is the strain rate sensitivity coefficient, given by:

$$m = \frac{d(\ln \sigma)}{d(\ln \dot{\varepsilon})} \qquad \text{(eqn. 2.2)}$$

In general, m increases with increased temperature or decreased grain size. Hart [Ref. 18] showed that a high resistance to localized necking is obtained in materials where the flow stress is highly strain rate sensitive. Typical superplastic materials have m values greater than 0.3, with maximum m values producing maximum tensile elongations. The strain rate sensitivity coefficient, m, is obtained by measuring the steady-state flow stress over a range of strain rates at constant temperature, and plotting the data logarithmically as σ versus $\dot{\varepsilon}$. The slope of the line is termed strain rate sensitivity coefficient, m. Equation 2.2 does not account for other failure modes such as cavitation, but only the development of a geometrical neck. Thus a high value of m, while a necessary condition, is not a sufficient condition for superplasticity.

3. Creep Mechanisms

Creep is the continuing plastic deformation of materials subjected to a constant load or constant stress. The temperature regime for which creep is important is $0.5\ Tm < T < Tm$; where Tm is the melting point in Kelvin. This is the temperature range in which diffusion is

sufficiently rapid to sustain recovery rates great enough to relieve strain hardening. Diffusion, being a thermally activated process, exhibits an exponential temperature dependence. Below 0.5 Tm the diffusion coefficient is so small that deformation modes exclusively dependent on it can effectively be neglected.

Current creep models may be combined in the form:

$$\dot{\varepsilon} = K_1 \frac{D_{eff}}{d^p} \sigma^{n_1} + K_2 D_L \sigma^{n_2} \qquad \text{(eqn. 2.3)}$$

where $\dot{\varepsilon}$ is the creep rate, K_1 and K_2 are constants, D_{eff} is the effective diffusion coefficient, d is the mean grain diameter, σ is the flow stress, D_L is the lattice diffusion coefficient, and n_1, n_2, and p are exponents. Each part of this constitutive equation represents different rate controlling mechanisms. When the applied stress is small the rate controlling mechanism is that of the first term on the right hand side, while at higher stress states the rate controlling mechanism is that of the second term, namely dislocation creep.

When $n_1 = 1$ and $p = 2$ with low stresses and high temperature, we have the Nabarro [Ref. 19] and Herring [Ref. 20] creep model. This type of creep results from diffusion of vacancies from regions of high chemical potential at grain boundaries subjected to normal tensile stresses to regions of low chemical potential where the

stresses on the grain boundaries are compressive. Atoms migrating in the opposite direction account for the creep strain. In this model, D_{eff} from Equation 2.3 is proposed to be that of volume diffusion. In subsequent work Coble [Ref. 21] proposed that grain boundary diffusion rather than volume diffusion controls. His model proposes n_1 of 1 and p value of 3.

Raj and Ashby [Ref. 22] reviewed in detail the various aspects of grain boundary sliding and diffusional creep. Their analysis shows that if diffusion is the only mechanism of accommodating the incompatibilities caused by grain boundary sliding, diffusional flow and sliding are not independent. They are interrelated and the resulting deformation is described by the combined contribution of Nabarro-Herring and Coble Creep. Although such a mechanism with its $n_1 = 1$ stress dependence could certainly control the deformation rate in fine-grained polycrystalline materials, it probably lies in a region separate from that of superplasticity which has typically an $n_1 = 2$ stress dependence of the strain rate.

Ashby and Verrall [Ref. 23] suggested a mechanism for producing the larger strains commonly encountered in superplasticity. It differs fundamentally from a combination of Nabarro-Herring and Coble creep in a topological sense; grains switch their neighbors (Figure 2.1) and do not elongate significantly. Their constitutive equation is

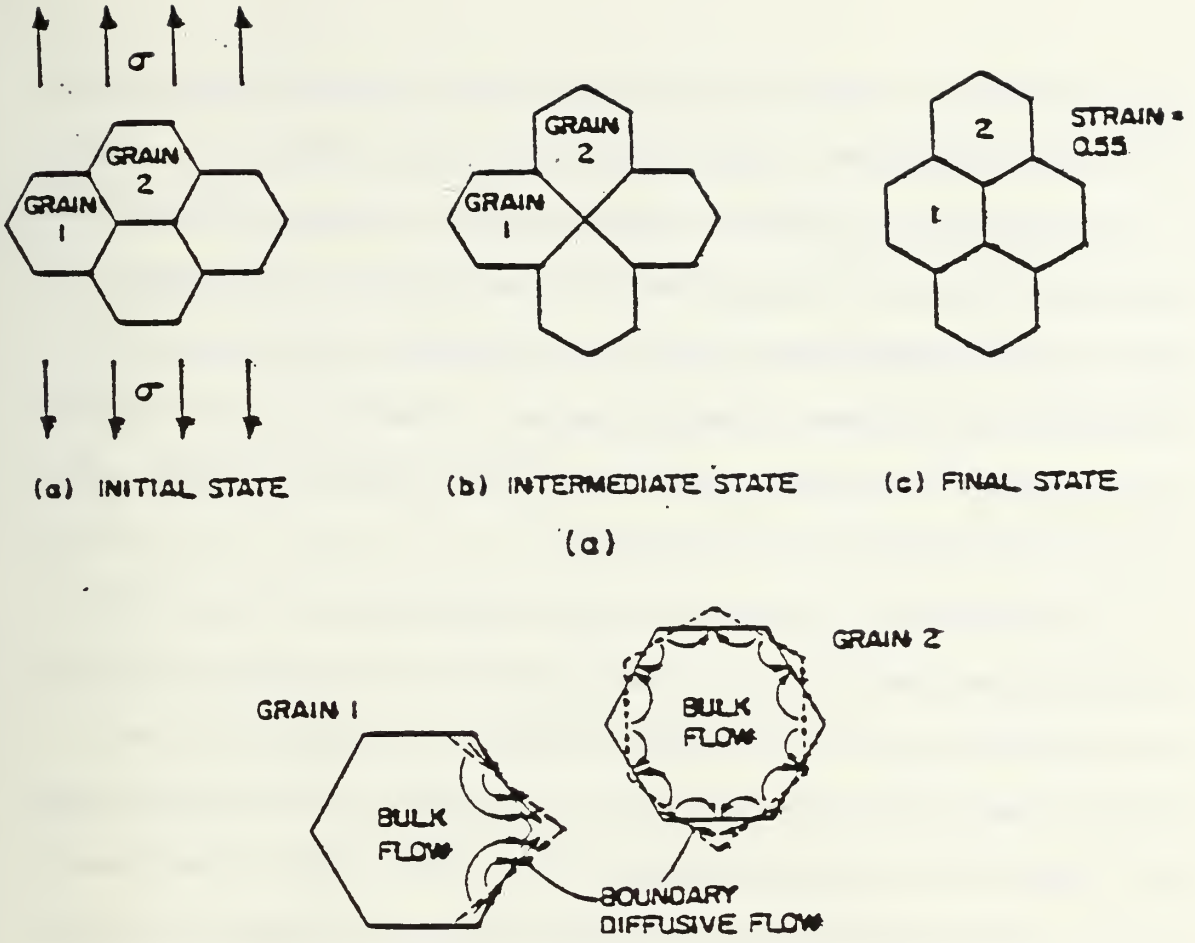

Figure 2.1 Ashby-Verrall grain boundary switching model

derived from the model that resembles the Nabarro-Herring-Coble equation but predicts strain rates which are approximately one order of magnitude faster. The flow behavior of superplastic alloys has been explained as the superposition of this mechanism and ordinary power law dislocation creep. However, the superposition principle that is involved in order to explain superplastic deformation may not be entirely correct. Experimental investigations by Misro and Mukherjee [Ref. 24] show that the second power stress dependence extends over quite a large range of strain rates. Hence, it is very likely

that superplasticity is not a transition region between two different mechanisms as envisaged by Ashby and Verrall, but is a mechanism by itself. Available data suggests that a realistic model for superplastic deformation should show a second power dependence, $n_1 = 2$, on stress, an inverse second or third power dependence, $p = 2$ or 3, on grain size, and an activation energy of the process probably close to that for grain boundary diffusion.

Nix [Ref. 25] argues that the diffusional model of switching proposed by Ashby and Verrall violates symmetry and does not account for grain rotation commonly observed during superplastic deformation. He further argues that any grain rotation that occurs must arise from slip within the grains, and thus slip must be involved in the superplastic flow process. The $\log \sigma - \log \dot{\varepsilon}$ curves are sigmoidal in nature and are usually divided into three regimes (I, II, III), distinguished by their slope changes; i.e., strain rate sensitivity. Maximum elongation to failure coincides with regime II where the strain rate sensitivity reaches a maximum value. In an attempt to explain the sigmoidal nature of these curves he proposed a transition model based on diffusional relaxation. He notes that although the curves appear to be straight in regime II, the corresponding elongation to failure curves show that the maximum elongation occurs at a single strain rate and this implies an inflection point in the stress-strain rate curves. His

model proposes there is no regime II, only a transition regime from regime I diffusional creep to regime III dislocation creep. Since the transition is brought about by a diffusional relaxation, the activation energy for flow in that regime should be the same as that for diffusion. The transition model does not explain how diffusion could give rise to the transition and not also produce a diffusional deformation regime at low strain rates. It should also be noted that the transition model does not indicate how the grain structure remains equiaxed during superplastic flow.

At high stress states creep tends to occur by dislocation glide aided by vacancy diffusion to overcome obstacles. Weertman [Ref. 26] developed a theory for minimum creep rate based on dislocation climb as the rate-controlling step. Dislocations are pinned by Cottrell-Lomer locks; they overcome them by climb, aided by either interstitial or vacancy generation or annihilation. Those that climb to another plane are replaced by other dislocations generated by Frank-Read sources and thus the process perpetuates itself. This model proposes a fourth or fifth order stress dependence (n_2 = 4 or 5) on strain rate. An alternate view, more applicable to the Al-Mg alloy being examined here was also developed by Weertman [Ref. 26] who proposes a mechanism of solute control of the dislocation glide step. This model results in the D of the second term

being replaced by D_s, the solute diffusion coefficient and $n_2 = 3$.

4. Activation Energy

The activation energy (Q), is a measure of the thermal energy required for temperature-dependent process. For a thermally activated deformation process:

$$\dot{\varepsilon} = f(\sigma) \exp(-Q/RT) \qquad \text{(eqn. 2.4)}$$

where R is the gas constant, and T the absolute temperature.

Values for the activation energy can be obtained by plotting log (strain rate) versus absolute temperature for data at a constant stress. Measurement of the activation energy provides insight into the mode of deformation at work in the material. Available data [Ref. 27] tends to suggest dislocation climb controlled creep activation energy has a value equal to, or lower than, the activation energy for lattice self-diffusion. With grain boundary sliding the activation energy values may be that for lattice diffusion, or lower and more closely related to the activation energy for grain boundary diffusion.

5. Microstructural Characteristics

In order to achieve superplasticity, a fine grain size, less than ten microns, is needed to achieve a high value of strain rate sensitivity coefficient, m. A thermally stable microstructure is necessary, which requires some form of grian boundary pinning, i.e., a fine dispersion

of intermetallic phase(s). A microstructure which has a high resistance to cavitation requires this intermetallic phase(s) to be deformable and similar in strength to the matrix. Enhanced ductility is associated with grains of small size which remain essentially equiaxed and unchanged in size during deformation. Grain growth suppresses ductility as greater diffusion distances are encountered in large grains, thus reducing the strain resulting from grain boundary sliding. Also if sliding is associated with slip, small grain size material can more easily accommodate sliding than large grain size material since larger grains enhance locallized slip while smaller grains enhance fine slip.

Effective use of intermetallic phase(s) to inhibit grain growth follows the Zener-McLean relationship [Ref. 28],

$$d = 4r/3f \qquad \text{(eqn. 2.5)}$$

where d is the grain size, r is the particle radius, and f is the volume fraction. Particles restrict grain growth by exerting a drag force on migrating boundaries. The origin of the drag force is the reduction of grain boundary energy when the boundary intersects the particle. Clearly, grain growth is arrested by fine particles given a fixed volume fraction.

B. ALLOYING ADDITIONS

The addition of magnesium to aluminum alloys results in a lighter, stronger alloy. Most of the increased strength in these alloys is due to Magnesium in solid solution, although precipitation does occur. These alloys are work-hardenable at both high and low temperatures. The aluminum end of the Al-Mg binary system, Figure 2.2 shows a eutectic at 450°C between Aluminum containing 15.35% Mg in solid solution and a β phase which in composition approaches the stoichiometric ratio Al_8Mg_5. This intermetallic phase is quite hard and brittle. The lever rule shows that the eutectic contains so much β phase that the structure will be brittle. Therefore, useful alloys must contain less Magnesium than the maximum soluble in the solid solution, i.e., less than 15.35% Mg.

Zirconium is an extremely effective addition for attaining a fine grain size from several points of view. It provides as-cast grain refinement and hence assists in providing homogeneity to the starting ingot. In addition, the Zirconium intermetallic in its metastable form is very fine and very slow to coarsen. Hence, it is excellent for microstructural stability at superplastic forming temperatures. The disadvantages of Zirconium are the high casting temperature and rapid solidification rates necessary to retain Zr in solid solution during the casting process. Coarse $ZrAl_3$ particles tend to be produced during casting

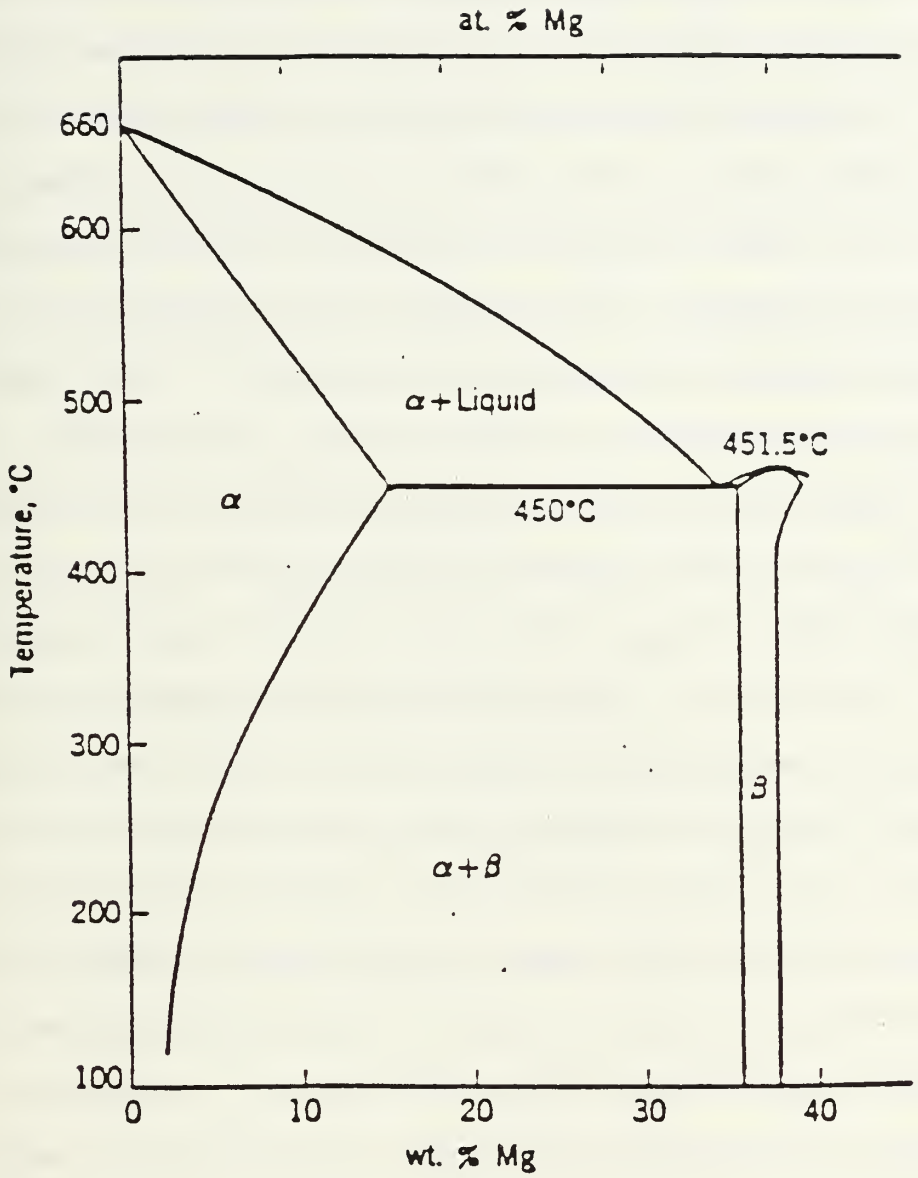

Figure 2.2 Aluminum-magnesium phase diagram

and are sites for cavity formation during superplastic forming. Thus good control over casting practice is essential for optimization of superplastic properties [Ref. 29].

C. PREVIOUS WORK AT THE NAVAL POSTGRADUATE SCHOOL

The Naval Postgraduate School materials science group has been investigating Al-Mg alloys since 1976 when Ness [Ref. 3] initiated the research with an 18%Mg aluminum alloy. This material was warm rolled in the two phase region in an effort to obtain improved mechanical properties and grain refinement. He reported that microstructural refinement could be obtained in an 18 percent alloy and a compressive strength of 655 MPa (95 KSI) was obtained. The disadvantage of this high Magnesium content alloy is that it is very brittle and subject to cracking during rolling.

Bingay [Ref. 4] and Glover [Ref. 5] in follow-on work studied variations of the thermomechanical processing on 15% to 19% Aluminum Magnesium alloys in an attempt to alleviate cracking. Bingay attempted to achieve microstructural refinement of alloys containing 15 and 19 weight percent Magnesium, through warm upset forging, both isothermally and non-isothermal. Due to cracking Bingay concluded that a lower Magnesium content alloy was required, and also recommended that solution treatment be carried out prior to thermomechanical processing. Glover subsequently shifted his work to a 7 weight percent Magnesium Aluminum alloy. His efforts were directed toward using forged material to produce rolling material, upon which tensile testing could be performed. This material was found to be rollable after forging and material for tensile testing was produced.

Grandon [Ref. 6] studied 7-10% Magnesium aluminum alloys. He revised the thermomechanical processing technique to include a twenty-four hour solution treatment at 440°C followed by air cooling and warm rolling at 300°C. This material exhibited high strength and good ductility at ambient temperature. It was also observed that the alloys did not recrystallize at temperatures below the solvus.

Speed [Ref. 7] followed Grandon's work by studying 10% and 12% Magnesium aluminum alloys. His contribution to the thermomechanical processing was resolution treatment following the hot upset forging process. This produced a more homogeneous, equiaxed grain structure in comparison to the initial processing used by Grandon.

Chesterman [Ref. 8] used optical microscopy to gain insight into the nature of precipitation and recrystallization in alloys containing a Magnesium content of 8-14 percent. These alloys were processed using the technique used by Speed, modified to include oil quenching following hot upset forging. This study showed that recrystallization for these alloys will not occur below the solvus temperature for material with either prior cold work, or material isothermally warm worked. Johnson [Ref. 9] examined alloys containing eight and ten weight percent Magnesium and the alloying effects of Copper and Manganese. Microstructural and mechanical properties at six warm rolling temperatures located above and below the solvus line of these alloys were

studied. He concluded that warm rolling between 200°C and 340°C controlled precipitation of the fine "beta" (Mg_5Al_8) intermetallic, the single most important factor in obtaining best strength and ductility. Shirah [Ref. 10] extended Johnson's work by investigating the influence of solution treatment time and quench rate on microstructure, strength and fracture resistance. He concluded that increasing the solution treatment time to 24 hours improved microstructural homogeneity.

Becker [Ref. 11] investigated the elevated temperature deformation characteristics of Al-8%Mg-0.4%Cu and Al-10%Mg-0.5%Mn alloys. He noted superplastic elongations of up to 400% are attainable in these alloys. He concluded that the higher Magnesium content alloy extended the range of superplastic behavior to higher temperatures. Mills [Ref. 12] did a comprehensive study on the Al-10%Mg-0.5%Mn alloy previously studied by Becker. He concluded that grain boundary sliding appears to be the predominant superplastic deformation mechanism at higher temperatures, above 300°C, based upon activation energy data.

Stengel [Ref. 13] studied the effects of various annealing treatments. She concluded that strain rate sensitivity and ductility of the as-rolled material can be controlled and improved by annealing below the rolling temperature, 300°C.

Self [Ref. 14] investigated the effects that various alloying elements have on superplasticity in high Magnesium Aluminum alloys. He concluded that the addition of Copper or Manganese, at the same weight percentage, has the same enhancing effect on superplasticity.

The purpose of this thesis was to investigate characteristics of a thermomechanically processed Al-10%Mg-0.1%Zr alloy. This work was undertaken concurrently with Berthold [Ref. 16] and Alcamo [Ref. 15]; the principal focus, as noted in Chapter I, was on the mechanical behavior of this alloy during deformation at elevated temperatures. This included obtaining strain rate sensitivity coefficients, and activation energies. Also studied were the effects of recrystallization or annealing treatments on the elevated temperature characteristics of this alloy.

III. EXPERIMENTAL PROCEDURE

A. MATERIAL PROCESSING

The aluminum alloy investigated was nominally 10 weight %Mg and 0.1%Zr. The direct-chill cast ingot was produced by ALCOA Technical Center using 99.99% pure aluminum base metal alloyed with commercially pure magnesium, Aluminum-Zirconium master alloy, Ti-B addition for grain size control in the as-cast condition, and Beryllium as 5% Be, Aluminum-Beryllium master alloy for oxidation control [Ref. 30]. The as-received ingot measured 127 mm (5 in) in diameter and 1016 mm (44 in) in length. Table I lists the complete chemical composition of the examined alloy [Ref. 30].

TABLE I

Serial Number	Si	Fe	Mg	Zn	Al
57286	0.02	0.02	9.90	0.09	Bal.

Processing followed the sequence shown in Figure 3.1 and Figure 3.2. The ingot was sectioned into billets 95.25 mm (3.75 in) long with a square cross section of width and thickness 31.75 mm (1.25 in). Following the procedure developed by Johnson [Ref. 9], and refined by Self [Ref. 14], the billets were solution treated above the solvus, at 440°C for 24 hours, upset forged at 440°C on heated platens

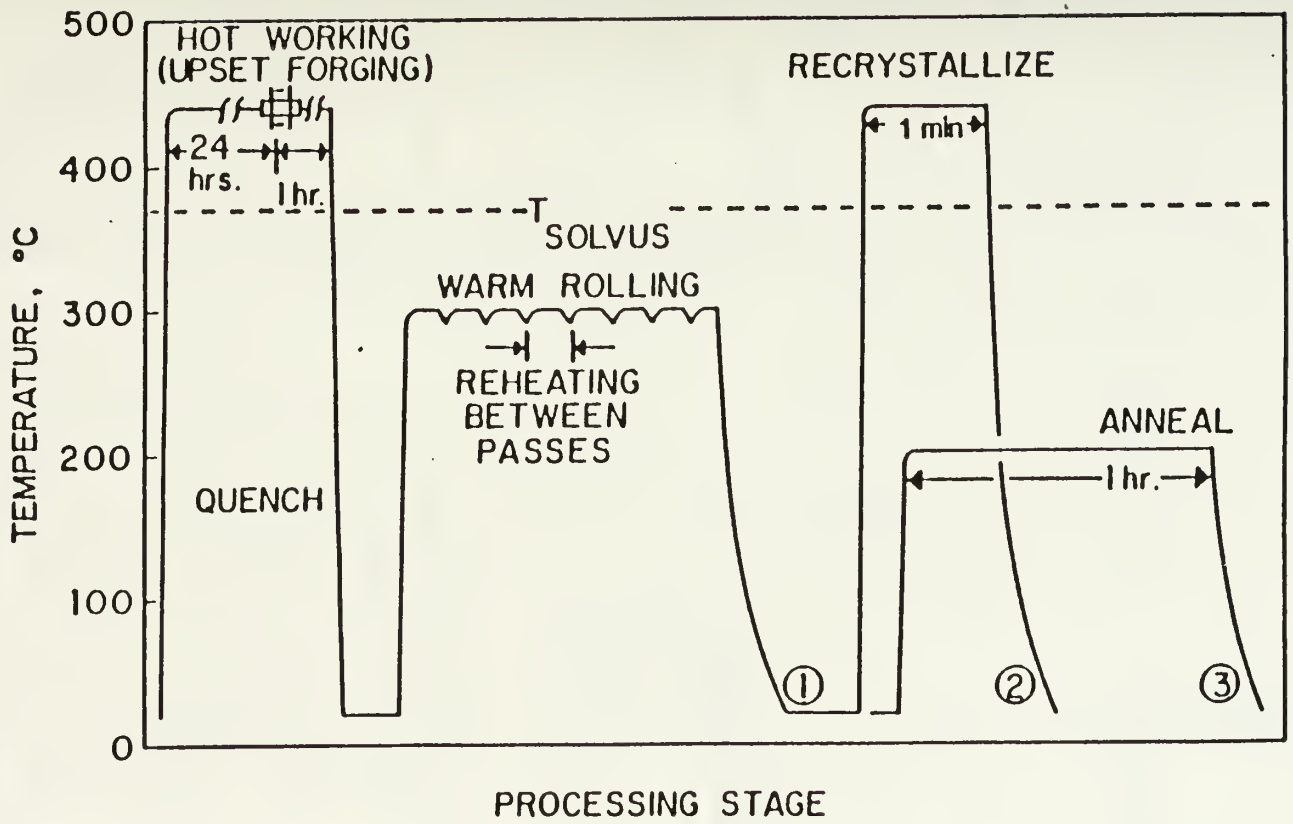

Figure 3.1 Thermomechanical processing technique

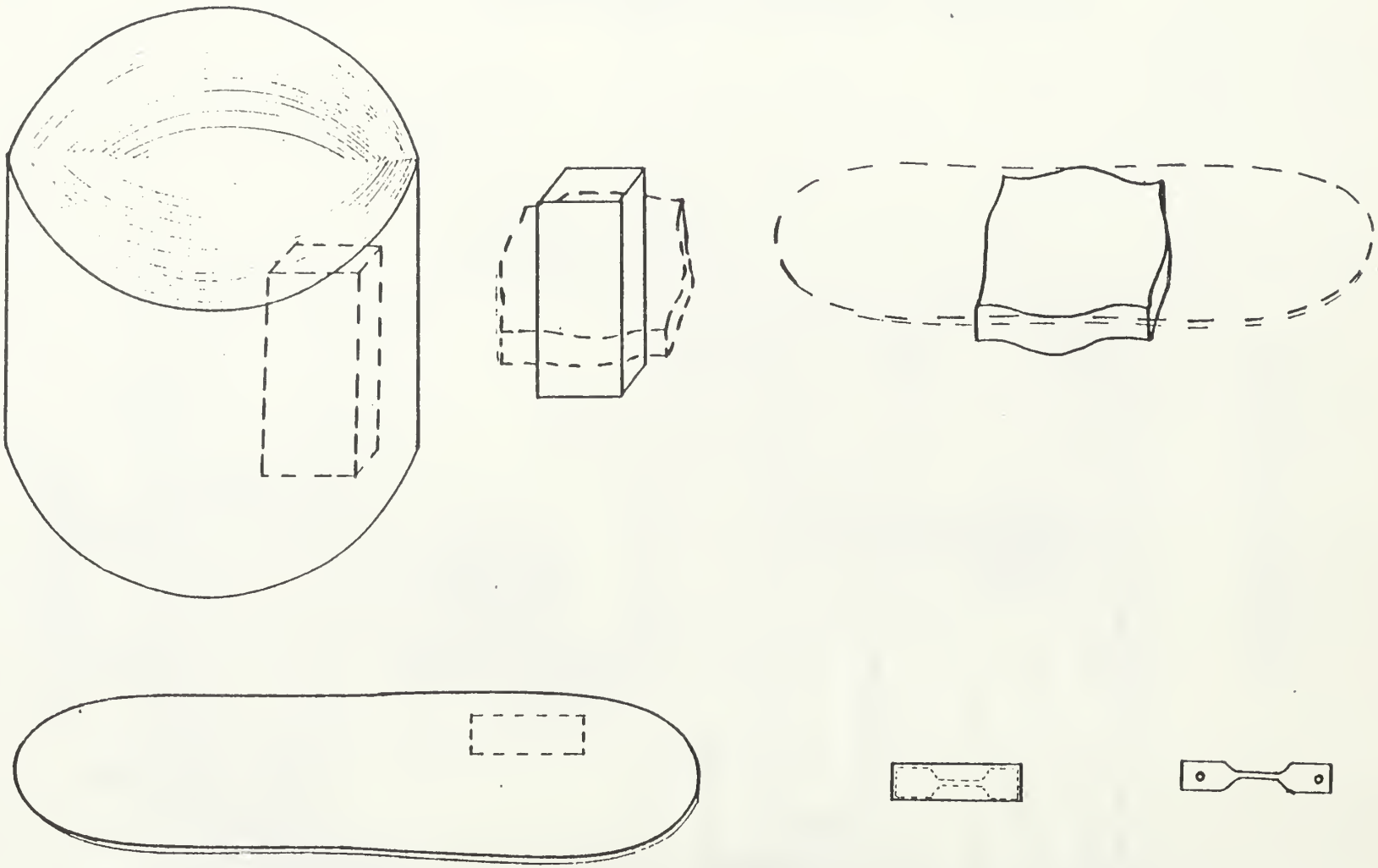

Figure 3.2 Evolution of tensile test specimens

to approximately 25.4 mm (1 in) in height. Subsequently, they were resolution treated at 440°C for 1 hour, and oil quenched. The billets were forged longitudinally, resulting in a reduction of approximately 71% for a true strain of 1.3.

B. WARM ROLLING

The billets were warmed rolled into sheets in accordance with the technique developed by Becker [Ref. 11] and modified by Self [Ref. 14]. The billet was heated to 300°C for 30 minutes to achieve isothermal conditions prior to the first rolling pass. This was accomplished to prevent cracking of forged billets during the rolling process, due to uneven heating. To achieve the isothermal condition the billets, two at a time, were placed on a large steel plate, which acted as a heat source, in a preheating furnace. The billet surface and steel plate temperatures were monitored using thermocouples. The billets were rolled with the upper roller lowered 0.762 mm (0.03 in) per pass to achieve a final average sheet 2.032 mm (0.08 in) thick, 101.6 mm (4 in) wide, and 965.2 mm (38 in) long. Between each successive pass the sheet was returned to the furnace for ten minutes in an attempt to maintain isothermal conditions. To reduce bowing of the rolled sheet, it was rotated endwise after each pass, maintaining the longitudinal direction, and also in the latter passes the sheet was manually pulled to

provide tension in the rolling mill. The final sheet reduction was approximately 92%, corresponding to a true strain of 2.5. The rolled sheets were cut into blanks, maintaining the rolling direction as the longitudinal dimension of the blanks, on a band saw. Conforming to the procedure established by Becker [Ref. 11], the blanks were cut into dimensions 69.85 mm (2.75 in) long, and 19.05 mm (0.75 in) wide. Depending upon sheet thickness and edge wastage each sheet yielded between 50 and 70 blanks. The blanks were skim cut in stacks of five on an end miller to true up the ragged edges. Then, the gage section was end milled, and guide pin holes drilled to conform to sketch of test specimens shown in Figure 3.3. This improved elevated temperature specimen design enhances the ability to determine gage section. It also distributes the gripping action of the wedges over the whole tab thus reducing slippage and tab deformation. Smaller guide pin holes enhance centering of specimen in wedge grips.

C. SPECIMEN TESTING

The tensile testing procedure was similar to that describe by Becker [Ref. 11] with minor modifications. Each test specimen was placed in wedge-action grips (Figure 3.4). The wedge-action grips, grip assemblies and pull rods were supplied by ATS, Butler, Pennsylvania, fabricated from Inconel 718 for elevated temperature testing. The grip

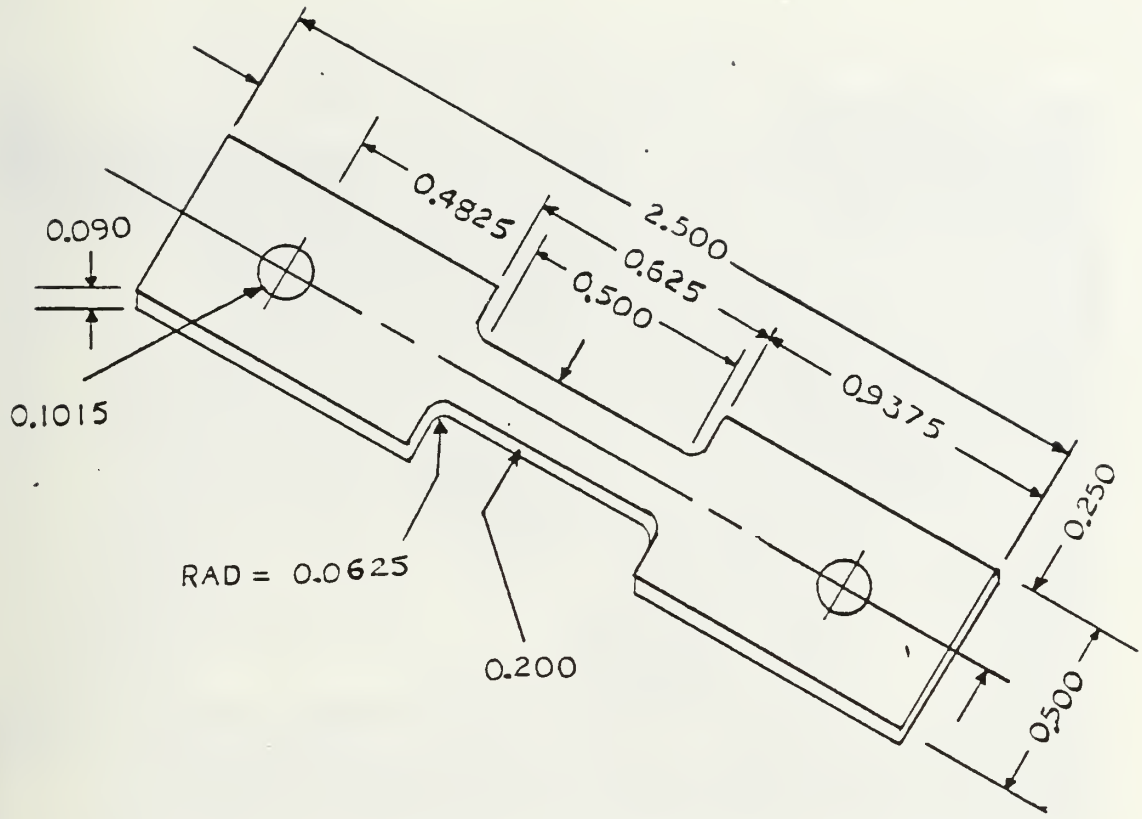

Figure 3.3 Tensile test specimen geometry

assemblies were threaded onto the pull rods which in turn were pin mounted to posts on the electro-mechanical Instron Machine, Figure 3.5.

To reduce slippage of the wedges in grip assemblies, the upper wedges, with specimen installed, were mounted in the assembly with the bottom end free. The upper wedges were then driven into the assembly by tapping with a hammer on a screw driver handle with the flat edge of screw driver between wedges and upper grip assembly. Next the lower wedges were installed while the chart scale was zeroed. Setting the full load scale on its lowest setting, 100 lb.,

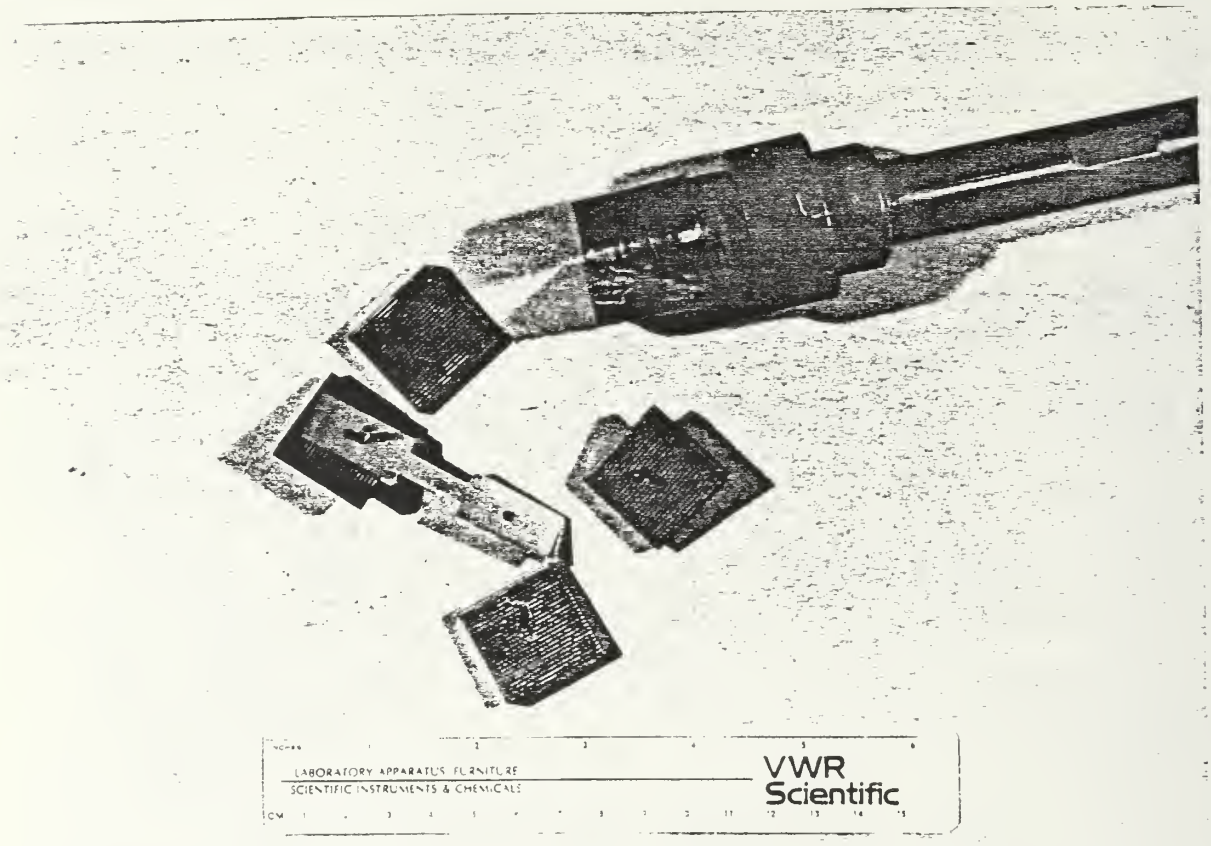

Figure 3.4 Wedge-action grips and grip assemblies

the crosshead was manually lowered, ensuring that no more than two pounds of load registers on the chart, effectively seating the bottom wedges.

Elevated temperature testing was conducted using a Marshall model 2232 three-zone clamshell furnace mounted on the Instron machine. Furnace temperature was maintained by three separate controllers, controlling the three vertically oriented heating elements. Each controller sensed the temperature of the individual zones from insulated

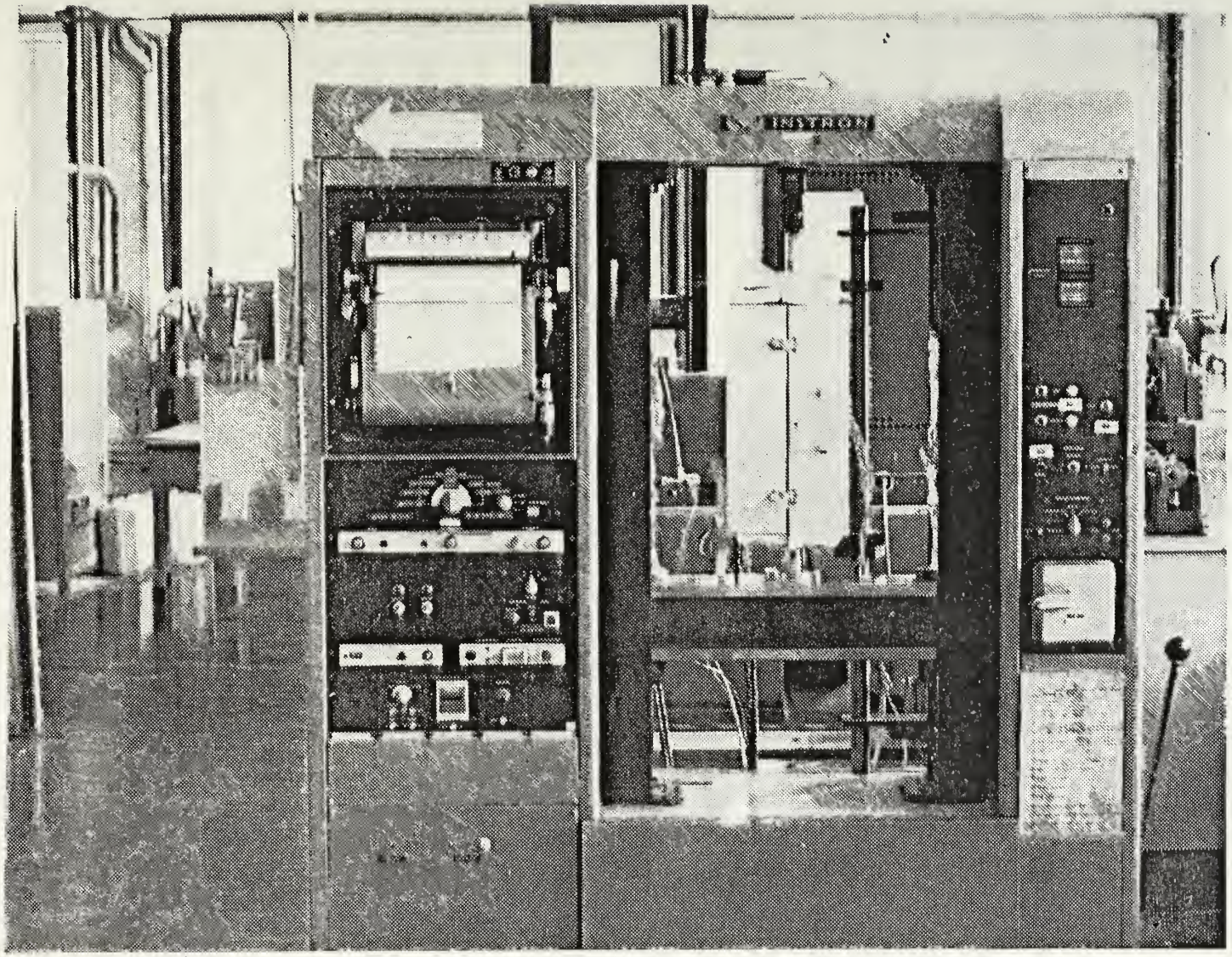

Figure 3.5 Electro-mechanical Instron machine

thermocouples, which passed into the furnace through a hole drilled into the furnace side. Sheathed thermocouples were used to reduce the chance of shorting the heated coils when opening and closing the furnace, and to facilitate placing the couple as close to each individual element as possible. The furnace was insulated by positioning thin strips of asbestos-impregnated paper on the front and rear mating surfaces and crescent-shaped insulation pads together with ceramic tiles on the top and bottom access holes for the pull rods. Insulation cloth was also wrapped around each pull rod and additional fiberglass pads placed around the pull rods on the exterior of the furnace. This was done to reduce the flue effect in the furnace, and to maintain an effective isothermal pull region.

Five thermocouples were installed inside the furnace to monitor temperature. Three were secured with wire to the upper pull rod, under the insulation cloth, and two along the lower pull rod. Of the upper three, one was positioned to monitor the upper grip assembly, one touched the upper specimen tab, and the last was positioned close to but not touching (to avoid bending) the gage length center. The lower thermocouples monitored the lower grip assembly and the bottom of the specimen tab temperatures. Temperatures were adjusted to remain within 1% of the desired temperature throughout the duration of the test.

The tensile testing was performed with crosshead speeds ranging from 0.05 mm per minute to 127.0 mm per minute (0.002 in/min to 5.0 in/min) at temperatures ranging from 20°C to 425°C. The magnification ratio used for the automatic chart recorder was 100 for the 0.05 mm/min crosshead speed, 40 for 0.13 mm/min speed, 20 for 0.25 mm/min speed, and ten for the remaining test crosshead speeds. Care was taken to ensure each specimen was pulled isothermally. The entire assembly was heated to a constant temperature overnight prior to commencing a series of tests. A test specimen was then mounted in the assembly and the test commenced immediately upon attaining a stable, isothermal test temperature. The specimen temperature was monitored and adjustments made to maintain the test temperature throughout the test. The lowest full load scale was selected for each test to achieve the best resolution. Figure 3.6 is a summary of one test sequence.

D. DATA REDUCTION

Elongation was determined by measuring both the gage length of the undeformed and fractured specimen. The Instron strip chart recorded elongation was corrected for grip slippage and tab elongation by multiplying the recorded elongation by the ratio of measured/recorded ductility. Engineering and true stress were computed from the strip chart data. The raw data from the tensile testing was

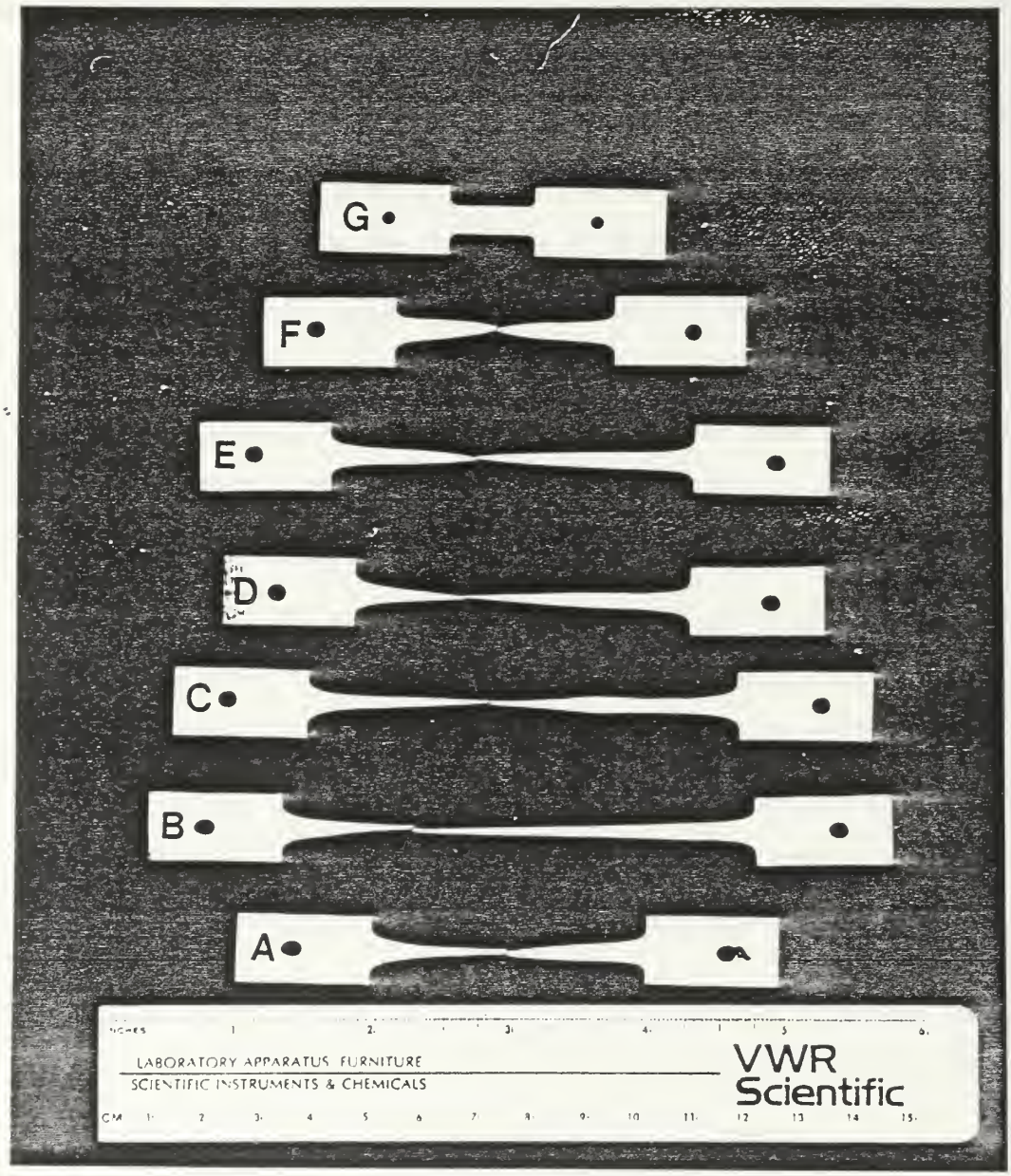

KEY

A. $6.67 \times 10^{-5}\ s^{-1}$
B. $6.67 \times 10^{-4}\ s^{-1}$
C. $1.67 \times 10^{-3}\ s^{-1}$
D. $6.67 \times 10^{-3}\ s^{-1}$
E. $6.67 \times 10^{-2}\ s^{-1}$
F. $1.67 \times 10^{-1}\ s^{-1}$
G. Untested sample

Figure 3.6 Test sequence at 325°C

reduced for analysis by a Fortran data reduction program run on an IBM 3033 computer. The data reduction program used was that developed by Alcamo [Ref. 15]. To remove the lumped elasticity of the Instron machine, grip assemblies, and specimen a "floating slope" calculation was made at each selected data point. The reduced data was loaded into computer data files for further computation and generation of graphics using the EASYPLOT routine.

IV. RESULTS AND DISCUSSION

A. MECHANICAL TESTING RESULTS FOR AS-ROLLED MATERIAL

To study the deformation characteristics of an Al-10%Mg-0.1%Zr alloy, tensile testing was conducted over a wide range of temperatures and strain rates using the procedures described in Chapter III. The temperatures varied from 20°C to 425°C and strain rates from 6.67×10^{-5} to 1.67×10^{-1} s^{-1} as illustrated in Table II.

As described in Chapter III at each test temperature, true stress and true plastic strain were computed. A graphical representation of true stress versus true plastic strain is shown in Figure 4.1 for test temperature 275°C, with data for other test temperatures shown in Appendix A. The solid lines on these curves reflect straining up to the onset of necking, while the dashed lines reflect straining from the onset of necking to fracture. This distinction was made as the assumption of uniform straining of the gage section does not apply once necking has begun. These curves exhibit prolonged necking during deformation, a common characteristic of superplastic materials. Particular attention was directed to the temperature interval from 275°C to 325°C since Mill's [Ref. 12] and Becker's [Ref. 11] data indicated superplastic behavior in this region.

TABLE II

Data for Al-10%Mg-0.1%Zr Alloy in the As-Rolled Condition

Temperature C	Strain Rate s^{-1}	UTS Mpa	True Strain at 0.1 Plastic Strain Mpa	Ductility %
20	6.67×10^{-2}	445.9	*	12.2
20	6.67×10^{-3}	457.6	*	13.2
20	6.67×10^{-4}	500.8	*	8.0
100	6.67×10^{-2}	498.2	493.6	22.8
100	6.67×10^{-3}	495.3	481.0	38.0
100	6.67×10^{-4}	467.5	437.9	53.2
100	6.67×10^{-5}	404.4	386.4	53.4
150	6.67×10^{-2}	441.6	438.7	45.2
150	6.67×10^{-3}	398.2	375.3	60.6
150	6.67×10^{-4}	317.4	300.1	94.0
150	3.33×10^{-4}	321.2	288.7	81.2
150	1.67×10^{-4}	278.3	260.7	87.0
150	6.67×10^{-5}	239.4	230.4	119.8
200	1.67×10^{-1}	337.0	334.0	54.4
200	6.67×10^{-2}	324.4	321.3	54.3
200	6.67×10^{-3}	297.5	264.8	100.2
200	1.67×10^{-3}	220.2	208.8	109.0
200	6.67×10^{-4}	179.6	164.6	115.2
200	3.33×10^{-4}	176.7	153.1	148.8
200	1.67×10^{-4}	130.7	110.2	213.8
200	6.67×10^{-5}	111.6	91.9	189.6
225	6.67×10^{-2}	279.3	269.9	75.0
225	1.67×10^{-2}	242.5	232.6	90.2
225	6.67×10^{-3}	214.0	196.9	109.2
225	3.33×10^{-3}	209.0	155.8	121.0
225	1.67×10^{-3}	157.0	142.7	271.4
225	6.67×10^{-4}	135.9	87.9	271.2
225	3.33×10^{-4}	114.2	69.1	251.4
225	1.67×10^{-4}	97.5	67.3	214.0
225	6.67×10^{-5}	81.3	54.3	181.0

*Specimen fractured before achieving 0.1 strain.

Temperature C	Strain Rate s^{-1}	UTS Mpa	True Strain at 0.1 Plastic Strain Mpa	Ductility %
250	6.67×10^{-2}	219.8	219.1	119.0
250	3.33×10^{-2}	223.8	213.5	119.0
250	1.67×10^{-2}	190.2	176.6	162.4
250	6.67×10^{-3}	159.6	150.6	235.0
250	3.33×10^{-3}	145.7	108.1	257.2
250	1.67×10^{-3}	127.1	70.8	165.6
250	6.67×10^{-4}	94.0	59.0	281.2
250	3.33×10^{-4}	60.2	46.9	268.4
250	1.67×10^{-4}	63.6	32.4	297.4
275	1.67×10^{-1}	197.0	194.1	110.4
275	6.67×10^{-2}	186.5	176.0	146.6
275	3.33×10^{-2}	169.7	154.9	200.8
275	1.67×10^{-2}	150.5	130.8	213.2
275	6.67×10^{-3}	119.6	92.3	220.0
275	3.33×10^{-3}	102.3	62.0	327.8
275	1.67×10^{-3}	79.6	54.7	444.8
275	6.67×10^{-4}	67.7	33.6	293.4
275	3.33×10^{-4}	57.1	29.8	484.4
275	1.67×10^{-4}	42.5	26.7	365.6
275	6.67×10^{-5}	28.1	16.2	353.0
325	1.67×10^{-1}	134.5	133.8	192.8
325	6.67×10^{-2}	107.4	105.8	296.6
325	3.33×10^{-2}	85.3	83.3	349.8
325	6.67×10^{-3}	63.4	48.5	463.8
325	1.67×10^{-3}	44.1	33.8	439.4
325	6.67×10^{-4}	28.9	20.1	576.0
325	6.67×10^{-5}	15.1	12.2	276.6
350	1.67×10^{-1}	143.2	142.8	138.0
350	6.67×10^{-2}	113.5	112.7	188.4
350	3.33×10^{-2}	88.2	87.4	212.8
350	6.67×10^{-3}	71.5	71.4	159.6
350	6.67×10^{-4}	36.2	34.8	246.6
350	6.67×10^{-5}	19.6	18.4	197.2
375	1.67×10^{-1}	118.2	118.1	131.6
375	6.67×10^{-2}	90.8	90.8	172.0
375	6.67×10^{-3}	47.4	47.1	193.6
375	6.67×10^{-4}	24.9	24.4	132.2
375	6.67×10^{-5}	13.1	12.3	170.0
400	1.67×10^{-1}	100.7	100.0	181.0
400	6.67x10-2	76.8	76.8	158.8
400	6.67×10^{-3}	44.9	44.0	196.3
400	6.67×10^{-4}	18.6	18.1	217.6

Temperature C	Strain Rate s^{-1}	UTS Mpa	True Strain at 0.1 Plastic Strain Mpa	Ductility %
425	1.67×10^{-1}	80.9	74.9	157.8
425	6.67×10^{-2}	60.8	59.7	194.8
425	1.67×10^{-2}	41.7	41.5	317.0
425	6.67×10^{-3}	30.8	30.0	258.0
425	3.33×10^{-3}	23.6	23.6	356.6
425	6.67×10^{-4}	15.5	15.5	309.4
425	3.33×10^{-4}	14.9	14.4	213.0
425	6.67×10^{-5}	9.4	8.7	121.8

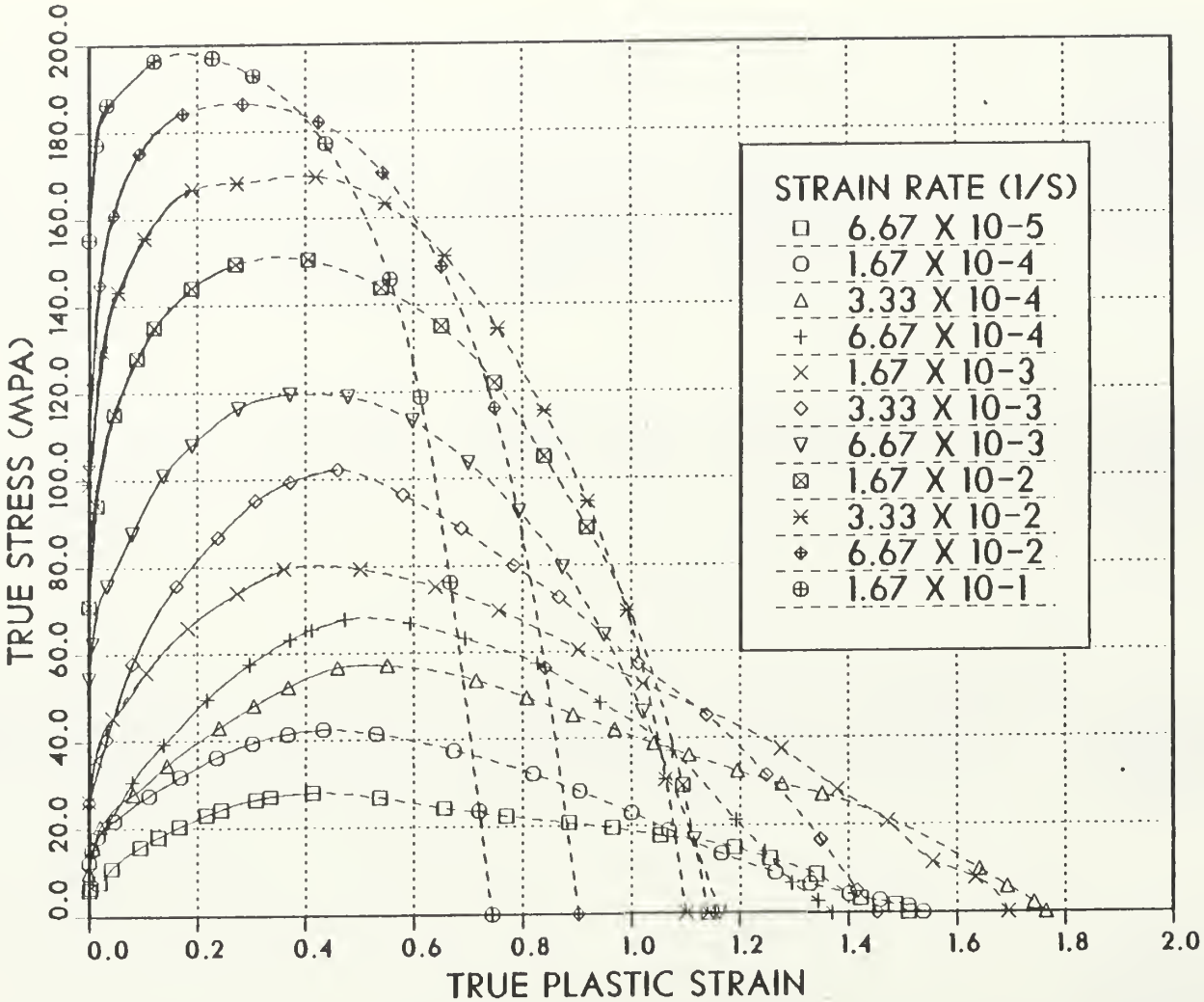

Figure 4.1 True stress vs. true plastic strain for testing conducted at 275 °C for Al-10%Mg-0.1%Zr. Solution treated at 440 °C for 24 hours, hot worked, resolution treated at 440 °C for 1 hour, oil quenched, and warm rolled at 300 °C to 92% reduction. Dashed lines indicate straining beyond onset of necking.

In contrast to Mill's data on the Mn containing alloy, the stress-strain plots for this Zr containing material exhibit a substantial work hardening at low strains. This is attributed to the microstructural instability of this material, as discussed by Berthold [Ref. 16]. Mill's work also showed that, at high strain rates, and temperatures near 300°C a strain softening occurs beginning at strains of 0.1 or less, with stress decreasing significantly with increasing strain. This he attributed not only to the diffuse necking that occurred during deformation, but also to a break-up of an initially fibered structure by continuous recrystallization and a stabilization of the structure by $MnAl_6$. The Zirconium in the Al-10%Mg-0.1%Zr alloy, in contrast, was not as effective as the Manganese in stabilizing the microstructure, as shown by Berthold [Ref. 16], and thus the flow softening is not as pronounced in this alloy.

In an attempt to compare the elevated temperature characteristics of this material with the characteristics predicted by the various creep models previously described in Chapter III, the strain rate sensitivity and activation energies for deformation in this alloy were studied. To obtain the strain rate sensitivity coefficient from Equation 2.2, values of true stress at a true plastic strain of 0.1 were plotted against strain rate on double logarithmic axes, for each test temperature. The slopes of these curves as

shown in Figure 4.2 and Figure 4.3, represent m, the strain rate sensitivity coefficient. These curves are separated into two figures; close examination will show that the data for 350°C suggests a stronger material at that temperature than at a lower temperature, e.g., 300°C. This inversion in temperature dependence represents strengthening due to static recrystallization prior to testing, which will be discussed in a subsequent section. The strain rate sensitivity coefficients obtained vary from m = 0.1 at 100°C to a maximum of m = 0.46 at 275°C. The region of greatest interest in this research centered around 275°C to 325° where maximum ductility was observed. The strain rate sensitivity coefficient m, at 275°C, gives a nearly second order strain rate dependence on stress: 1/0.46 = 2.17. The lower m value at 300°C and 325°C are believed to result from microstructural coarsening as documented by Alcamo [Ref. 15] in concurrent work. It was suggested [Ref. 15] that a strain rate change test as described by Ghosh [Ref. 29] be used to obtain the strain rate sensitivity coefficient at constant structure; likely this would be closer to a second order strain rate dependence on stress.

In contrast to Mill's work with the Manganese containing alloy, which showed a continuous increase in strain rate sensitivity with increasing temperature, this Zirconium containing alloy has its greatest strain rate sensitivity at temperatures coinciding with maximum superplasticity.

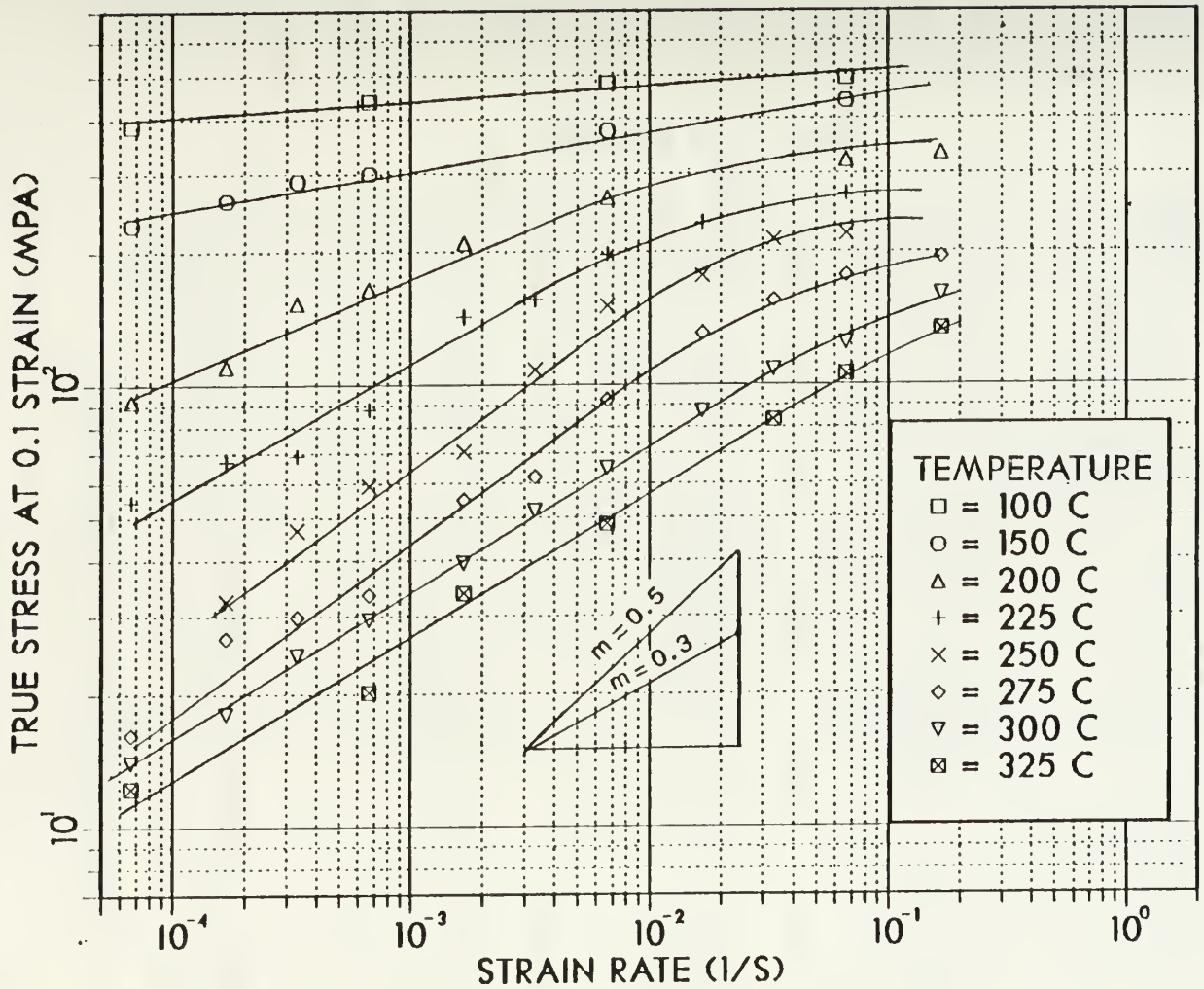

Figure 4.2 True stress at 0.1 strain vs. strain rate for Al-10%Mg-0.1Zr. Solution treated at 440°C for 24 hours, hot worked, resolution treated at 440°C for 1 hour, oil quenched, and warm rolled at 300°C to 92% reduction.

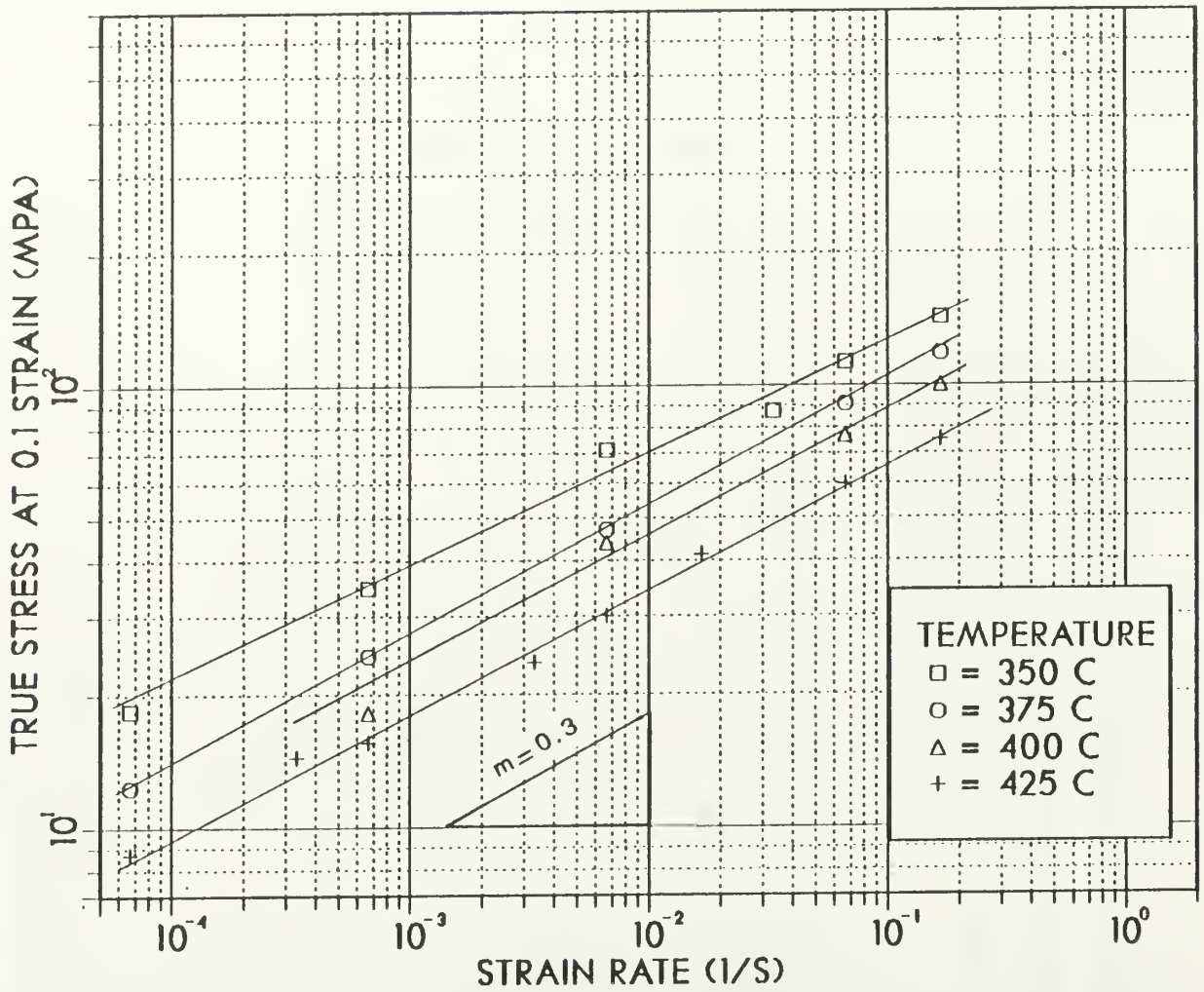

Figure 4.3 True stress at 0.1 strain vs. strain rate for Al-10%Mg-0.1%Zr. Solution treated at 440°C for 24 hours, hot worked, resolution treated at 440°C for 1 hour, oil quenched, and warm rolled at 300°C to 92% reduction.

Again, as shown by Berthold [Ref. 16], recrystallization and growth occurs more readily and extensively in this alloy, resulting in substantial strengthening at elevated temperatures.

To obtain the temperature dependence of deformation of this Al-10%Mg-0.1%Zr alloy, values of true stress at 0.1 true plastic strain were plotted against temperature, for each strain rate as shown in Figure 4.4. Generally, as the temperature increases the stress decreases, and as the strain rate increases the stress increases. The trend of the curves suggest a weakening of the temperature dependence above the rolling temperature, 300°C. These curves also show an anomalous behavior from 325°C to 375°C, in the form of increased strength with temperature. Optical microscopy by Berthold [Ref. 16] revealed that this behavior is due to the material recrystallizing in the testing furnace while waiting for the specimen to become isothermal prior to the start of the tensile test. This increased strength is due to the recrystallized grains being much larger than the size of the substructure produced in rolling and initially present at the start of lower-temperature tests. The diffusional models listed in Chapter III predict this increased strength with increased grain size for stresses and temperatures where they dominate deformation.

Based on the stress-temperature data of Figure 4.4, activation energies can be determined by plotting strain

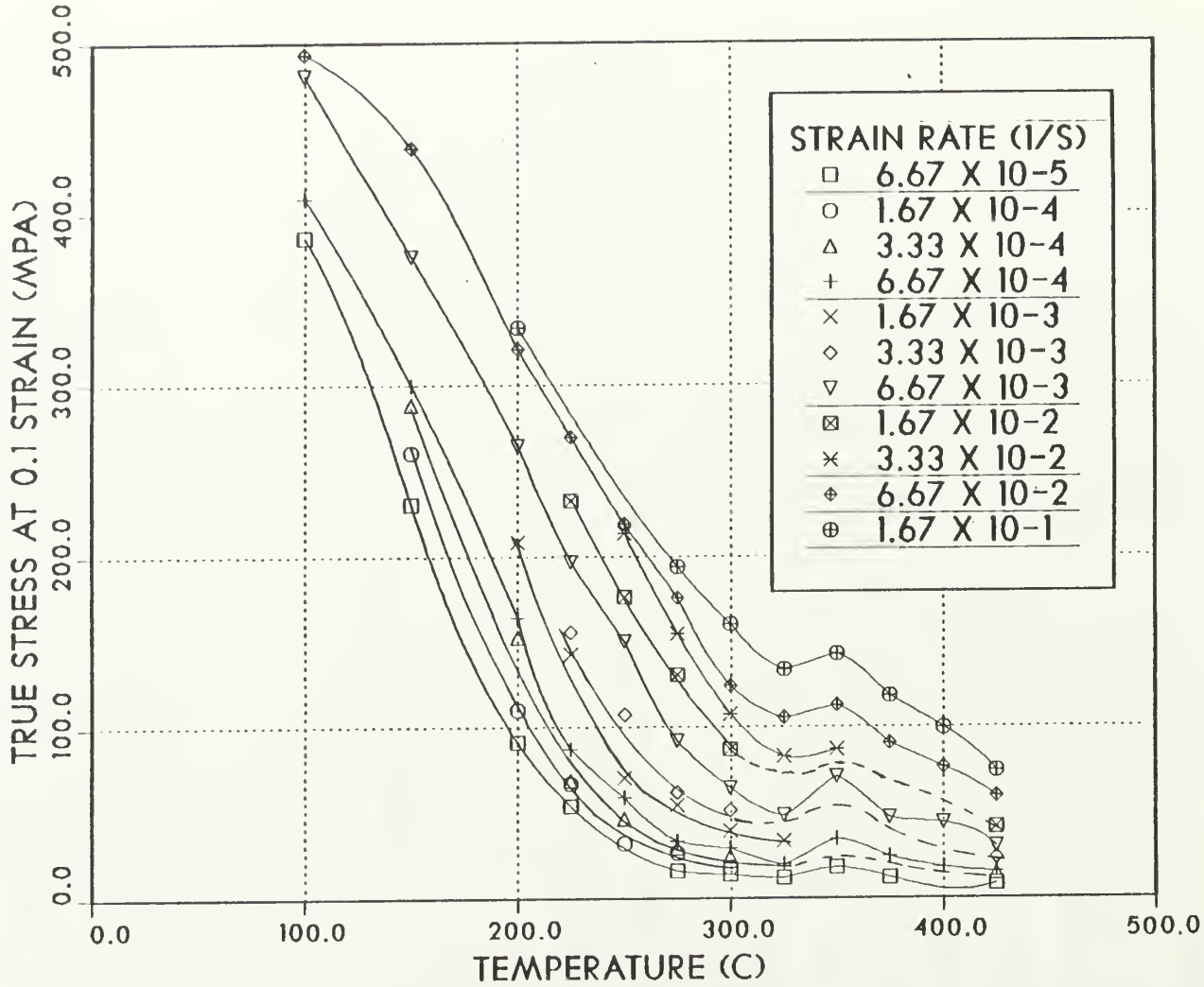

Figure 4.4 True strain at 0.1 strain vs. temperature for Al-10%Mg-0.1%Zr. Solution treated at 440 °C for 24 hours, hot worked, resolution treated at 440 °C for 1 hour, oil quenched, and warm rolled at 300 °C to 92% reduction.

rate versus inverse temperature at constant values of stress as shown in Figure 4.5. By taking the logarithm of each side of Equation 2.4, holding stress constant, and rearranging terms the equation takes the form:

$$Q = -R \left. \frac{d(\ln \dot{\varepsilon})}{d(1/T)} \right|_{\sigma} \qquad \text{(Eqn. 4.1)}$$

that is, the slope of each constant stress line is the activation energy, Q, of the process at that stress.

The activation energy over a broad range of temperature and strain rates was found to be 32.5 Kcal/mole. This value is consistent with lattice diffusion control of deformation, with a rate controlling mechanism of either dislocation climb or glide or grain boundary sliding with accommodation by lattice diffusion. At temperatures around 350°C the curves indicate a negative activation energy. To understand this, a closer look at the parameters held constant in deriving Equation 4.1 is required. Equation 2.4 as written implies strain rate is only a function of stress and temperature, but all models for the superplastic regime show an inverse dependence on grain size. Hence, taking the derivative of strain rate with respect to 1/T in Equation 4.1 implies that the grain size was held constant. Berthold [Ref. 16] in concurrent work showed that the structure/substructure was not stable in this temperature region. If recrystallization and growth takes place in this temperature

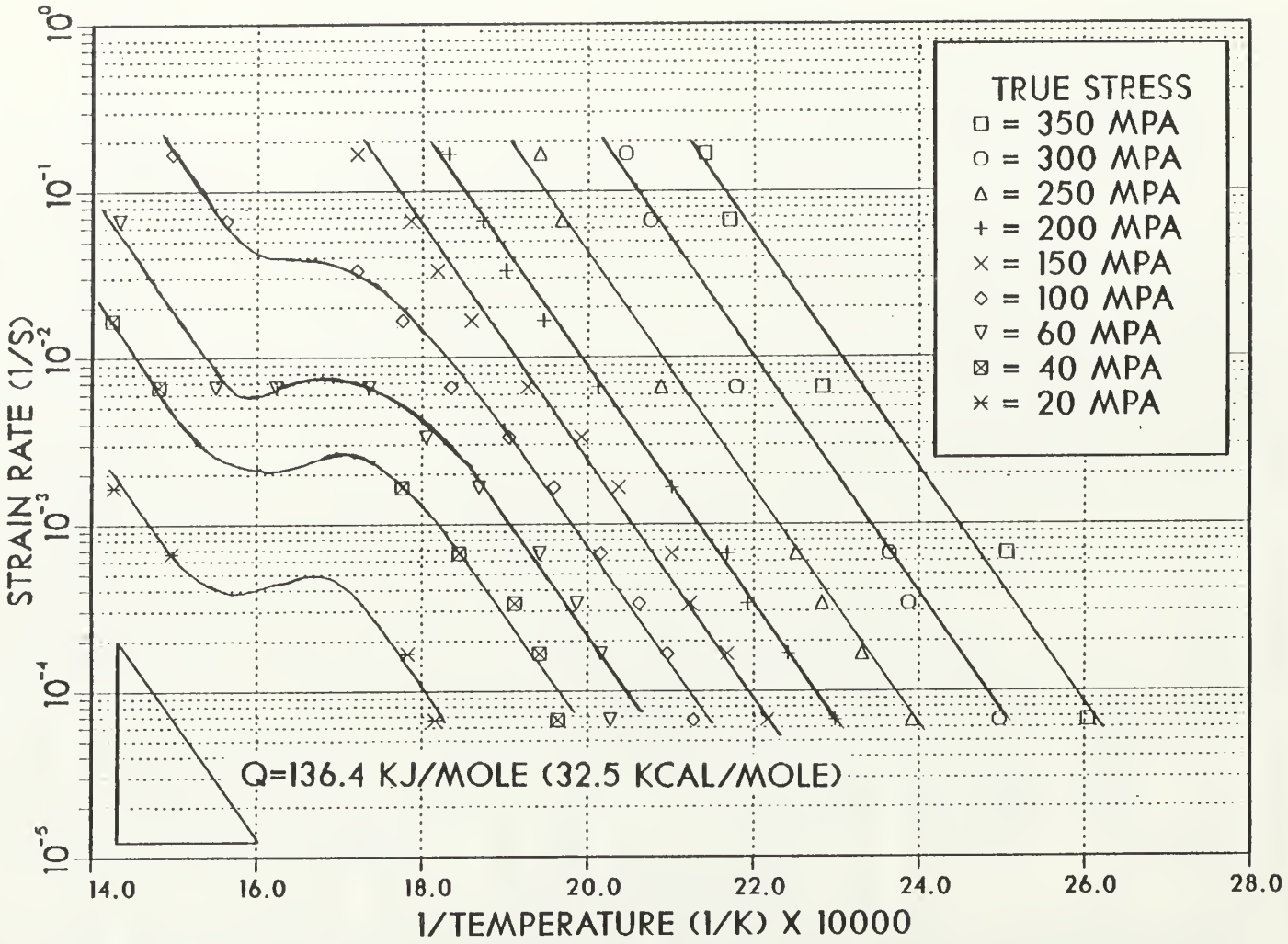

Figure 4.5 Strain rate vs. 1/T for Al-10%Mg-0.1%Zr. Solution treated at 440°C for 24 hours, hot worked, resolution treated at 440°C for 1 hour, oil quenched, and warm rolled at 300°C to 92% reduction.

range, the growth, reflected in an increase in d in Equation 2.4, will have a temperature dependence associated with it. If d increases with increasing temperature, this will result in a reduced strain rate at a given stress and a decrease in the slope of $d(\ln \dot{\varepsilon})/d(\ln 1/T)$. A sufficiently pronounced coarsening with increased temperature may cause an anomalous appearance of a negative value for Q. Hence, this structure/substructure change is believed to be the major contributor to the anomalous behavior of the activation energy in the optimum superplastic temperature region for this material. The most significant result from the activation energy plots is that the activation energy indicates lattice diffusion control over the whole range of temperatures and strain rates, even in the region where the material statically recrystallizes.

B. MECHANICAL TESTING RESULTS FOR RECRYSTALLIZED MATERIAL

One method commonly used to achieve the fine grain size required for superplasticity is to recrystallize deformed material. To study the effects recrystallization has on Al-10%Mg-0.1%Zr alloys, the as-rolled material was recrystallized using the procedures described in Chapter III. Tensile testing was then conducted on this material at tempertaures varying from 250°C to 400°C and strain rates from 6.67×10^{-5} to 1.67×10^{-1} s^{-1}, using the procedure

described in Chapter III. Tabulated results from these tests are presented in Table III.

A graphical representation of true stress versus true plastic strain is shown in Figure 4.6, for test temperature 250°C, with other test temperatures shown in Appendix A. The solid lines on these curves reflect straining up to the onset of necking, while the dashed lines reflect straining from the onset of necking to fracture, as previously discussed. In comparison with the as-rolled material, the recrystallized material exhibits increased strength at all temperatures for a given strain and strain rate. Due to its coarser structure, as previously discussed, this increased strength was expected. As with the as-rolled material, the recrystallized specimens exhibited substantial work hardening at low strain values. Berthold [Ref. 16], in this microscopy study of these specimens, showed that extensive grain growth occurred during the tensile test. This would account for the degree of work hardening that has occurred. Berthold further showed that the Zirconium, which was added to be a grain refiner, is actually present as coarse primary $ZrAl_3$ particles formed in the liquid-β two phase region. Less Zr was available to precipitate as a fine dispersoid in the solid state to control grain growth.

The strain rate sensitivity for the recrystallized material was obtained in the manner previously discussed. Figure 4.7 shows that the recrystallized material exhibits

TABLE III

Data for Al-10%Mg-0.1%Zr Alloy in the Recrystallized Condition

Temperature C / Strain Rate s^{-1}		UTS Mpa	True Strain at 0.1 Plastic Strain Mpa	Ductility %
250	1.67×10^{-1}	267.2	250.4	56.4
250	6.67×10^{-2}	246.1	235.9	49.0
250	2.67×10^{-3}	210.5	201.8	87.2
250	6.67×10^{-4}	152.9	152.7	123.0
250	6.67×10^{-5}	90.4	85.4	216.6
300	1.67×10^{-1}	195.2	192.1	81.6
300	6.67×10^{-2}	196.5	189.4	98.2
300	6.67×10^{-3}	145.0	142.7	150.8
300	6.67×10^{-4}	84.8	79.6	178.4
300	6.67×10^{-5}	38.8	36.1	180.4
325	1.67×10^{-1}	171.9	170.1	88.0
325	6.67×10^{-2}	159.3	158.9	112.6
325	6.67×10^{-3}	109.0	104.4	188.6
325	6.67×10^{-4}	60.6	57.3	260.8
325	6.67×10^{-5}	38.8	24.4	180.4
350	1.67×10^{-1}	153.3	152.9	107.0
350	6.67×10^{-2}	130.3	130.1	145.8
350	6.67×10^{-3}	78.5	75.9	227.0
350	6.67×10^{-4}	38.3	36.9	241.6
350	6.67×10^{-5}	16.6	16.4	186.0
400	1.67×10^{-1}	110.4	109.8	155.0
400	6.67×10^{-2}	87.7	81.4	242.0
400	6.67×10^{-3}	42.5	40.0	297.8
400	6.67×10^{-4}	20.0	19.4	291.4
400	6.67×10^{-5}	11.3	10.9	187.0

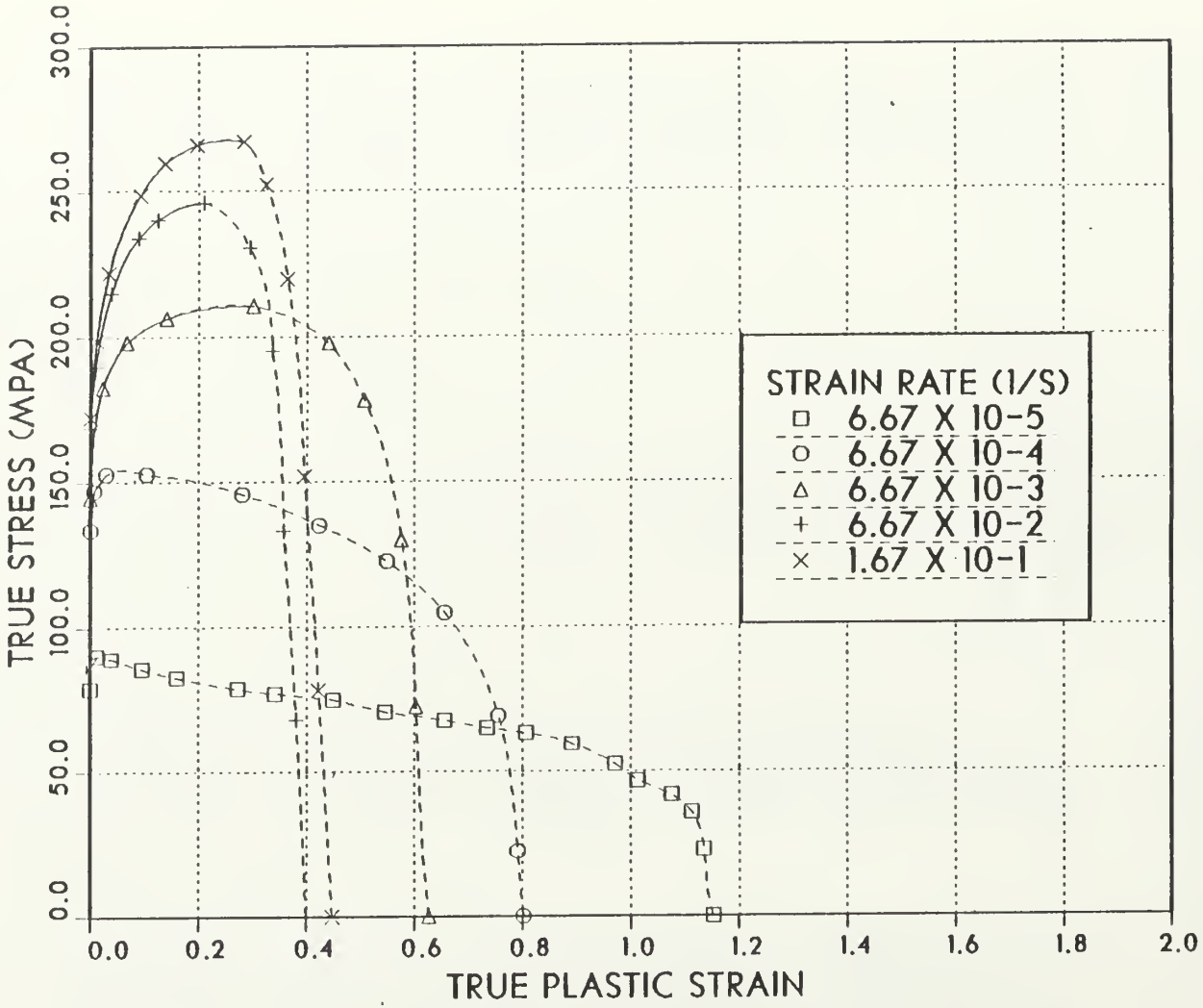

Figure 4.6 True strain vs. true plastic strain for testing conducted at 250 °C for Al-10%Mg-0.1%Zr. Solution treated at 440 °C for 24 hours, hot worked, resolution treated at 440 °C for 1 hour, oil quenched, warm rolled at 300 °C to 92% reduction and recrystallized at 440 °C for 1 minute. Dashed lines indicate straining beyond onset of necking.

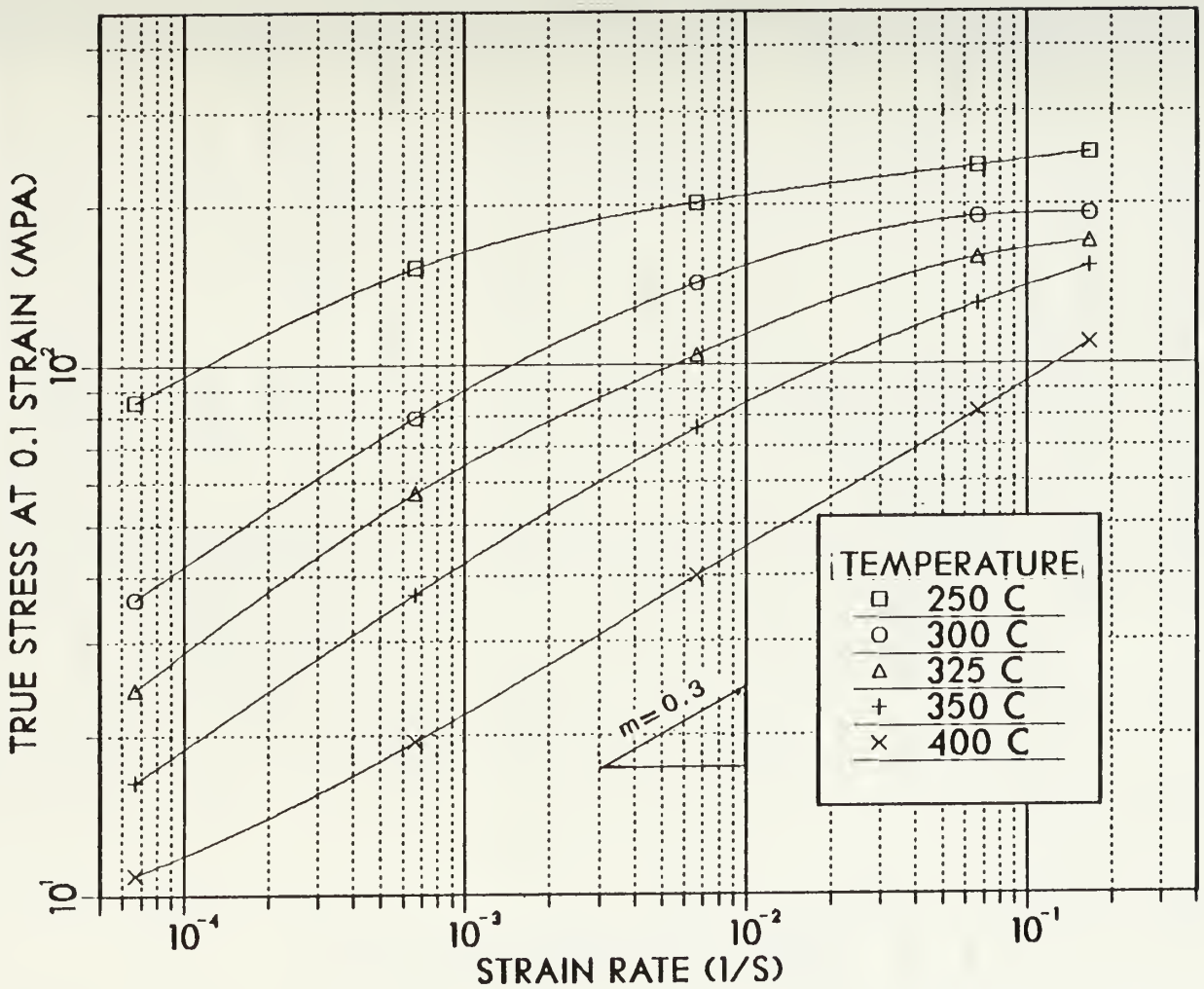

Figure 4.7 True stress at 0.1 strain vs. strain rate for Al-10%Mg-0.1%Zr. Solution treated at 440 °C for 24 hours, hot worked, resolution treated at 440 °C for 1 hour, oil quenched, warm rolled at 300 °C to 92% reduction, and recrystallized at 440 °C for 1 minute.

strain rate sensitivity coefficients, m = 0.3 at lower strain rates for all temperatures tested. Again, it can be argued that the instability of the microstructure has lowered the m value from a higher true value, and thus a second order strain rate dependence on stress cannot be ruled out. Detailed study of grain growth and deformation mechanisms would be required to determine if this pattern of grain growth observed in the rolled material is also observed with this recrystallize material. In contrast to the as-rolled material the maximum ductility of the recrystallized material is observed at higher temperature, 400°C, and does not coincide with the maximum m value. A more comprehensive study of recrystallized, than was performed in this research, would be required to explain this.

Activation energy for the recrystallized material was obtained following the same procedure outlined in the as-rolled section. The activation energy, Q, was computed to be 32.5 Kcal/mol, Figure 4.8, identical to that for the as-rolled material. Significant in this is that the recrystallized material does not exhibit the anomalous behavior in the 300°C to 350°C temperature region that the as-rolled material did. This provides conclusive evidence that the structural change in the as-rolled material by static recrystallization prior to commencing straining gave rise to the apparent negative activation energy in this

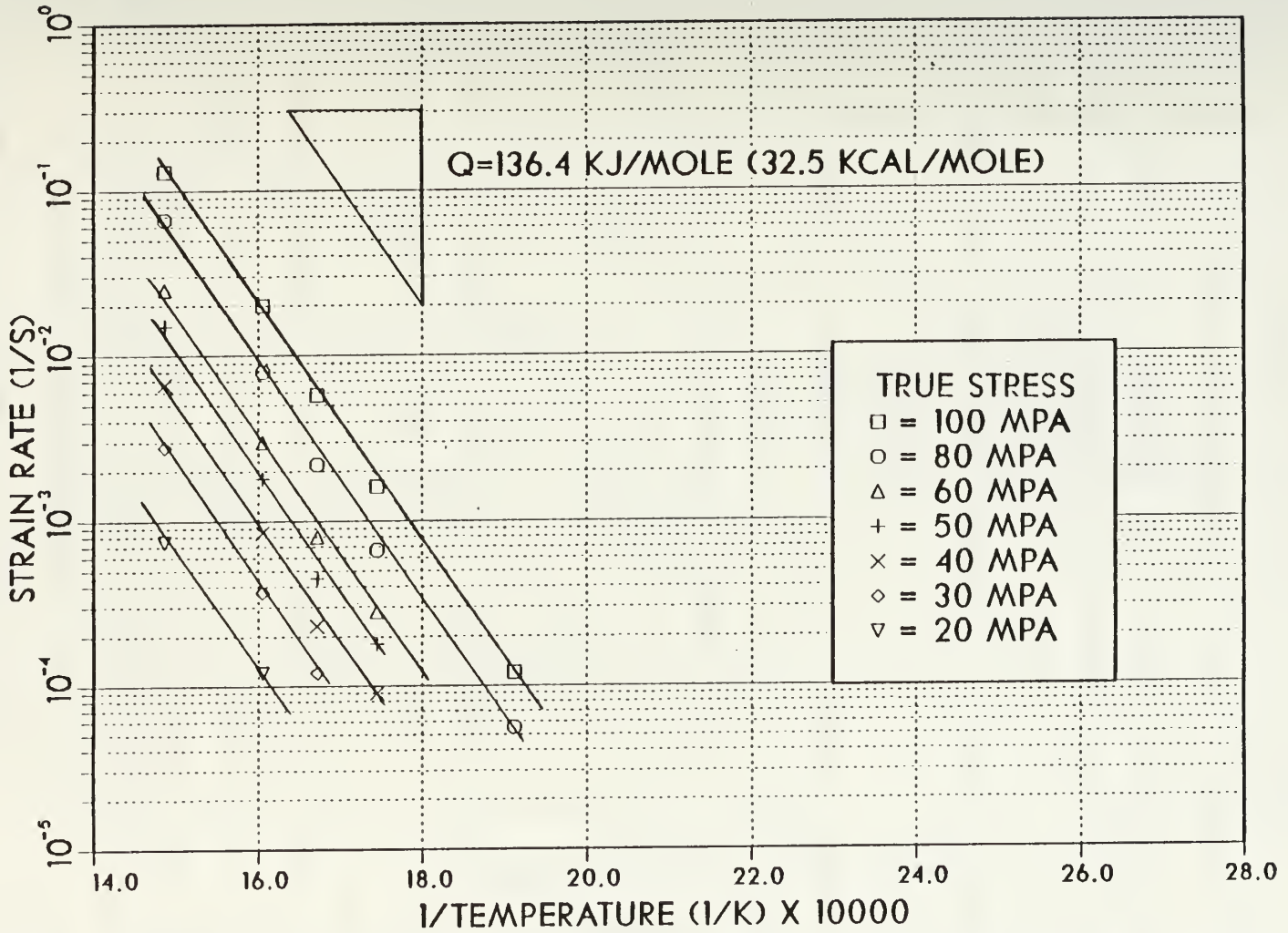

Figure 4.8 Strain rate vs. 1/T for Al-10%Mg-0.1%Zr. Solution treated at 440°C for 24 hours, hot worked, resolution treated at 440°C for 1 hour, oil quenched, warm rolled at 300°C to 92% reduction, and recrystallized at 440°C for 1 minute.

temperature region. From this it can be argued that the activation energy over the entire temperature range is that for lattice diffusion control. Also, superimposing the activation energy curves for selected stresses of as-rolled and recrystallized material, as illustrated in Figure 4.9, shows that at higher temperatures the activation energies are identical. This further supports the contention that the as-rolled material statically recrystallized prior to testing in the 325°C to 375°C temperature region.

C. MECHANICAL TESTING RESULTS FOR ANNEALED MATERIAL

Stengel [Ref. 13] in previous research of Al-1-%Mg-0.5%Mn alloys reported enhanced ductility in as-rolled material if it was annealed at a temperature below the solvus, prior to stress-strain testing. To see if this also applied to Al-10%Mg-0.1%Zr alloys, specimens were annealed using the procedure outlined in Chapter III, and tensile tested. Results for these tests are shown in Table IV. Figure 4.10, a graphical representation of ductility versus strain rate at 325°C, for the three heat treatment conditions shows that while the annealing produces better ductility than recrystallizing, the annealed material is not as ductile as the as-rolled material. This may be attributed to the ineffectiveness of the Zirconium in stabilizing the microstructure, as compared to the Manganese in Stengel's work.

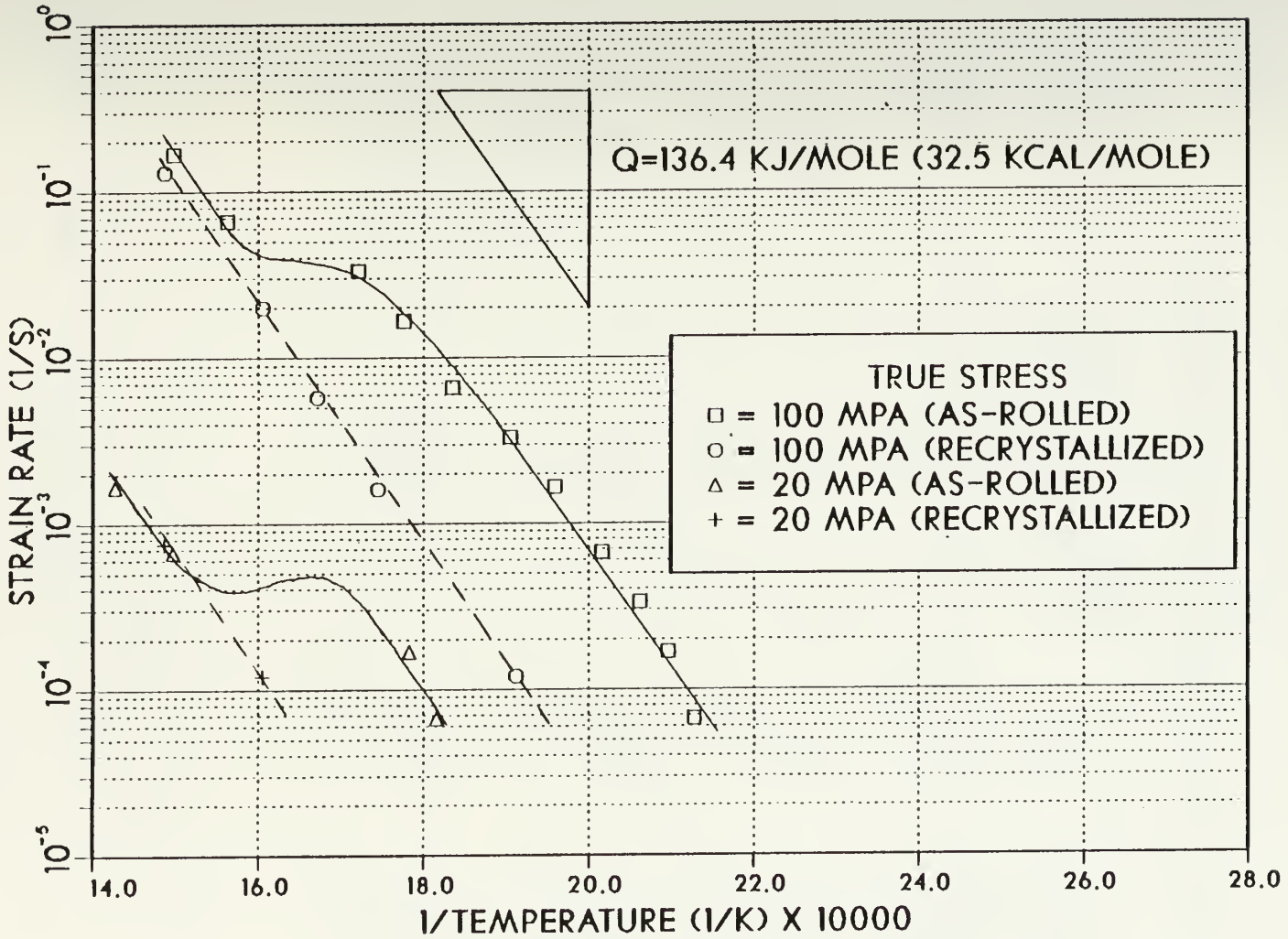

Figure 4.9 Strain rate vs. 1/T for Al-10%Mg-0.1%Zr. Solution treated at 440°C for 24 hours, hot worked, resolution treated at 440°C for 1 hour, oil quenched, warm rolled at 300°C to 92% reduction. Solid lines indicate as-rolled condition, dashed lines indicate material recrystallized at 440°C for 1 minute.

TABLE IV

Data for Al-10%Mg-0.1%Zr Alloy Annealed at 200°C for 1 Hour

Temperature C	Strain Rate s^{-1}	UTS Mpa	True Stress at 0.1 Plastic Strain Mpa	Ductility %
250	1.67×10^{-1}	242.4	242.0	71.4
250	6.67×10^{-2}	207.2	206.3	72.0
250	6.67×10^{-3}	157.7	147.6	155.2
250	6.67×10^{-4}	84.9	65.5	226.8
250	6.67×10^{-5}	51.1	36.7	250.6
275	1.67×10^{-1}	195.4	193.6	119.6
275	6.67×10^{-2}	166.8	164.5	163.4
275	6.67×10^{-3}	94.3	80.2	177.2
275	6.67×10^{-4}	55.2	38.8	426.0
275	6.67×10^{-5}	25.3	18.3	281.6
300	1.67×10^{-1}	156.1	156.1	117.4
300	6.67×10^{-2}	129.6	116.5	131.4
300	6.67×10^{-3}	77.6	68.8	304.6
300	6.67×10^{-4}	35.9	28.4	313.6
300	6.67×10^{-5}	14.3	11.5	452.8
325	1.67×10^{-1}	134.9	134.6	174.4
325	6.67×10^{-2}	111.2	110.0	372.0
325	6.67×10^{-3}	60.4	55.8	320.6
325	6.67×10^{-4}	31.3	24.7	445.0
325	6.67×10^{-5}	13.2	11.1	308.0

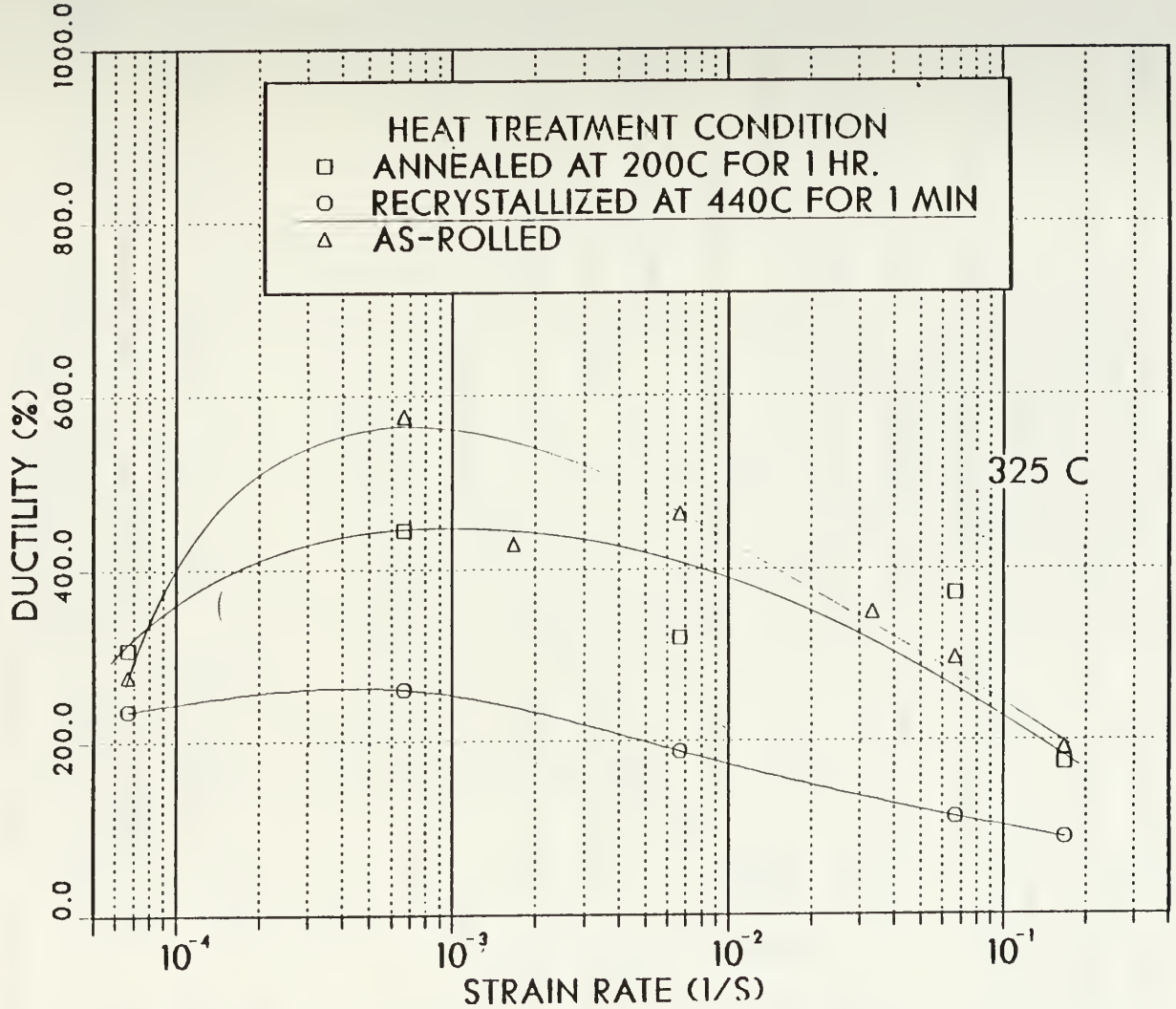

Figure 4.10 Percent ductility vs. strain rate for Al-10%Mg-0.1%Zr. Solution treated at 440°C for 24 hours, hot worked, resolution treated at 440°C for 1 hour, oil quenched, warm rolled at 300°C to 92% reduction.

A true stress versus true plastic strain plot, Figure 4.11, at 250°C shows that in the annealed condition this material is substantially weaker than either the recrystallized or as-rolled material, as expected. The strain rate sensitivity of the annealed material was in the same range as the as-rolled and recrystallized material, i.e., had a strain rate sensitivity coefficient, m = 0.3, Figure 4.12. The peculiar characteristic of this material is that, at certain temperatures, it shows a continuous increase in ductility with decreasing strain rate. This is contrary to the behavior of the as-rolled and recrystallized material, which exhibited peak ductilities at moderate strain rates. The narrowness of the test temperature range for which testing was performed on the annealed material, makes any indepth analysis for this condition impossible. A greater range of strain rates and temperatures would be required to understand the affects annealing has on this alloy.

D. CREEP MODELS

As noted in Chapter III, there are numerous creep models that have been proposed to explain superplastic behavior. There are two major schools of thought in characterizing this behavior. One proposes a separate mechanism for superplasticity, while the other believes that superplasticity occurs as a result of a transition in flow behavior from

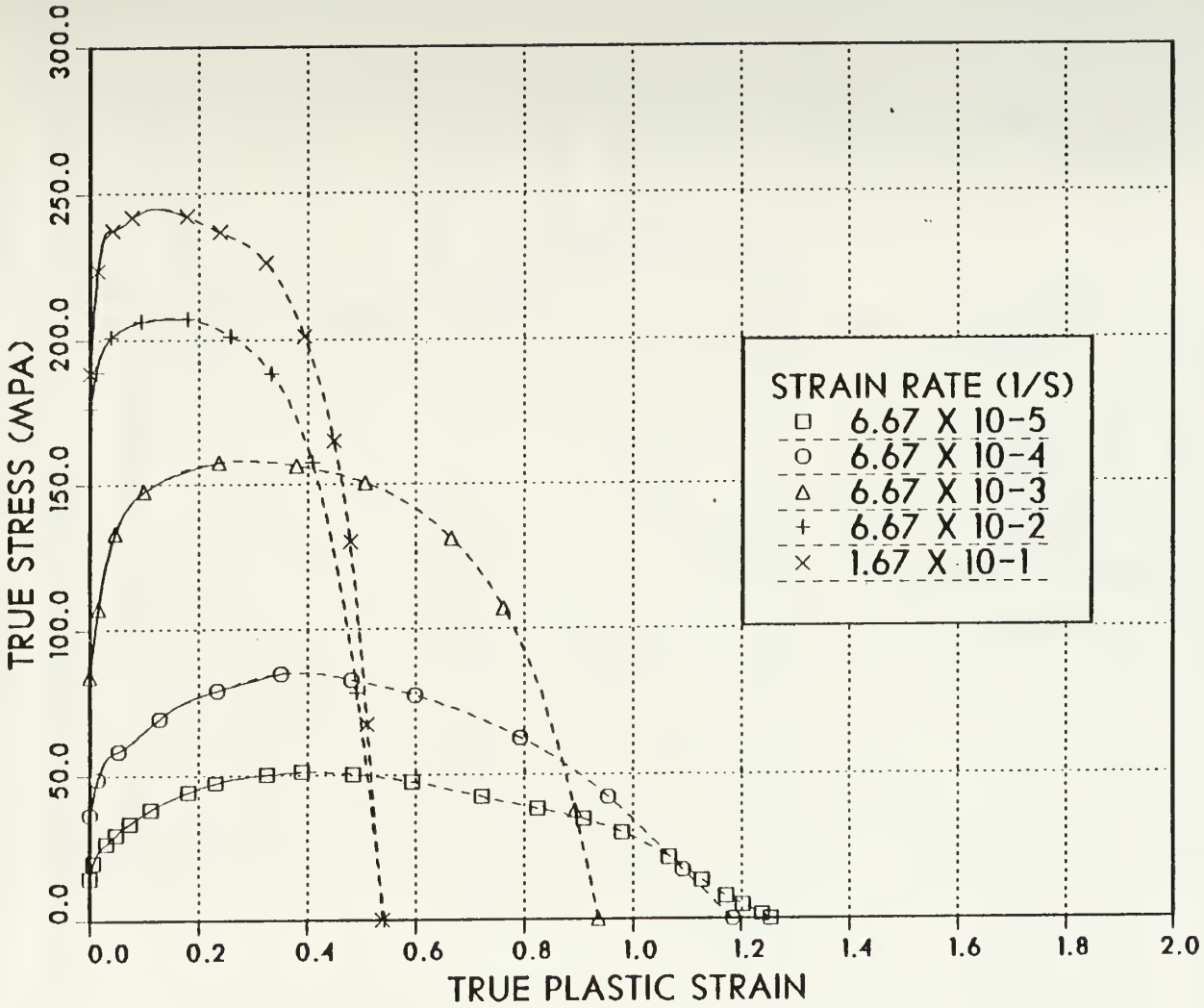

Figure 4.11 True stress vs. true plastic strain for testing conducted at 250 °C for Al-10%Mg-0.1%Zr. Solution treated at 440 °C for 24 hours, hot worked, resolution treated at 440 °C for 1 hour, oil quenched, warm rolled at 300 °C to 92% reduction, and annealed at 200 °C for 1 hour. Dashed lines indicate straining beyond onset of necking.

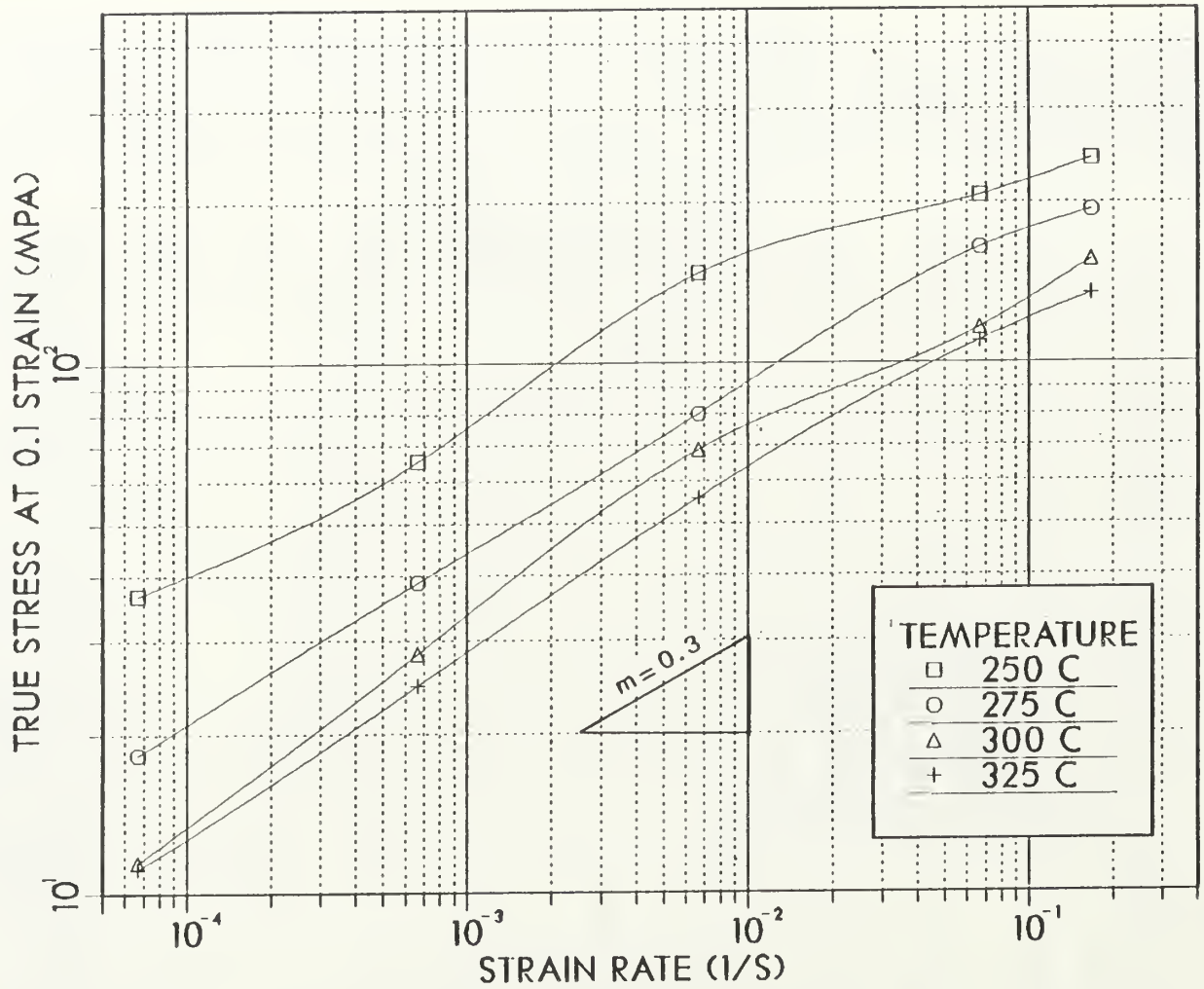

Figure 4.12 True stress at 0.1 strain vs. strain rate for Al-10%Mg-0.1%Zr. Solution treated at 440°C for 24 hours, hot worked, resolution treated at 440°C for 1 hour, oil quenched, warm rolled at 300°C to 92% reduction, and annealed at 200°C for 1 hour.

regime I to regime III deformation. An attempt will be made here to match the characteristics of Al-10%Mg-0.1%Zr alloys with a few of the current creep models.

Nabarro [Ref. 19] and Herring [Ref. 20] creep model discussed in Chapter III, is attractive in the sense that it predicts lattice diffusion as the controlling process, which is exhibited by this alloy. But it is less than satisfactory in that it proposes a first order strain rate dependence on stress, which this material does not exhibit. The Coble [Ref. 21] creep model is unsatisfactory in predicting the behavior of this material, in that it proposes grain boundary diffusion control and a first order strain rate dependence on stress, neither of which is observed in this alloy. The Raj and Ashby [Ref. 22] model, grain boundary sliding accommodated by lattice diffusion, could explain this alloy's diffusion controlled deformation, but it is hard to perceive how this alloy, with such a high dislocation density, is not also slip accommodated. Their model also does not predict the second order strain rate dependence on stress exhibited by this material.

The Ashby and Verrall [Ref. 23] transitional model discussed in Chapter III, with its grain switching, is attractive in that it explains how grains remain fine and equiaxed during deformation which concurrent work by Berthold [Ref. 16] has shown is the case with this alloy. But contrary to their model, this alloy exhibits a much

wider range of strain rates for which the second order stress dependence is observed. The Misro and Mukherjee [Ref. 24] model could explain this wider range of second power strain rate dependence on stress, but with its grain boundary diffusion control prediction it is not applicable to this alloy. Nix's [Ref. 25] model, also transitional with its diffusional relaxation, is attractive from many standpoints, but again the range of strain rate for second order stress dependence in transition is much too narrow to explain the behavior of this alloy. Also, his model fails to show how grains remain equiaxed during superplastic flow.

The Weertman [Ref. 26] model based on dislocation glide control with its fourth or fifth order strain rate dependence on stress probably lies outside the regime or transition range for superplastic behavior. Thus its applicability to predict deformation behavior in this material is limited. Weertman's [Ref. 26] microcreep model or dislocation glide for solid solutions with solute diffusion control and third order strain rate dependence fails to totally predict the behavior of this alloy although it may be useful with the data for the recrystallized condition. Thus, although several models have attractive aspects in predicting the behavior of this alloy, no one model can explain completely the behavior for this alloy. And although the activation energy for this material was

established to be that of lattice diffusion, no single rate mechanism has clearly been established. This rate controlling mechanism may be either dislocation deformation or diffusional deformation or a combination of the two. If this mechanism can be found, a satisfactory model could be devised to predict the behavior of this material.

V. CONCLUSIONS AND RECOMMENDATIONS

The following conclusions are drawn from this research: 1) superplastic elongations up to 500% are attainable in Al-10%Mg-0.1%Zr alloys at temperatures from 275°C-325°C, and strain rates of 7×10^{-3} to 7×10^{-4} s^{-1}; 2) warm-rolled materials tend to exhibit the greatest degree of superplasticity; 3) the activation energy for elevated temperature deformation of this material is that of lattice diffusion; 4) the material exhibits a second order strain rate dependence on stress.

Continued research in the following areas is recommended: 1) step strain rate tests be performed to determine the true strain rate sensitivity coefficient for tempertures 300°C and 325°C; 2) further investigation of the anomalous behavior annealed material exhibits at low strain rates be initiated; 3) once the Zirconium premature precipitation problem has been resolved, further study of the effect recrystallizing has on this material; 4) continued, more detailed, elevated temperature testing of the warm rolled material in the temperature range 275°C-325°C; 4) expansion of this research both mechanically and microstructurally to enable the development of a model that will predict the superplastic behavior of this material.

APPENDIX A

MECHANICAL TESTING DATA

This appendix provides a graphical summary of the elevated-temperature mechanical characteristics for the Al-10%Mg-0.1%Zr alloy of this research. The data includes that for material in the as-rolled condition, after recrystallizing at 440°C for one minute, and after annealed at 200°C for one hour.

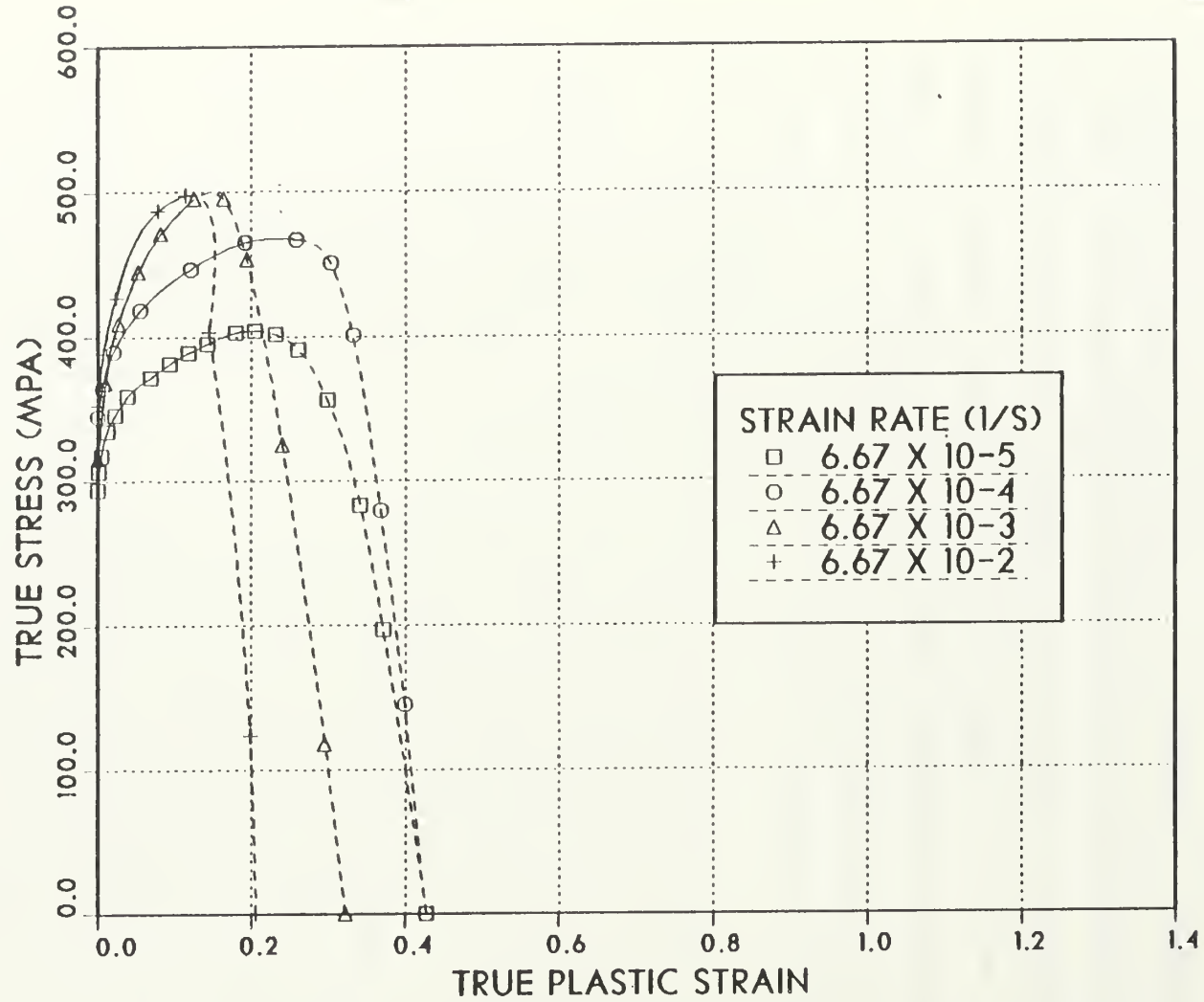

Figure A.1 True stress vs. true plastic strain for testing conducted at 100 °C for Al-10%Mg-0.1%Zr. Solution treated at 440 °C for 24 hours, hot worked, resolution treated at 440 °C for 1 hour, oil quenched, and warm rolled at 300 °C to 92% reduction. Dashed lines indicate straining beyond onset of necking.

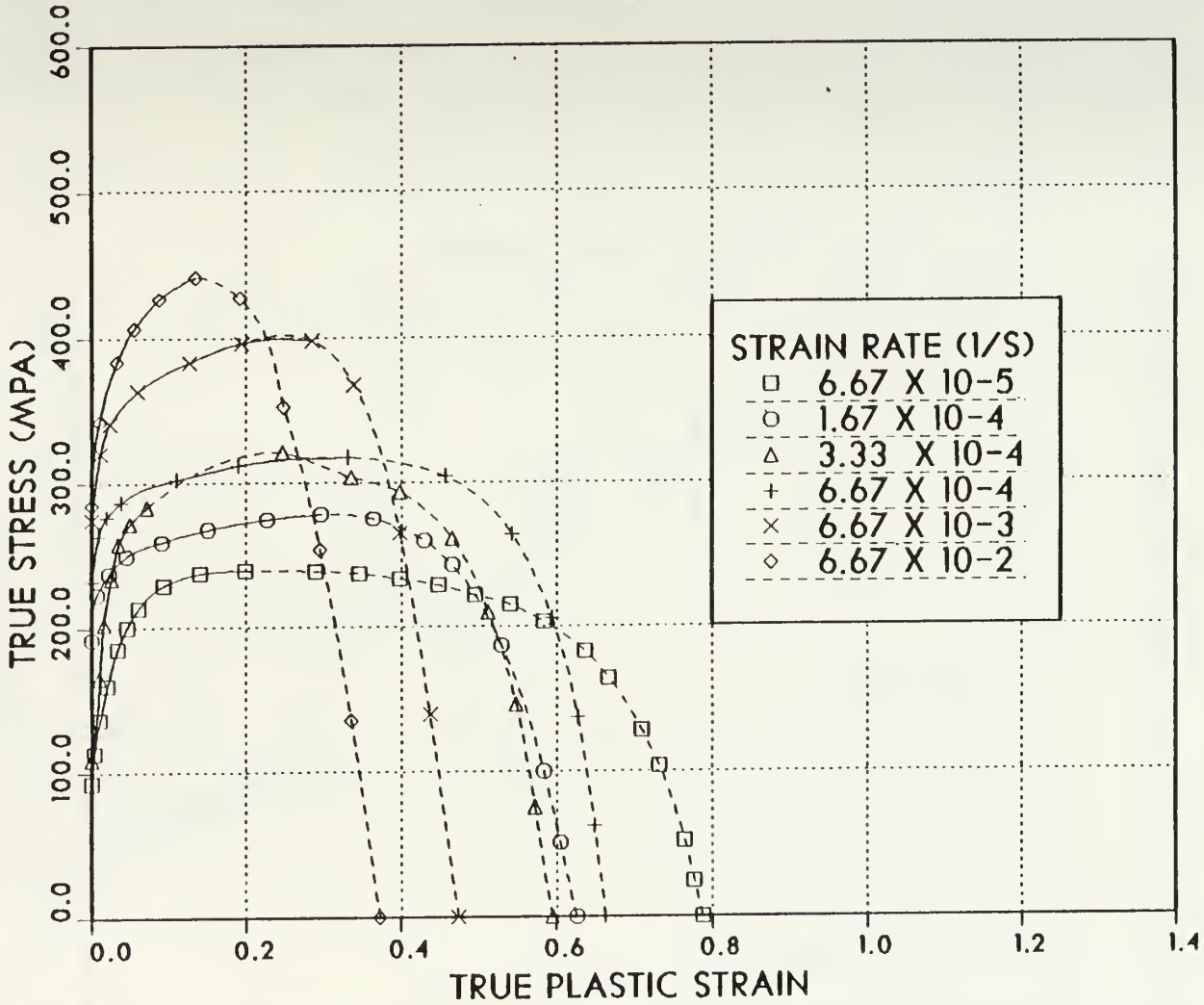

Figure A.2 True stress vs. true plastic strain for testing conducted at 150 °C for Al-10%Mg-0.1%Zr. Solution treated at 440 °C for 24 hours, hot worked, resolution treated at 440 °C for 1 hour, oil quenched, and warm rolled at 300 °C to 92% reduction. Dashed lines indicate straining beyond onset of necking.

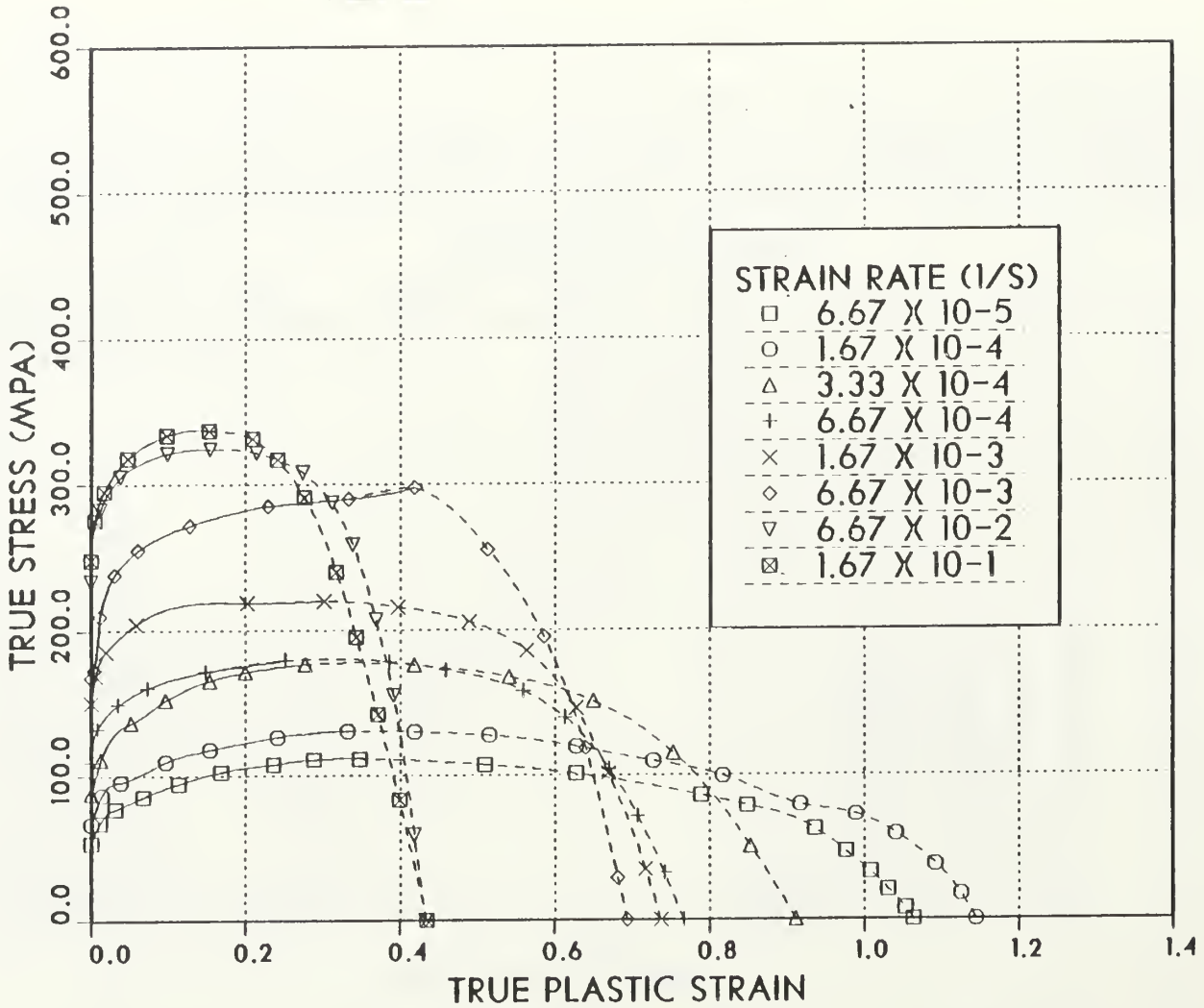

Figure A.3 True stress vs. true plastic strain for testing conducted at 200 °C for Al-10%Mg-0.1%Zr. Solution treated at 440 °C for 24 hours, hot worked, resolution treated at 440 °C for 1 hour, oil quenched, and warm rolled at 300 °C to 92% reduction. Dashed lines indicate straining beyond onset of necking.

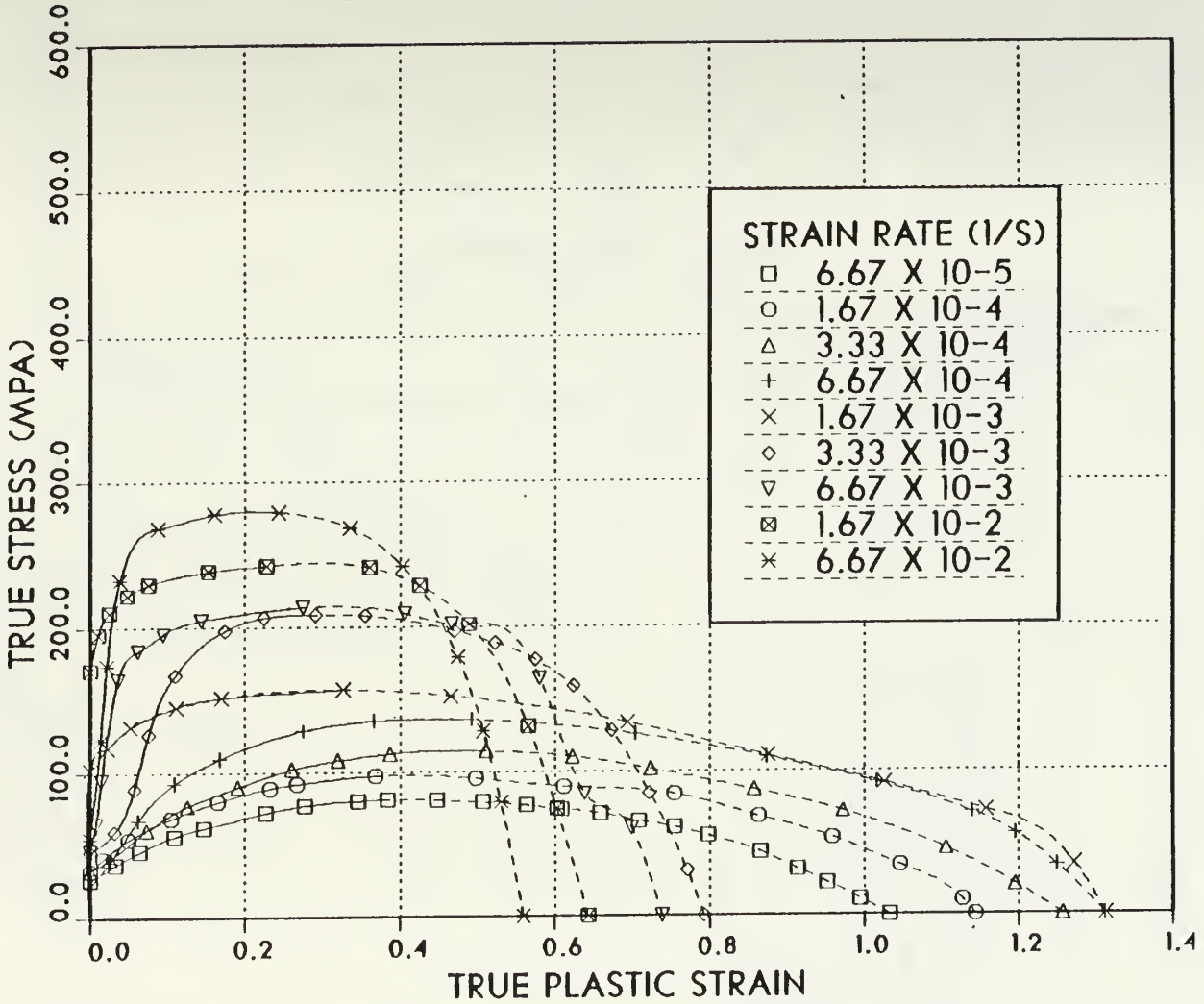

Figure A.4 True stress vs. true plastic strain for testing conducted at 225 °C for Al-10%Mg-0.1%Zr. Solution treated at 440 °C for 24 hours, hot worked, resolution treated at 440 °C for 1 hour, oil quenched, and warm rolled at 300 °C to 92% reduction. Dashed lines indicate straining beyond onset of necking.

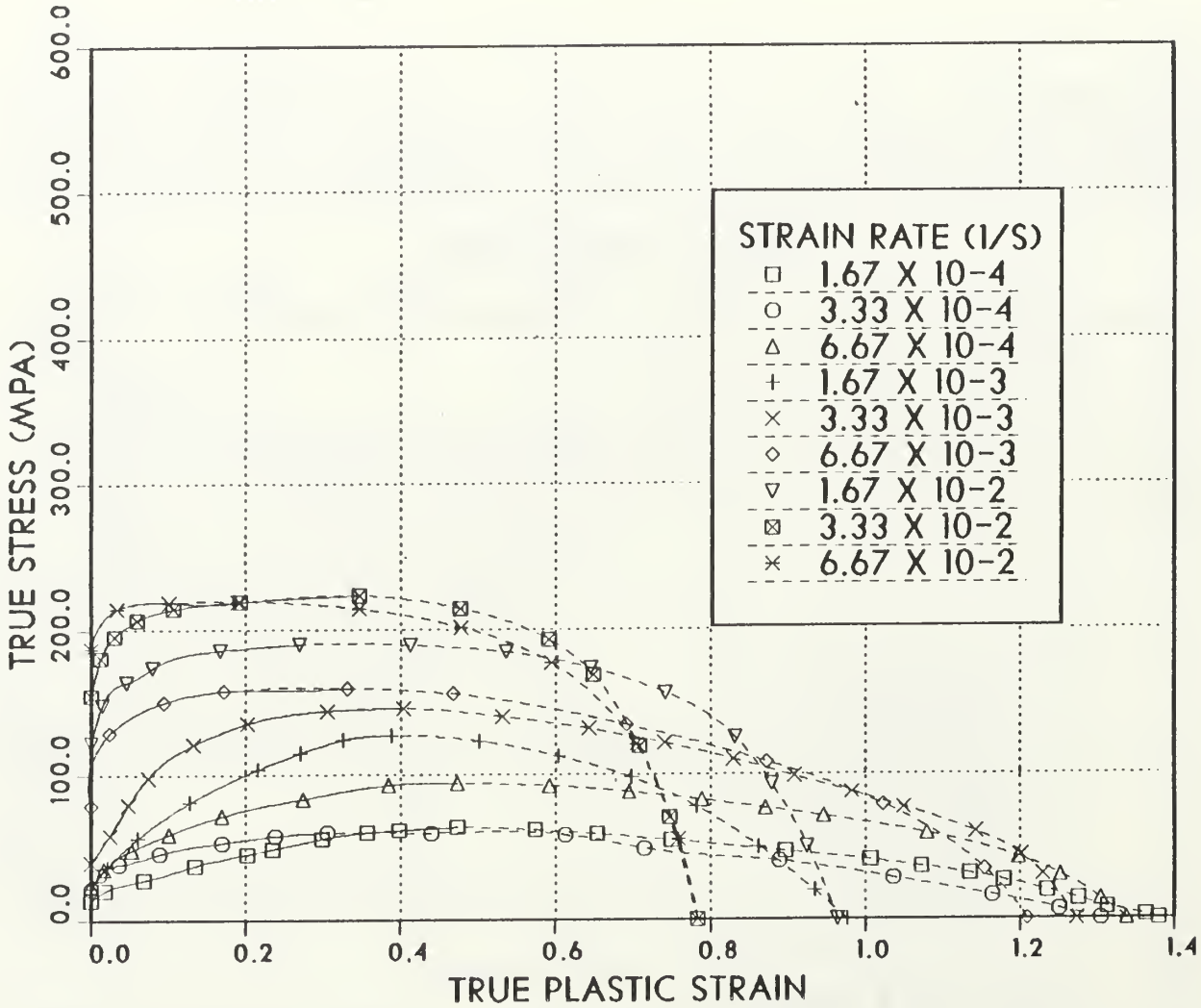

Figure A.5 True stress vs. true plastic strain for testing conducted at 250 °C for Al-10%Mg-0.1%Zr. Solution treated at 440 °C for 24 hours, hot worked, resolution treated at 440 °C for 1 hour, oil quenched, and warm rolled at 300 °C to 92% reduction. Dashed lines indicate straining beyond onset of necking.

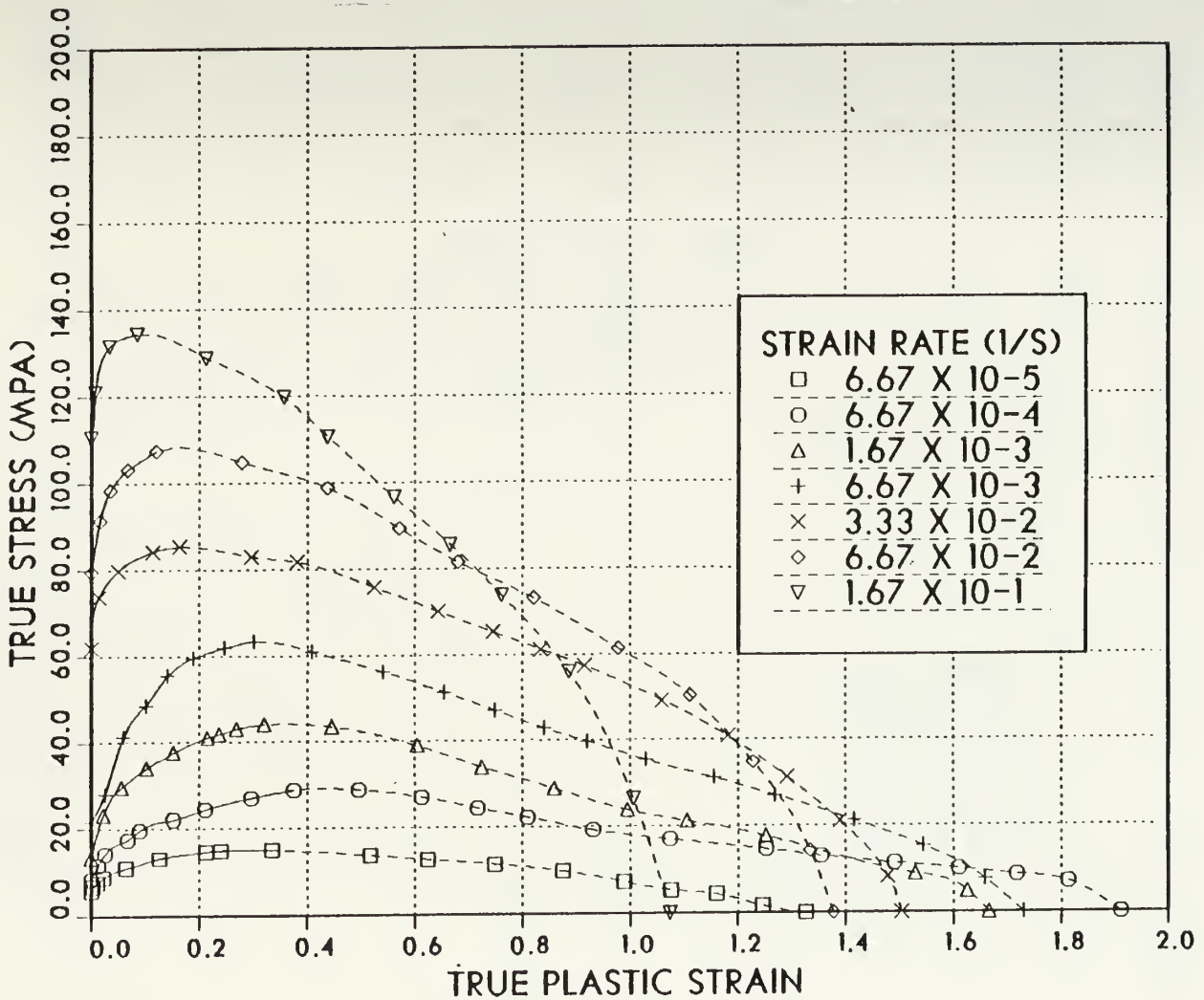

Figure A.6 True stress vs. true plastic strain for testing conducted at 325 C for Al-10%Mg-0.1%Zr. Solution treated at 440°C for 24 hours, hot worked, resolution treated at 440°C for 1 hour, oil quenched, and warm rolled at 300°C to 92% reduction. Dashed lines indicate straining beyond onset of necking.

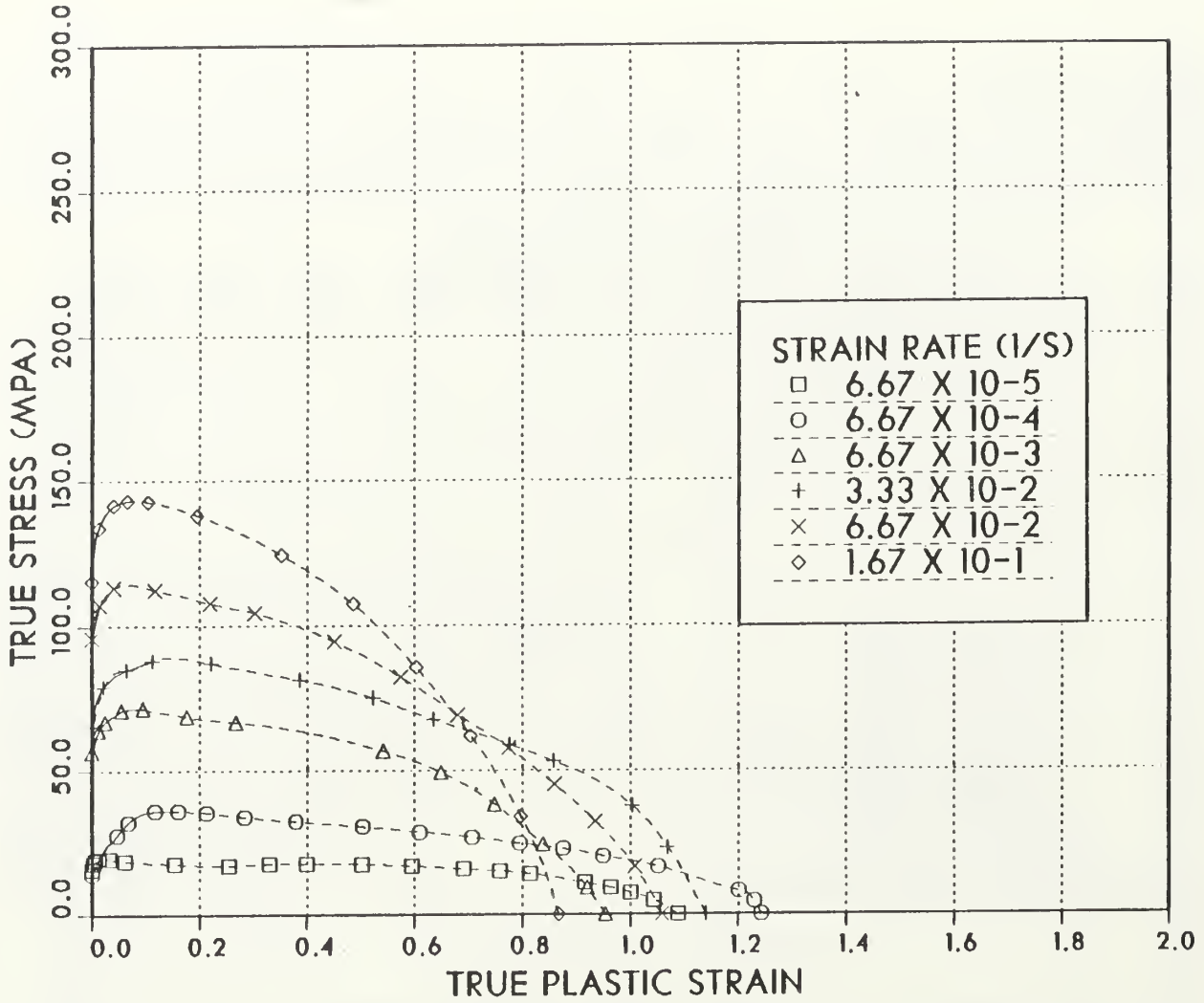

Figure A.7 True stress vs. true plastic strain for testing conducted at 350 °C for Al-10%Mg-0.1%Zr. Solution treated at 440 °C for 24 hours, hot worked, resolution treated at 440 °C for 1 hour, oil quenched, and warm rolled at 300 °C to 92% reduction. Dashed lines indicate straining beyond onset of necking.

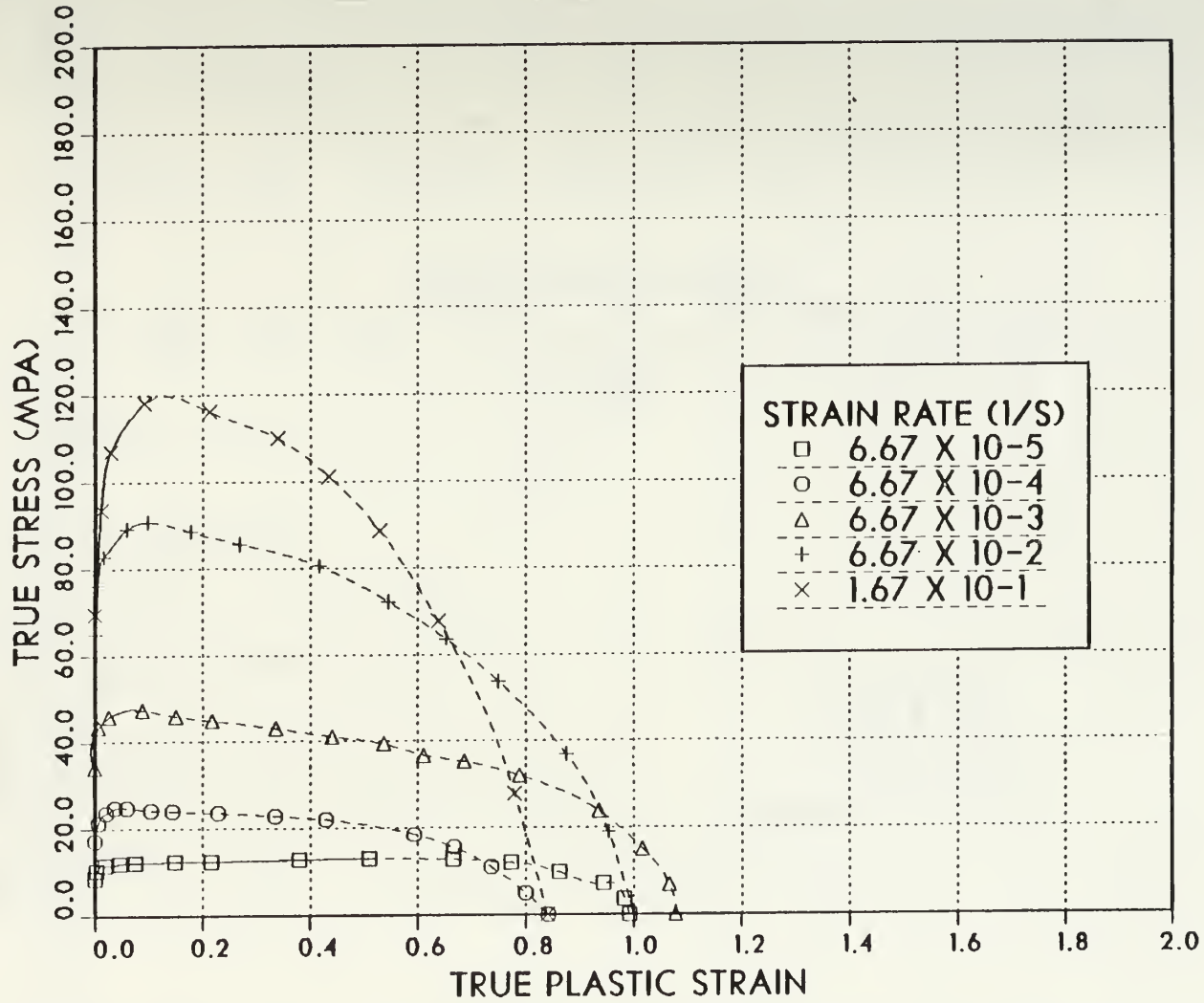

Figure A.8 True stress vs. true plastic strain for testing conducted at 375 °C for Al-10%Mg-0.1%Zr. Solution treated at 440 °C for 24 hours, hot worked, resolution treated at 440 °C for 1 hour, oil quenched, and warm rolled at 300 °C to 92% reduction. Dashed lines indicate straining beyond onset of necking.

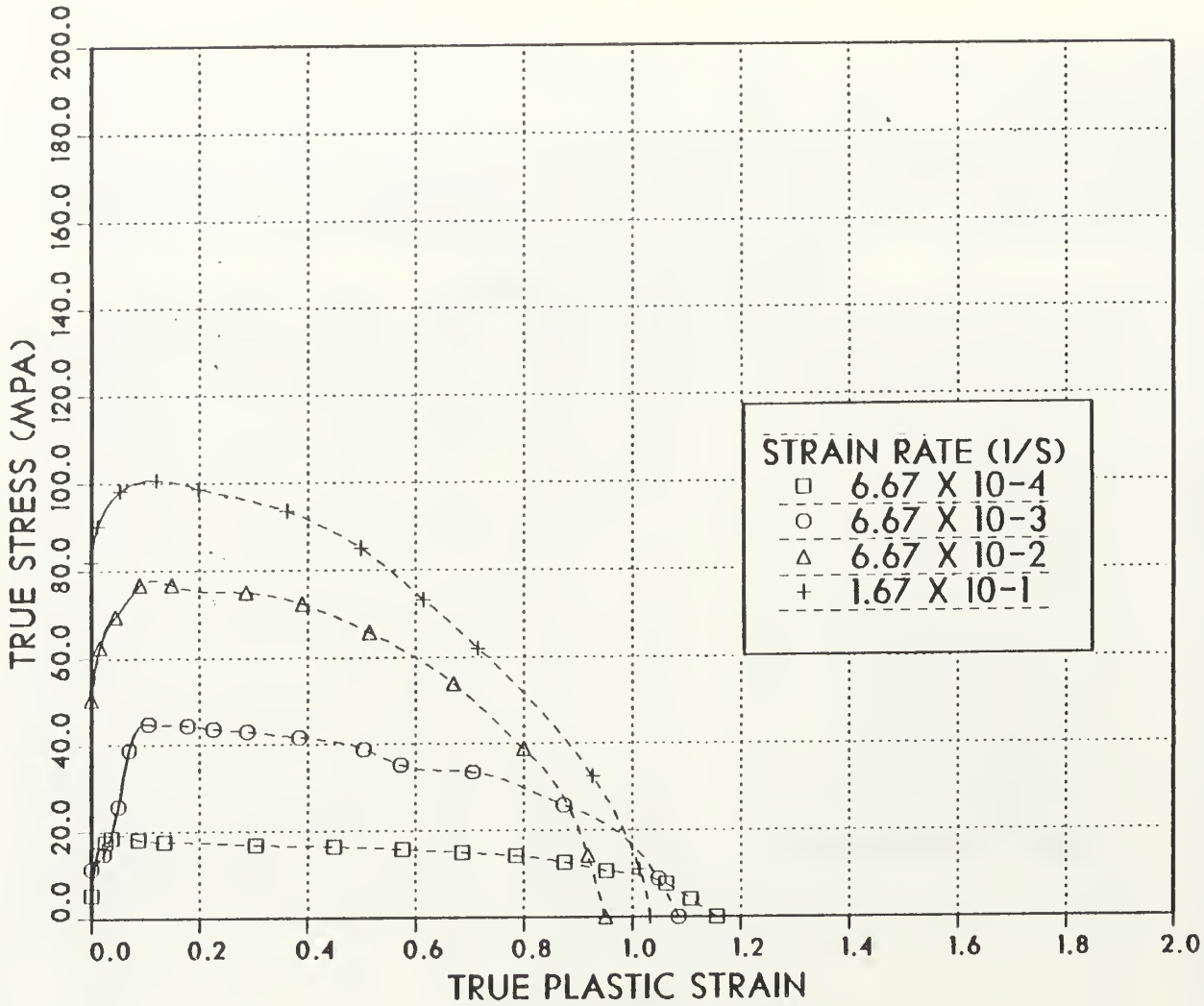

Figure A.9 True stress vs. true plastic strain for testing conducted at 400 °C for Al-10%Mg-0.1%Zr. Solution treated at 440 °C for 24 hours, hot worked, resolution treated at 440 °C for 1 hour, oil quenched, and warm rolled at 300 °C to 92% reduction. Dashed lines indicate straining beyond onset of necking.

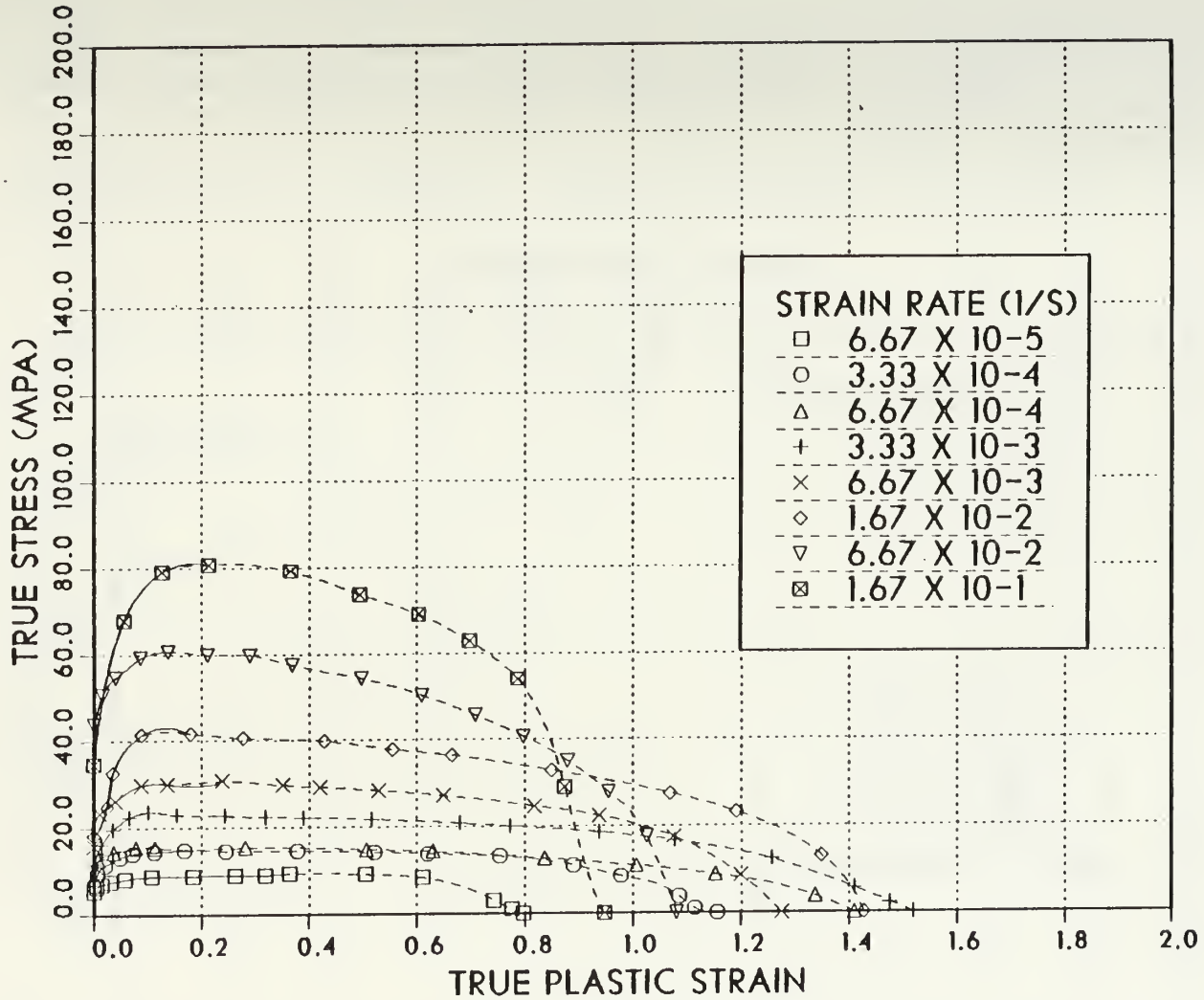

Figure A.10 True stress vs. true plastic strain for testing conducted at 425 °C for Al-10%Mg-0.1%Zr. Solution treated at 440 °C for 24 hours, hot worked, resolution treated at 440 °C for 1 hour, oil quenched, and warm rolled at 300 °C to 92% reduction. Dashed lines indicate straining beyond onset of necking.

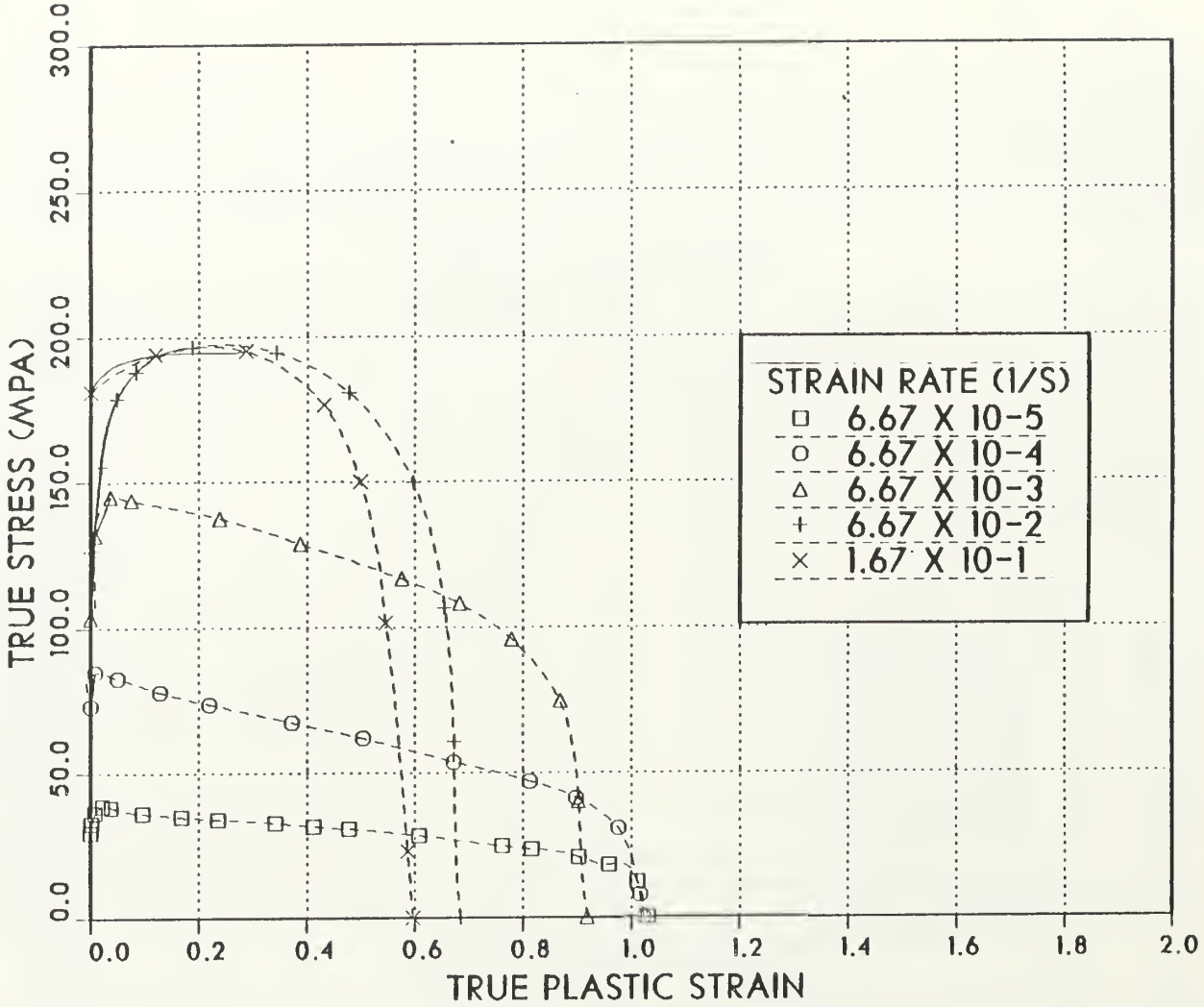

Figure A.11 True stress vs. true plastic strain for testing conducted at 300 °C for Al-10%Mg-0.1%Zr. Solution treated at 440 °C for 24 hours, hot worked, resolution treated at 440 °C for 1 hour, oil quenched, warm rolled at 300 °C to 92% reduction, and recrystallized at 440 °C for 1 minute. Dashed lines indicate straining beyond onset of necking.

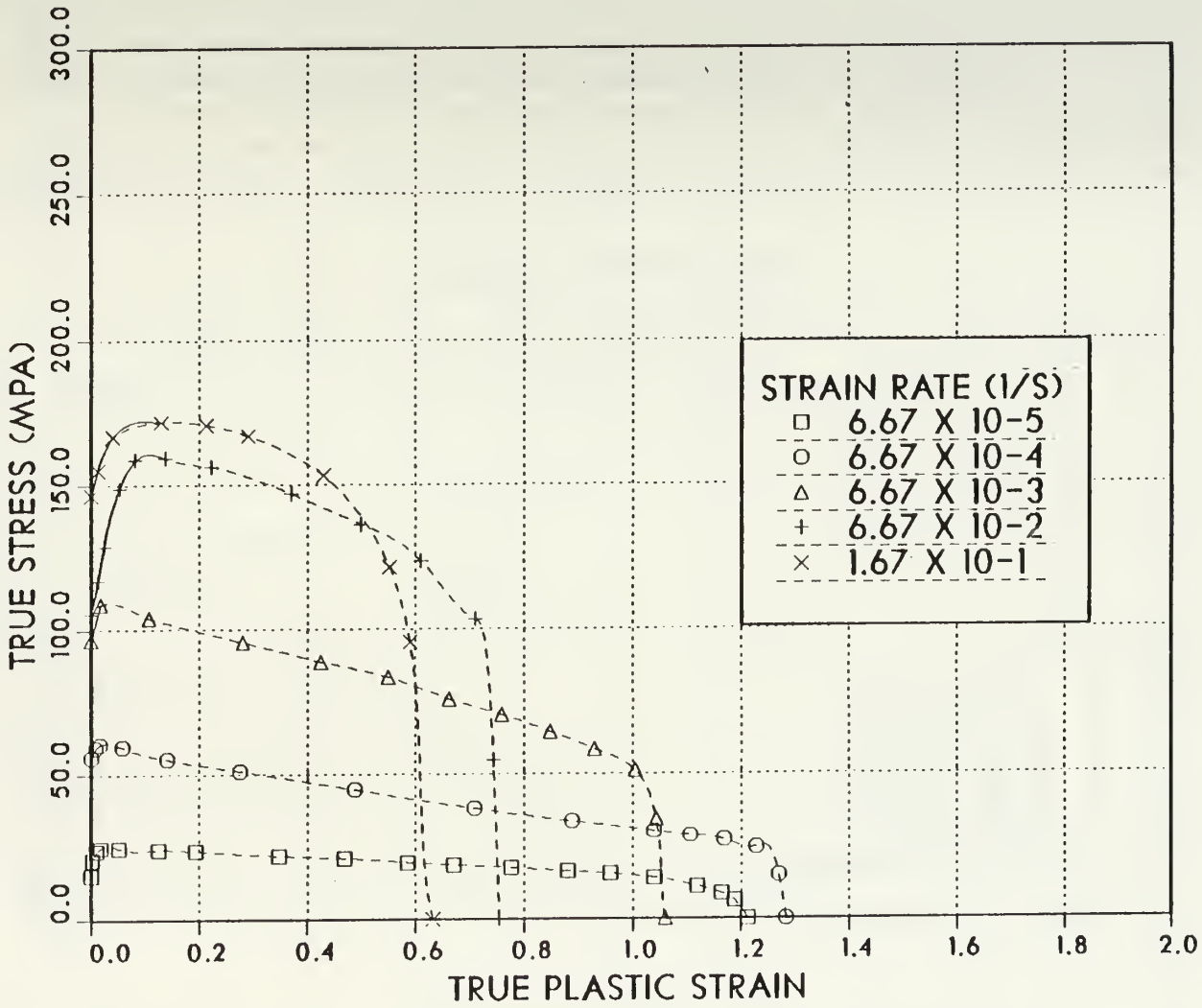

Figure A.12 True stress vs. true plastic strain for testing conducted at 325 °C for Al-10%Mg-0.1%Zr. Solution treated at 440 °C for 24 hours, hot worked, resolution treated at 440 °C for 1 hour, oil quenched, warm rolled at 300 °C to 92% reduction, and recrystallized at 440 °C for 1 minute. Dashed lines indicate straining beyond onset of necking.

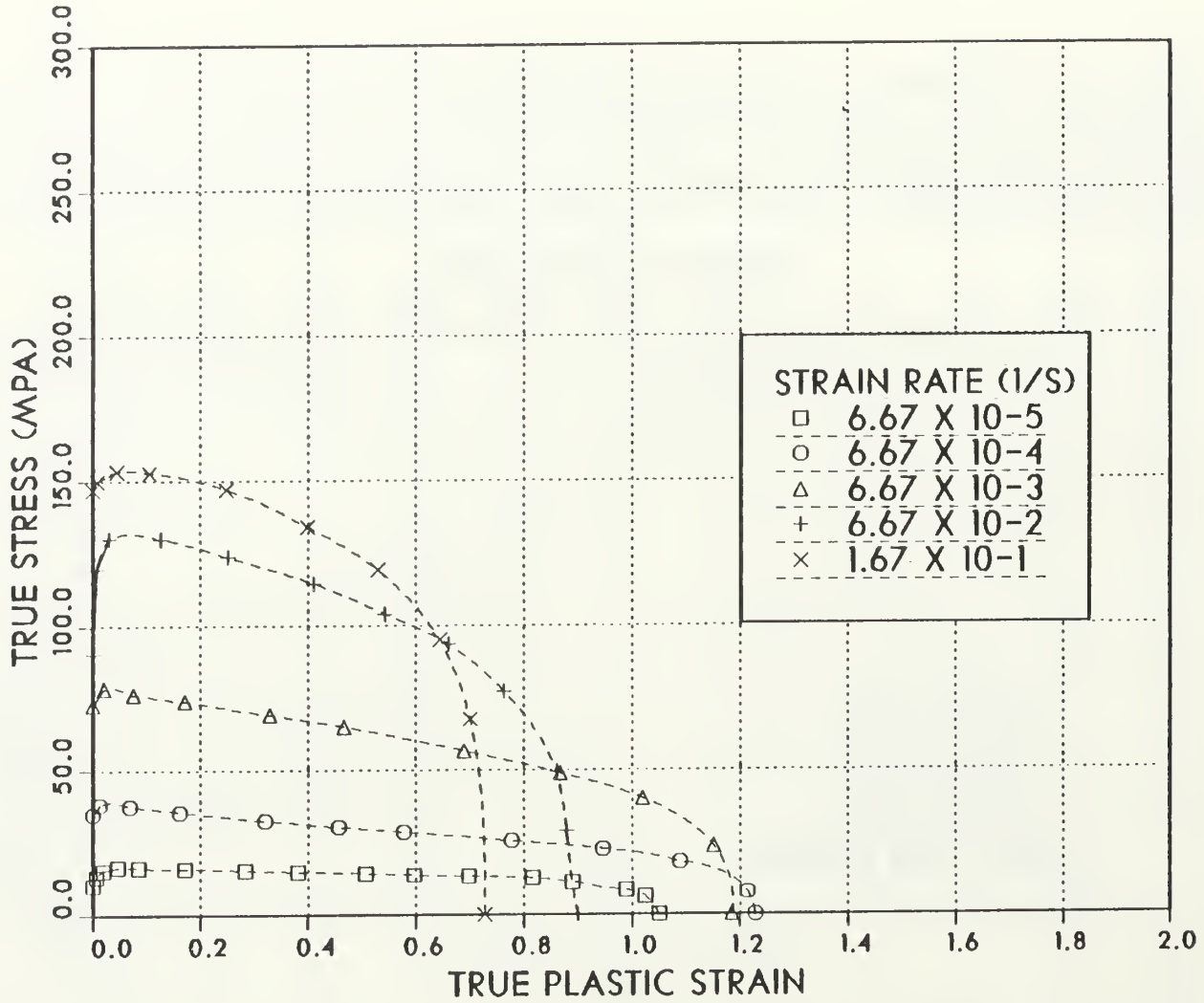

Figure A.13 True stress vs. true plastic strain for testing conducted at 350 °C for Al-10%Mg-0.1%Zr. Solution treated at 440 °C for 24 hours, hot worked, resolution treated at 440 °C for 1 hour, oil quenched, warm rolled at 300 °C to 92% reduction, and recrystallized at 440 °C for 1 minute. Dashed lines indicate straining beyond onset of necking.

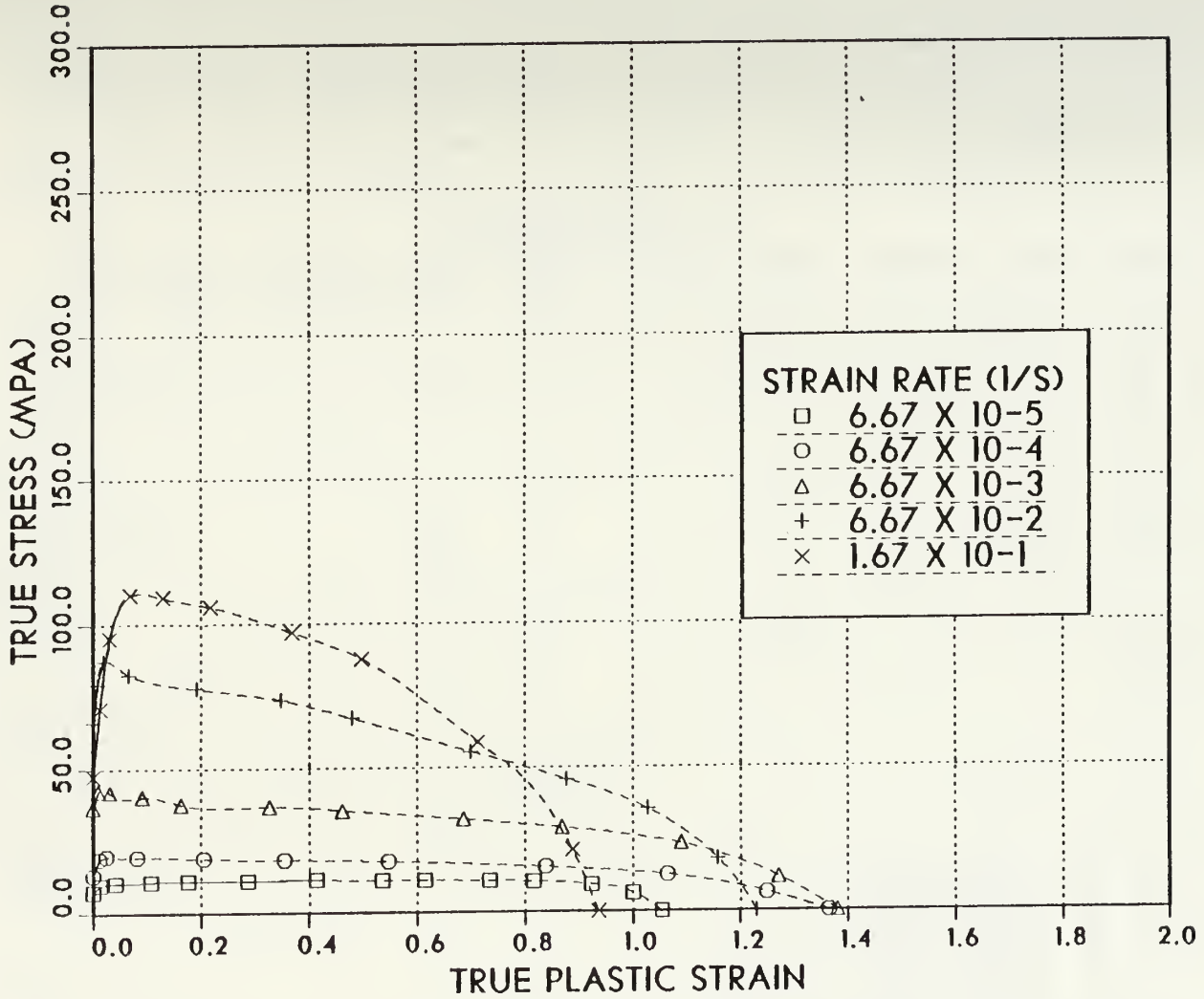

Figure A.14 True stress vs. true plastic strain for testing conducted at 400°C for Al-10%Mg-0.1%Zr. Solution treated at 440°C for 24 hours, hot worked, resolution treated at 440°C for 1 hour, oil quenched, warm rolled at 300°C to 92% reduction, and recrystallized at 440°C for 1 minute. Dashed lines indicate straining beyond onset of necking.

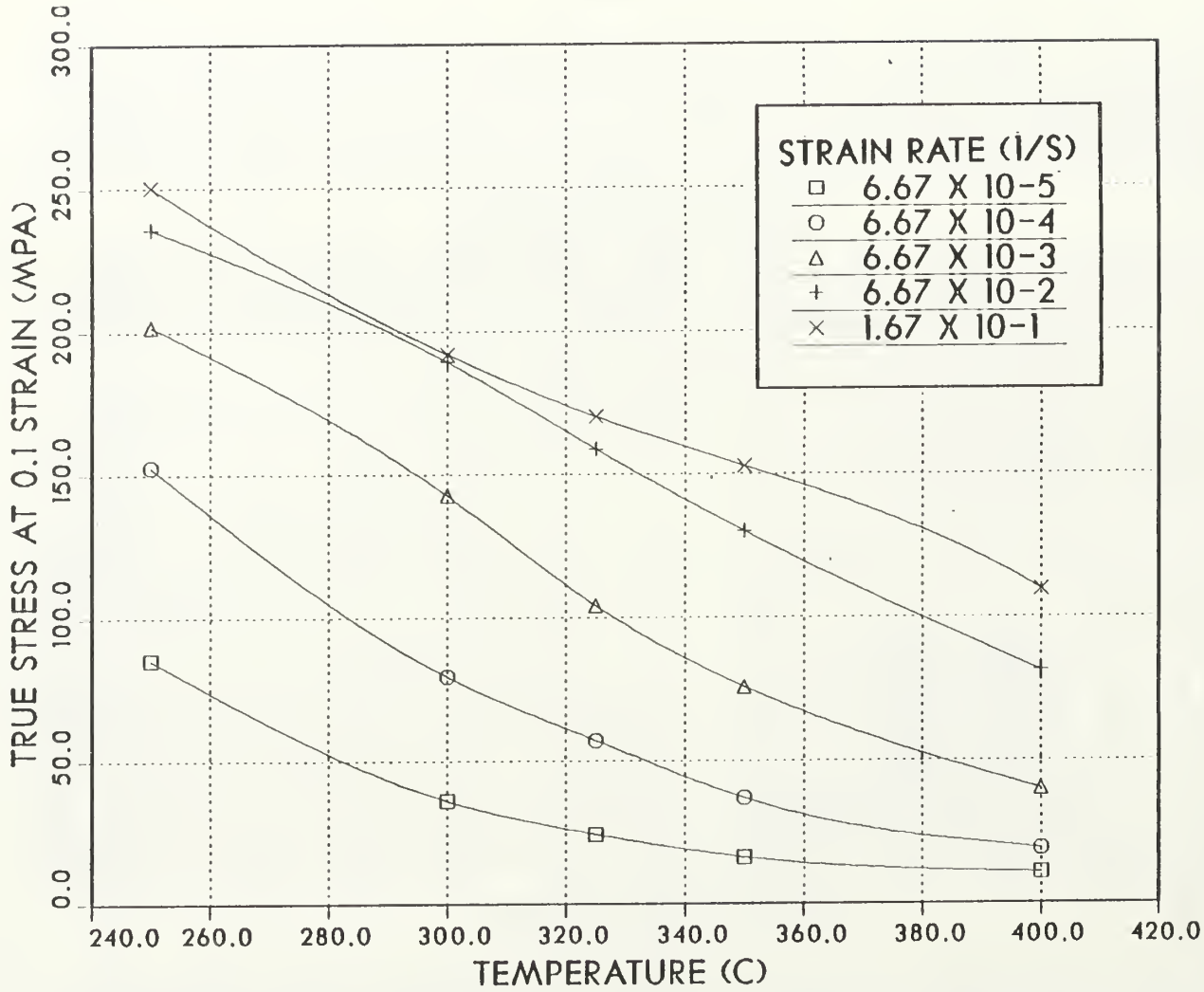

Figure A.15 True stress at 0.1 strain vs. temperature for Al-10%Mg-0.1%Zr. Solution treated at 440°C for 24 hours, hot worked, resolution treated at 440°C for 1 hour, oil quenched, warm rolled at 300°C to 92% reduction, and recrystallized at 440°C for 1 minute.

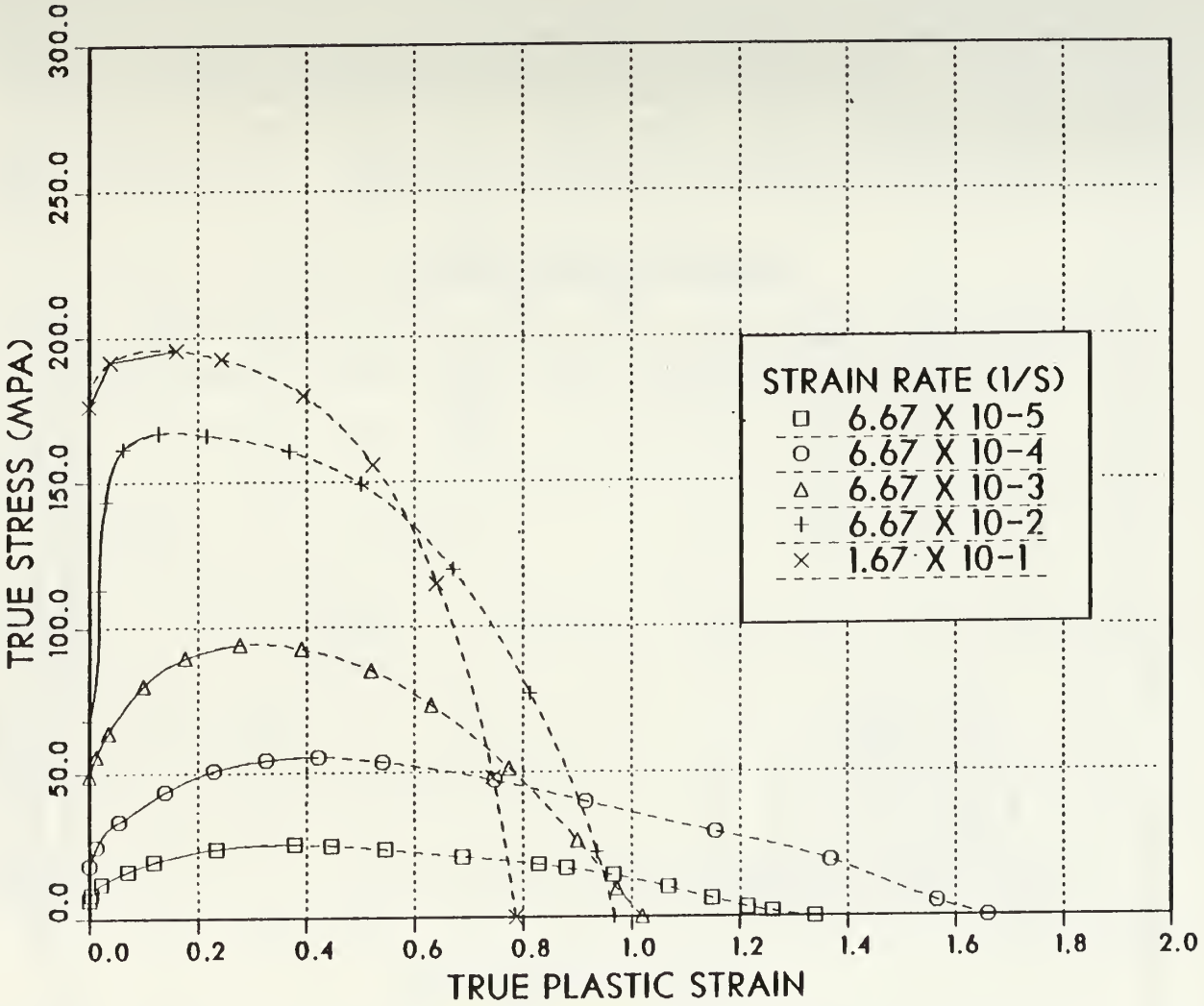

Figure A.16 True stress vs. true plastic strain for testing conducted at 275 °C for Al-10%Mg-0.1%Zr. Solution treated at 440 °C for 24 hours, hot worked, resolution treated at 440 °C for 1 hour, oil quenched, warm rolled at 300 °C to 92% reduction, and annealed at 200 °C for 1 hour. Dashed lines indicate straining beyond onset of necking.

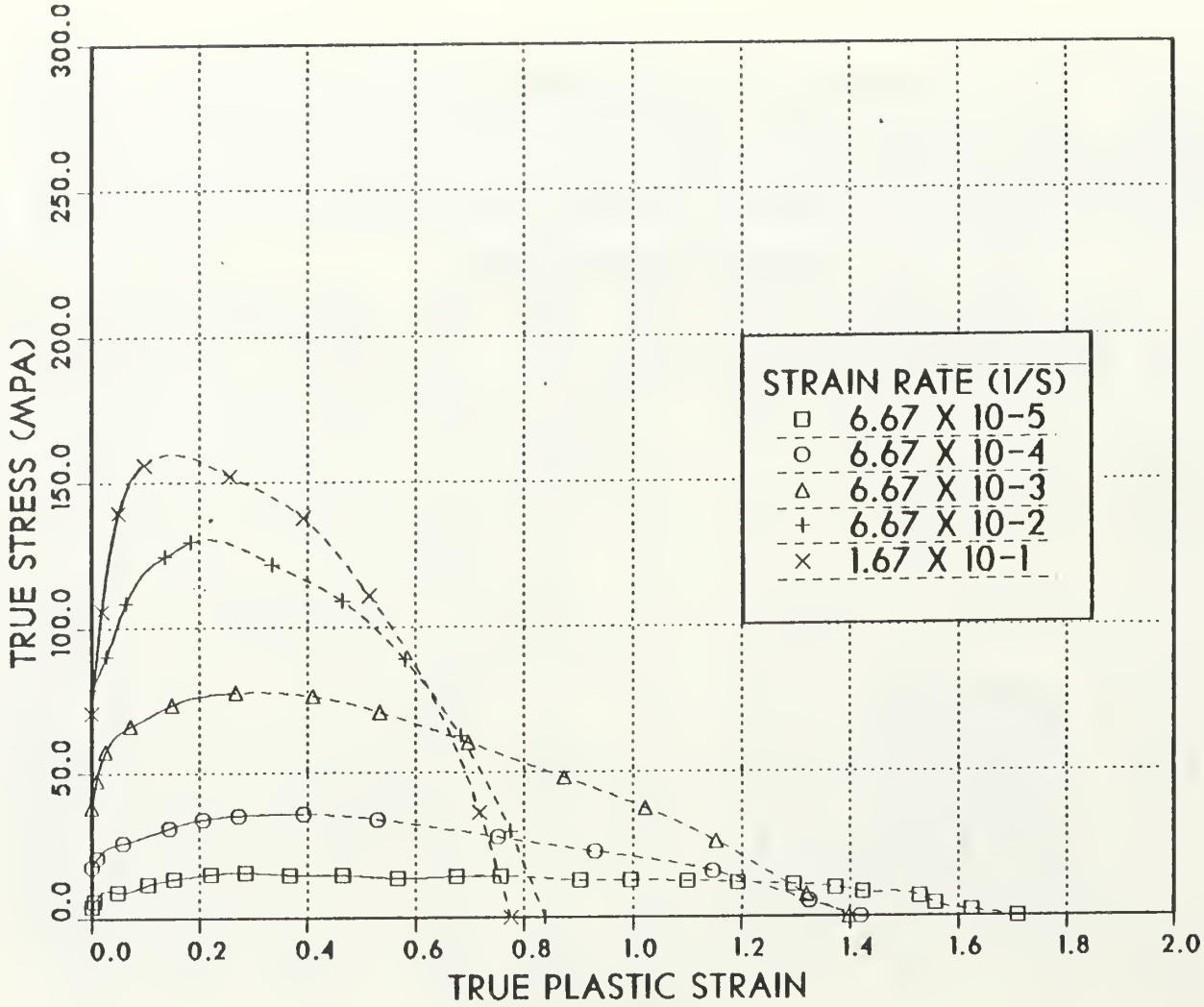

Figure A.17 True stress vs. true plastic strain for testing conducted at 300 °C for Al-10%Mg-0.1%Zr. Solution treated at 440 °C for 24 hours, hot worked, resolution treated at 440 °C for 1 hour, oil quenched, warm rolled at 300 °C to 92% reduction, and annealed at 200 °C for 1 hour. Dashed lines indicate straining beyond onset of necking.

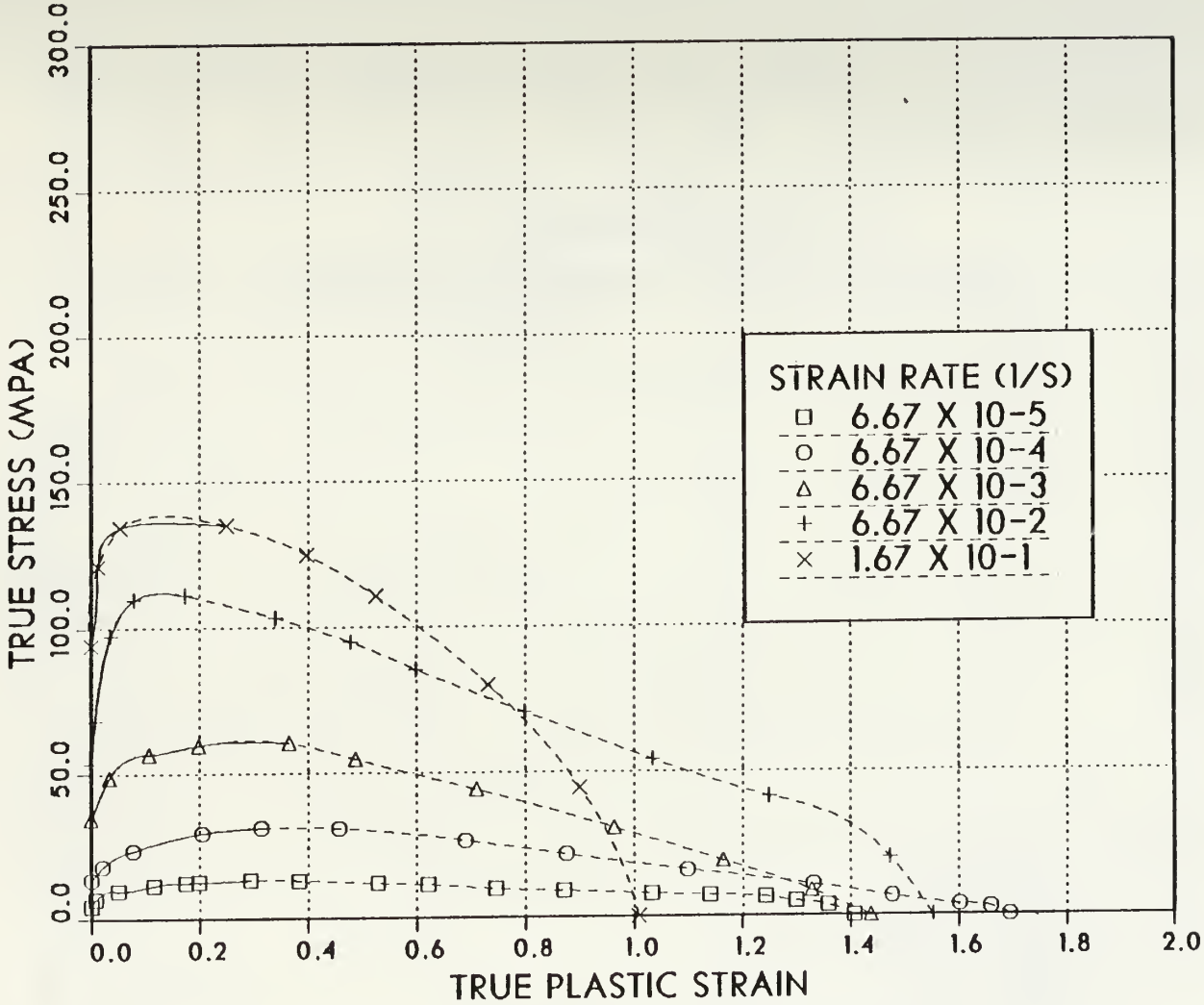

Figure A.18 True stress vs. true plastic strain for testing conducted at 325 °C for Al-10%Mg-0.1%Zr. Solution treated at 440 °C for 24 hours, hot worked, resolution treated at 440 °C for 1 hour, oil quenched, warm rolled at 300 °C to 92% reduction, and annealed at 200 °C for 1 hour. Dashed lines indicate straining beyond onset of necking.

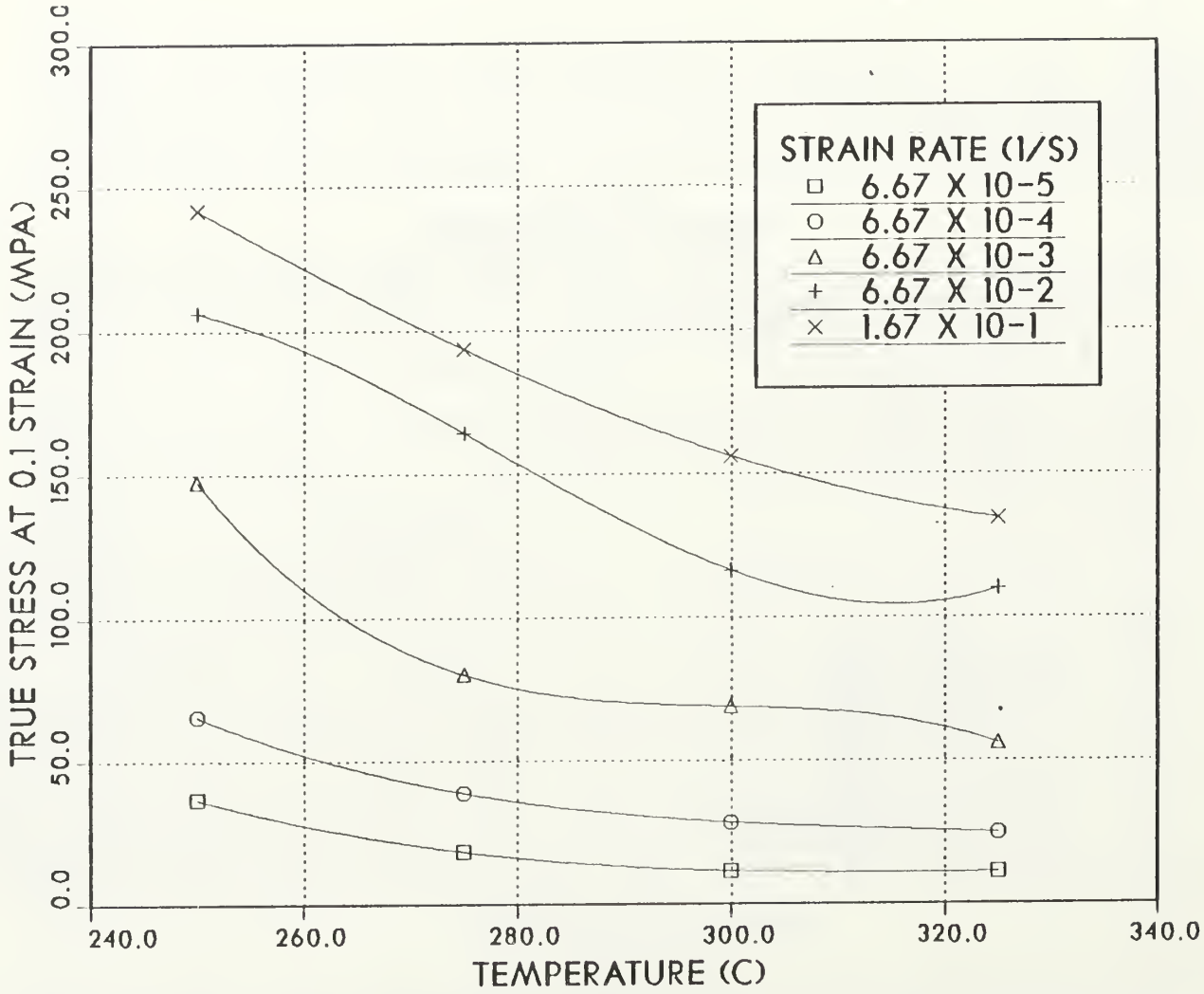

Figure A.19 True stress at 0.1 strain vs. temperature for Al-10%Mg-0.1%Zr. Solution treated at 440°C for 24 hours, hot worked, resolution treated at 440°C for 1 hour, oil quenched, warm rolled at 300°C to 92% reduction and annealed at 200°C for 1 hour.

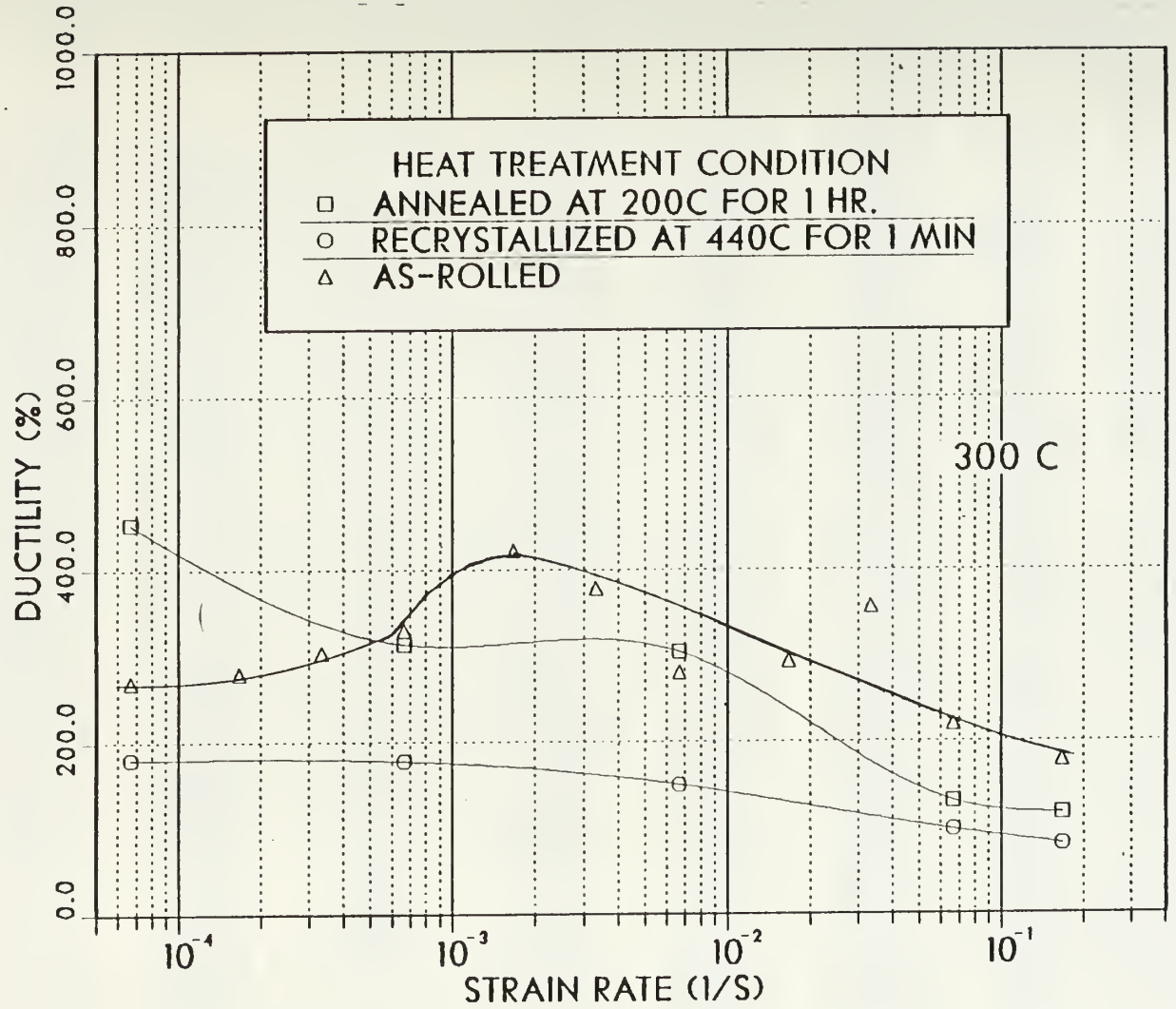

Figure A.20 Percent ductility vs. strain rate for Al-10%Mg-0.1%Zr. Solution treated at 440°C for 24 hours, hot worked, resolution treated at 440°C for 1 hour, oil quenched, warm rolled at 300°C to 92% reduction.

LIST OF REFERENCES

1. Lloyd, D. J. and Moore, D. M., "Aluminum Alloy Design for Superplasticity," Superplastic Forming of Structural Alloys, Conference Proceedings of TME-AIME, pp. 147-172, June 1982.

2. Stewart, M. J., "Closed Die Forging of Superplastic Alloys," Canadian Metallurgy Quarterly, Volume 12, pp. 159-169, 1973.

3. Ness, F. G., Jr., High Strength to Weight Aluminum-18 Weight Percent Magnesium Alloy Through Thermomechanical Processing, M.S. Thesis, Naval Postgraduate School, Monterey, California, December 1976.

4. Bingay, C. P., Microstructural Response of Aluminum-Magnesium Alloys to Thermomechanical Processing, M.S. Thesis, Naval Postgraduate School, Monterey, California, December 1977.

5. Glover, T. L., Effects of Thermomechanical Processing of Aluminum-Magnesium Alloys Containing High Weight Percent Magnesium, M.S. Thesis, Naval Postgraduate School, Monterey, California, December 1977.

6. Grandon, R. A., High Strength Aluminum-Magnesium Alloys: Thermomechanical Processing, Microstructure and Tensile Mechanical Properties of High Strength Aluminum-Magnesium Alloys, M.S. Thesis, Naval Postgraduate School, Monterey, California, March 1980.

7. Speed, W. G., An Investigation into the Influence of Thermomechanical Processing on Microstructure and Mechanical Properties of High Strength Aluminum-Magnesium Alloys, M.S. Thesis, Naval Postgraduate School, Monterey, California, December 1977.

8. Chesterman, C. W., Jr., Precipitation, Recovery and Recrystallization Under Static and Dynamic Conditions for High Magnesium Aluminum-Magnesium Alloys, M.S. Thesis, Naval Postgraduate School, Monterey, California, March 1980.

9. Johnson, R. B., The Influence of Alloy Composition and Thermomechanical Processing Procedure on Microstructural and Mechanical Properties of High

Magnesium Aluminum-Magnesium Alloys, M.S. Thesis, Naval Postgraduate School, Monterey, California, June 1980.

10. Shirah, R. H., The Influence of Solution Time and Quench Rate on the Microstructure and Mechanical Properties of High Magnesium Aluminum-Magnesium Alloys, M.S. Thesis, Naval Postgraduate School, Monterey, California, December 1981.

11. Becker, J. J., Superplasticity in Thermomechanically Processed High-Magnesium Aluminum Magnesium Alloys, M.S. Thesis, Naval Postgraduate School, Monterey, California, March 1984.

12. Mills, M. E., Superplasticity in Thermomechancially Processed Aluminum-10.2%Mg-0.52%Mn Alloy, M.S. Thesis, Naval Postgraduate School, Monterey, California, September 1984.

13. Stengel, A. R., Effects of Annealing Treatments on Superplasticity in a Thermomechanically Processed Aluminum-10.2%Mg-0.52%Mn Alloy, M.S. Thesis, Naval Postgraduate School, Monterey, California, December 1984.

14. Self, R. J., The Effect of Alloy Additions on Superplasticity in Thermomechanically Processed High Magnesium Aluminum Magnesium Alloys, M.S. Thesis, Naval Postgraduate School, Monterey, California, December 1984.

15. Alcamo, M.E., Effects of Strain and Strain Rate on the Microstructure of a Superplastically Deformed Al-10%Mg-0.1%Zr Alloy, M.S. Thesis, Naval Postgraduate School, Monterey, California, June 1985.

16. Berthold, D. B., Effects of Temperature and Strain Rate on the Microstructure of a Deformed, Superplastic Al-10%Mg-0.1%Zr Alloy, M.S. Thesis, Naval Postgraduate School, Monterey, California, June 1985.

17. Bly, D. C., Sherby, O. D., and Young, C. M., "Influence of Thermal Mechanical Treatments on the Mechanical Properties of a Finely Spheroidized Eutectic Composition Steel," Material Science and Engineering, Volume 2, pp. 41-46, 1973.

18. Hart, E. W., "Theory of the Tensile Test," Acta Metallurgica, Volume 15, pp. 351-355, 1967.

19. Nabarro, F. R. M., Report of a Conference on the Strength of Solids, Physical Society (Publishers), London, p. 75, 1948.

20. Herring, C., "Diffusional Viscosity of A Polycrystalline Solid," Journal Applied Physics, Volume 21, p. 437, 1950.

21. Coble, R. L., "A Model for Boundary Diffusion Controlled Creep in Polycrystalline Materials," Journal Applied Physics, Volume 34, p. 1679, 1963.

22. Raj, R. and Ashby, M. F., "Grain Boundary Sliding and Diffusional Creep," Metallurgical Transactions, Volume 2, p. 1113, 1971.

23. Ashby, M. F., "A First Report on Deformation-Mechanism Maps," Acta Metallurgica, Volume 20, p. 887, 1972.

24. Misro, S. C. and Mukherjee, A. K., "Experimental Observations for Superplastic Deformation," Transactions of the ASM, Volume 64, pp. 755-768, 1973.

25. Nix, W. D., "On Some Fundamental Aspects of Superplastic Flow," Metals/Materials Technology Series, 8401-004, 1984.

26. Weertman, J., "Dislocation Climb Theory of Steady-State Creep," Transactions of the ASM, Volume 61, p. 681, 1968.

27. Langdon, T. G., "Experimental Observations in Superplasticity," Superplastic Forming of Structural Alloys, Conference Proceedings of TMS-AIME, pp. 27-40, June 1982.

28. Zener, C., as quoted by C. S. Smith, "Grains, Phases, Phase and Interphases: An Interpretation of Microstructure," Transactions American Institute of Metallurgical Engineering, Volume 175, pp. 15-51, 1948.

29. Ghosh, A. K., "Characterization of Superplastic Behavior of Metals," Superplastic Forming of Structural Alloys, Conference Proceedings of TMS-AIME, pp. 85-103, June 1982.

30. Alcoa Technical Center, Ltr, August 1984.

INITIAL DISTRIBUTION LIST

		No. Copies
1.	Defense Technical Information Center Cameron Station Alexandria, Virginia 22304-6145	2
2.	Library, Code 0142 Naval Posgraduate School Monterey, California 93943-5100	2
3.	Department Chairman, Code 69Mx Department of Mechanical Engineering Naval Postgraduate School Monterey, California 93943-5100	1
4.	Professor T. R. McNelley, Code 69Mc Department of Mechanical Engineering Naval Postgraduate School Monterey, California 93943-5100	5
5.	Mr. Richard Schmidt, Code AIR 320A Naval Air Systems Command Naval Air Systems Command Headquarters Washington, D.C. 20361	1
6.	Dr. Eu Whee Lee, Code 6063 Naval Air Development Center Warminster, Pennsylvania 18974	1
7.	LCDR Thomas S. Hartmann, USN U.S. Naval Ship Repair Facility, Subic Bay, P.I. Box 34 FPO San Francisco, California 96651-1400	5